CHAPTER IV

RESULTS AND DISCUSSION

Results of various measurements carried out in the present work on samples of carbonatites, alkaline rocks, metasomatic rocks and country rocks from different Mesozoic carbonatite-alkaline complexes of India are presented in this chapter and their implications are discussed. This chapter consists of two parts. The first part discusses the results of different studies on the complexes of Deccan Province (Western India) and the second part discusses the results from complexes of Assam-Meghalaya plateau (Eastern India). For the sake of convenience each part is divided into several sections and each section deals with a particular method of investigation.

PART-A: CARBONATITE-ALKALINE COMPLEXES OF DECCAN PROVINCE

In this part, the results of different studies on the rocks of the three carbonatite alkaline complexes (Amba Dongar, Mundwara and Sarnu-Dandali) are presented and discussed in light of the evolution of these complexes. This part is again divided into five sections describing the results of ^{40}Ar-^{39}Ar chronology, strontium isotopic studies, trace and rare earth elements studies of Amba Dongar complex and stable isotopic studies of all the three complexes, respectively.

4.1. ^{40}Ar-^{39}Ar CHRONOLOGY OF AMBA DONGAR COMPLEX

4.1.1. Results

The Amba Dongar alkaline complex is one of the several alkaline complexes that are spatially associated with the Deccan Traps. According to the present notion these complexes represent magmatic activity either older or younger than the main tholeiitic volcanism (Basu et al., 1993; Sen, 1995) of the Deccan Province. As discussed in Chapter II the only chronological study by Deans et al. (1973) of the Amba Dongar complex failed to provide a reliable age for this complex, as the K-Ar dates given by these authors varied from 37.5 Ma to 76 Ma.

To establish the temporal relationship between the Amba Dongar alkaline complex and the Deccan Traps, precise ^{40}Ar-^{39}Ar dating of samples from Amba Dongar was undertaken following the procedures described in Chapter III. Three fresh alkaline rock samples (AD-16, AD-45 and AD-47) and a phlogopite separate from a carbonatite (AD-46) were dated. The description of these samples are given in Table 3.1 of Chapter-III. The argon isotopic compositions, fractions of ^{39}Ar released, apparent ages and percent of radiogenic argon ($^{40}Ar^*$) released, for each temperature step are given in Tables 4.1 - 4.4. The tables also give modified J factors, determined from horizontal neutron fluence variation in the irradiation can.

Table 4.1. Step heating argon isotopic compositions and apparent ages of sample AD-16 (Amba Dongar Nephelinite). Errors on age are without and with (bracketed) error on J. Errors quoted are at 1σ.

(J = 0.00218 ± 0.00002)

Temp. (°C)	$^{36}Ar/^{39}Ar$ ±1σ	$^{37}Ar/^{39}Ar$ ±1σ	$^{40}Ar/^{39}Ar$ ±1σ	AGE (Ma) ±1σ	^{39}Ar (%)	$^{40}Ar^*$ (%)
450	2.201	0.0362	654.0	16	0.02	0.61
	0.099	0.003	21.0	81 (81)		
500	0.2513	0.0362	91.48	67	0.14	18.82
	0.0093	0.0036	0.93	11 (11)		
550	0.0383	0.0363	27.90	64.1	1.56	59.47
	0.0012	0.0036	0.26	1.6 (1.7)		
650	0.02081	4.740	22.79	64.33	5.27	73.02
	0.00038	0.074	0.15	0.67 (0.95)		
700	0.03599	4.35	27.46	65.04	5.0	61.27
	0.00059	0.22	0.18	0.88 (1.11)		
750	0.01950	3.74	22.54	64.9	4.07	74.43
	0.00059	0.11	0.16	1.1 (1.3)		
800	0.01567	5.63	21.25	64.26	4.78	78.21
	0.00066	0.83	0.16	0.89 (1.11)		

850	0.02445	11.02	23.91	64.5	3.60	69.78
	0.00074	0.11	0.21	1.1 (1.3)		
900	0.04381	1.89	29.79	65.1	3.67	56.54
	0.00081	0.16	0.22	1.2 (1.4)		
950	0.01782	3.57	21.93	64.44	5.67	75.99
	0.00047	0.11	0.16	0.77 (1.02)		
1000	0.00962	3.58	19.71	65.22	11.34	85.58
	0.00045	0.40	0.12	0.65 (0.93)		
1050	0.00531	3.442	18.34	64.82	26.0	91.44
	0.00040	0.060	0.12	0.57 (0.88)		
1100	0.00329	1.75	17.86	65.27	17.51	94.56
	0.0006	0.15	0.10	0.75 (1.01)		
1150	0.00817	4.941	19.26	65.11	7.61	87.46
	0.00062	0.062	0.15	0.88 (1.11)		
1200	0.0416	8.32	28.77	63.8	1.8	57.32
	0.0019	0.81	0.60	3.1 (3.2)		
1250	0.0924	10.6	45.7	70.9	0.72	40.23
	0.0055	1.1	1.5	8.4 (8.5)		
1300	0.219	0.416	94.7	114.0	0.41	31.51
	0.017	0.042	3.5	23.0 (23.0)		
1400	0.317	0.417	103.7	39	0.82	9.59
	0.010	0.042	3.3	16 (16)		
Integrated Values	0.01784	3.774	22.061	64.91	100.0	76.11
	0.00022	0.072	0.058	0.31 (0.74)		

Table 4.2. Step heating argon isotopic compositions and apparent ages of sample AD-45 (Amba Dongar Tinguaite). Errors on age are without and with (bracketed) error on J. Errors quoted are at 1σ.

(J = 0.00218 ± 0.00002)

Temp. (°C)	$^{36}Ar/^{39}Ar$ ±1σ	$^{40}Ar/^{39}Ar$ ±1σ	$^{40}Ar/^{39}Ar$ ±1σ	AGE (Ma) ±1σ	^{39}Ar (%)	$^{40}Ar^*$ (%)
450	0.643	0.259	221.2	119	0.02	14.14
	0.021	0.026	2.9	25 (25)		
500	0.1240	0.519	52.9	62.8	0.34	30.74
	0.0038	0.052	1.2	4.2 (4.2)		
550	0.05598	0.550	33.71	66.2	0.82	50.94
	0.00055	0.055	0.36	1.4 (1.5)		
600	0.01252	0.551	20.69	65.54	3.26	82.12
	0.00015	0.055	0.17	0.90 (1.13)		
650	0.005673	0.551	18.66	65.51	6.59	91.02
	0.000076	0.055	0.17	0.60 (0.91)		
700	0.01151	0.552	20.25	64.98	8.45	83.20
	0.00011	0.055	0.17	0.63 (0.92)		
750	0.0046	0.841	18.18	64.39	11.20	92.52
	0.0001	0.084	0.14	0.50 (0.84)		
800	0.00166	0.842	17.18	64.39	10.33	97.15
	0.00013	0.084	0.12	0.43 (0.43)		
850	0.00142	1.12	17.15	64.56	7.11	97.56
	0.00021	0.11	0.12	0.49 (0.83)		
900	0.00126	0.281	17.01	64.20	4.24	97.81
	0.00054	0.028	0.17	0.88 (1.10)		
950	0.00229	0.286	17.35	64.34	3.07	96.10
	0.00067	0.028	0.14	0.89 (1.11)		

1000	0.00173	0.893	17.43	65.2	3.21	97.07
	0.00074	0.089	0.35	1.3 (1.4)		
1050	0.00078	2.518	16.91	64.37	7.58	98.63
	0.00038	0.051	0.11	0.57 (0.87)		
1100	0.00105	3.58	16.94	64.18	15.69	98.17
	0.00026	0.11	0.11	0.47 (0.87)		
1150	0.00245	2.553	17.50	64.71	14.30	95.86
	0.00024	0.050	0.13	0.52 (0.85)		
1200	0.00188	1.58	17.32	64.7	2.42	96.80
	0.00096	0.16	0.30	1.5 (1.7)		
1250	0.0183	1.58	22.88	67.3	0.75	76.34
	0.0031	0.16	0.78	4.5 (4.6)		
1300	0.226	0.0316	74.2	29.0	0.40	10.09
	0.012	0.0032	4.2	16 (16)		
1400	4.463	0.0316	1327	33.0	0.22	0.64
	0.084	0.0032	24	55 (55)		
Integrated Values	0.01502	1.586	21.153	64.49	100.00	79.02
	0.00012	0.026	0.051	22 (70)		

Table 4.3. Step heating argon isotopic compositions and apparent ages of sample AD-46 (Phlogopite from Amba Dongar Carbonatite). Errors on age are without and with (bracketed) error on J. Errors quoted are at 1σ.

$J = 0.00239 \pm 0.00002$

Temp. (°C)	$^{36}Ar/^{39}Ar$ ±1σ	$^{40}Ar/^{39}Ar$ ±1σ	$^{40}Ar/^{39}Ar$ ±1σ	AGE (Ma) ±1σ	^{39}Ar (%)	$^{40}Ar^*$ (%)
500	2.565	0.00686	804	189	0.01	5.75
	0.097	0.00069	32	57 (57)		
550	0.9362	0.00687	279.8	14	0.05	1.14
	0.0076	0.00069	2.4	13 (13)		

600	0.2930	0.00688	106.91	85.5	0.22	19.01
	0.0027	0.00069	0.88	4.4 (4.5)		
650	0.3897	0.00688	128.71	57.5	2.07	10.54
	0.0034	0.00069	0.80	4.7 (4.8)		
700	0.1902	0.00689	71.65	65.4	4.24	21.58
	0.0011	0.00069	0.44	2.0 (2.0)		
750	0.05629	0.00699	31.86	64.5	3.87	47.79
	0.00029	0.0007	0.26	1.0 (1.2)		
800	0.04732	0.00701	29.67	66.38	7.73	52.87
	0.00017	0.0007	0.23	0.91 (1.1)		
850	0.03839	0.00702	26.84	65.59	7.73	57.74
	0.00018	0.00018	0.21	0.82 (1.02)		
900	0.04767	0.00702	29.60	65.65	7.85	52.41
	0.00019	0.0007	0.25	0.96 (1.14)		
950	0.04702	0.00714	29.28	65.1	6.49	52.54
	0.0002	0.00071	0.26	1.0 (1.2)		
1000	0.036651	0.00715	26.46	66.32	27.34	59.23
	0.00022	0.00072	0.25	1.0 (1.18)		
1050	0.0390	0.00742	27.2	66.2	17.85	57.62
	0.0028	0.00074	2.0	1.5 (1.6)		
1100	0.021954	0.00743	21.71	64.45	10.52	70.12
	0.000097	0.00074	0.24	0.95 (1.13)		
1150	0.01666	0.00744	20.30	65.1	2.21	75.75
	0.00027	0.00074	0.59	2.3 (2.4)		
1200	0.00113	0.00745	13.72	56.8	1.28	97.57
	0.00074	0.00075	0.48	2.2 (2.3)		
1250	0.0094	0.00747	12.7	42.4	0.49	78.14
	0.0022	0.00075	1.2	5.9 (5.9)		

1300	0.0669	0.00757	37.5	75.0	0.06	47.31
	0.0099	0.00076	2.8	17 (17)		
Integrated Values	0.05274	0.00719	31.04	65.4	100.0	49.79
	0.00068	0.00027	0.41	0.45 (0.76)		

Table 4.4. Step heating argon isotopic compositions and apparent ages of sample AD-47 (Amba Dongar Tinguaite). Errors on age are without and with (bracketed) error on J. Errors quoted are at 1σ.

(J = 0.00232 ± 0.00002)

Temp. (°C)	$^{36}Ar/^{39}Ar$ ±1σ	$^{40}Ar/^{39}Ar$ ±1σ	$^{40}Ar/^{39}Ar$ ±1σ	AGE (Ma) ±1σ	^{39}Ar (%)	$^{40}Ar^*$ (%)
450	0.03744	0.0461	28.39	70.95	3.22	61.03
	0.00018	0.0021	0.17	0.64 (0.92)		
500	0.01877	0.13644	22.61	69.90	19.46	92.96
	0.00009	0.00027	0.13	0.47 (0.80)		
600	0.01004	0.34765	18.99	65.72	11.12	84.38
	0.00011	0.0007	0.11	0.41 (0.74)		
650	0.00146	0.0916	16.261	64.94	10.87	97.34
	0.00033	0.0026	0.094	0.52 (0.80)		
700	0.00312	0.0426	16.84	65.29	5.31	94.53
	0.00033	0.0010	0.10	0.73 (0.95)		
750	0.00255	0.03771	16.55	64.81	3.99	95.45
	0.00049	0.00062	0.11	0.70(0.93)		
800	0.01162	0.0520	19.40	65.49	4.26	82.30
	0.00053	0.0023	0.13	0.77 (0.99)		
850	0.00956	0.0589	18.71	65.49	4.63	84.90
	0.00043	0.0019	0.12	0.67 (0.91)		
900	0.00368	0.00320	17.05	65.49	7.54	93.63
	0.00033	0.00032	0.11	0.55 (0.82)		

950	0.00361	0.0793	16.92	65.03	7.48	93.69
	0.0003	0.0027	0.12	0.55 (0.82)		
1000	0.0502	0.04774	17.51	65.76	5.85	91.53
	0.0002	0.00095	0.13	0.54 (0.82)		
1050	0.01805	0.0774	21.78	67.4	0.92	75.51
	0.00076	0.0017	0.76	3.2 (3.2)		
1100	0.05421	0.168	40.2	98.2	0.24	60.12
	0.00072	0.014	2.4	9.7 (9.7)		
1150	0.1015	1.382	48.5	76.0	0.17	38.14
	0.0024	0.021	3.3	13 (13)		
1200	0.265	1.02	87.2	36.0	0.14	10.11
	0.011	0.33	4.6	23 (23)		
Integrated Values	0.009001	0.15533	19.036	67.15	100.0	86.03
	0.000073	0.00076	0.039	0.17 (0.65)		

The age spectra along with isotope correlation plots for all four samples are shown in Figures 4.1 - 4.4. The plateau ages along with percent ^{39}Ar included for the plateaus; isochron ages and inverse isochron ages of plateau steps along with ratios of trapped argon and MSWD values; and integrated (total) ages are summarized in Table 4.5. Errors quoted in all the values are at 2σ level. Two alkaline rocks (AD-16 and AD-45) and the phlogopite separate from a carbonatite (AD-46) yielded good plateaus in the age spectra (Figs.4.1a, 4.2a and 4.3a) giving ages of 64.8±0.6 Ma, 64.7±0.5 Ma, and 65.5±0.8 Ma, respectively. The third alkaline rock (AD-47) yielded a 10 step high temperatures plateau (from 600°C to 1050°C) with an age of 65.3±0.6 Ma (Fig.4.4a). The three low temperature steps of AD-47 (Fig.4.4a) showed higher apparent ages, perhaps due to recoil effect. The one or more initial and final temperature steps (Figs. 4.1a, 4.2a, 4.3a and 4.4a), which are not included in the plateaus, showed large errors in their apparent ages due to the very small amount of ^{39}Ar-release in these steps. For all the four samples, there is an excellent agreement between plateau and isochron ages indicating that these samples have not lost any significant amount

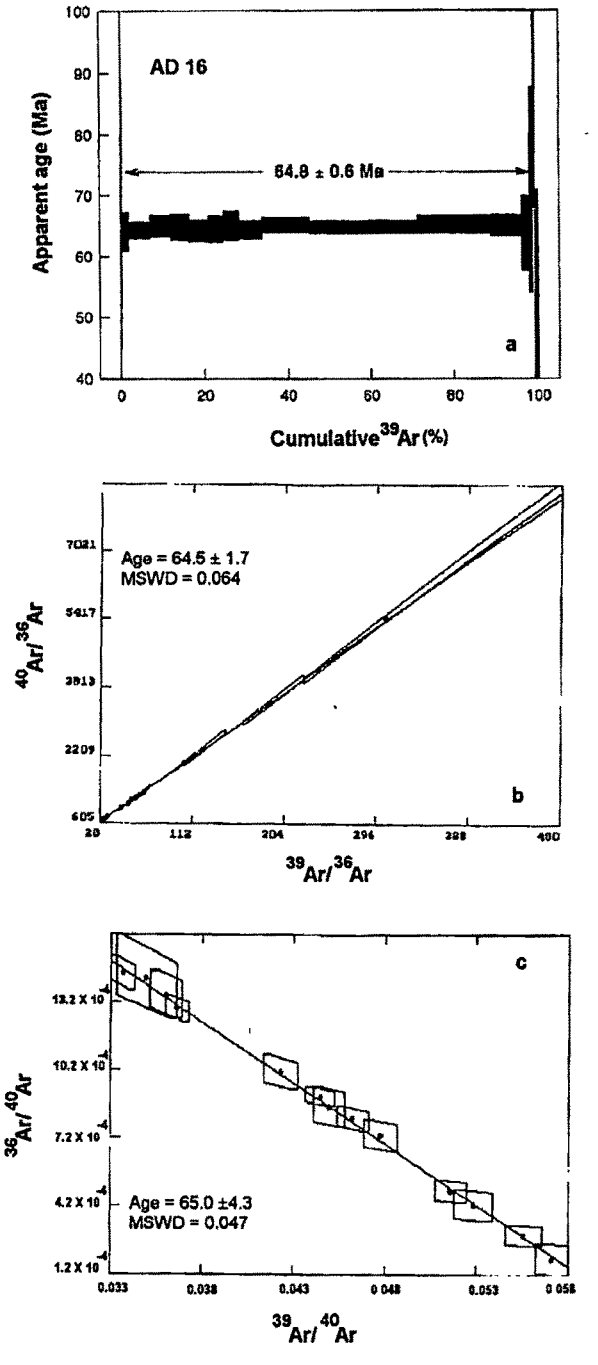

Fig. 4.1. *(a) Step heating of $^{40}Ar/^{39}Ar$ apparent age spectrum for AD-16 (Amba Dongar Nephelinite). The age shown is plateau age, which includes 2σ error on J but the vertical width of plateau boxes indicate 2σ errors calculated without error on J. (b) $^{40}Ar/^{36}Ar$ vs. $^{39}Ar/^{36}Ar$ correlation diagram of AD-16 showing 2σ error envelopes and regression line. Error on isochron age is at 2σ. (c) $^{36}Ar/^{40}Ar$ vs. $^{39}Ar/^{40}Ar$ correlation diagram of AD-16 showing 2σ error envelopes and regression line. Error on inverse isochron age is at 2σ.*

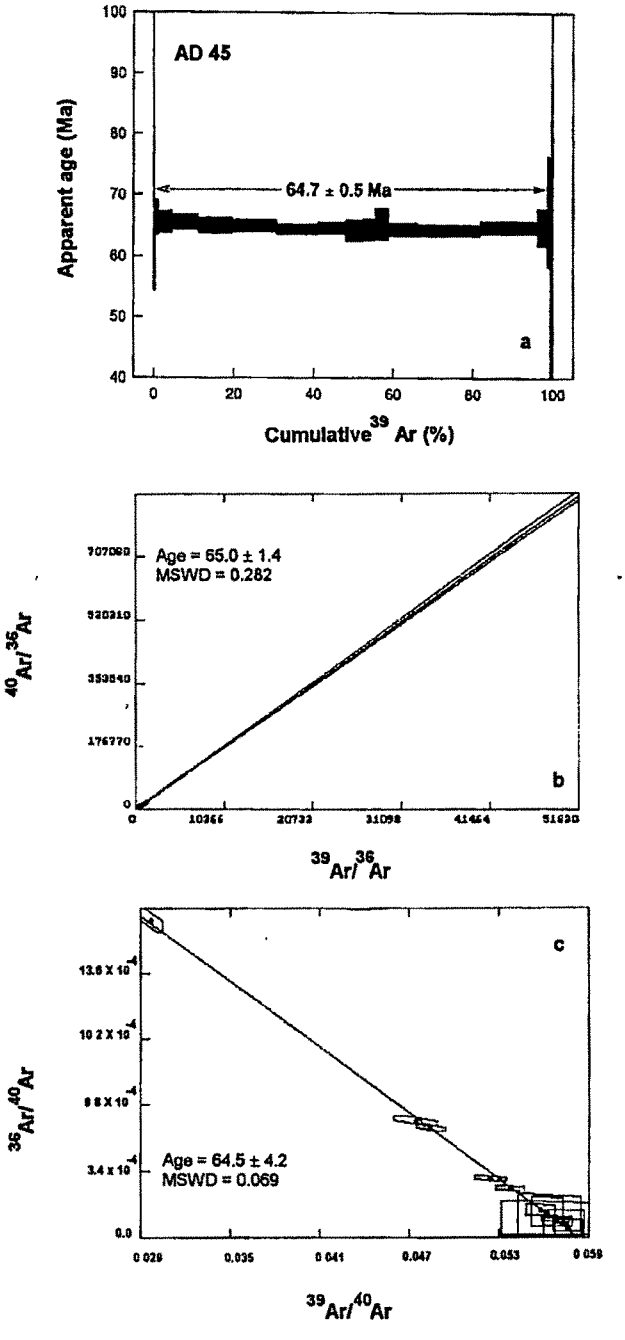

Fig.4.2 *(a) Step heating $^{40}Ar/^{39}Ar$ apparent age spectrum for AD-45 (Amba Dongar Tinguaite)with plateau age.(b) $^{40}Ar/^{36}Ar$ vs. $^{39}Ar/^{36}Ar$ correlation diagram of AD-45 with isochron age and MSWD value. (c) $^{36}Ar/^{40}Ar$ vs. $^{39}Ar/^{40}Ar$ correlation diagram of AD-45 with inverse isochron age and MSWD value. Please also see the caption of Fig. 4.1.*

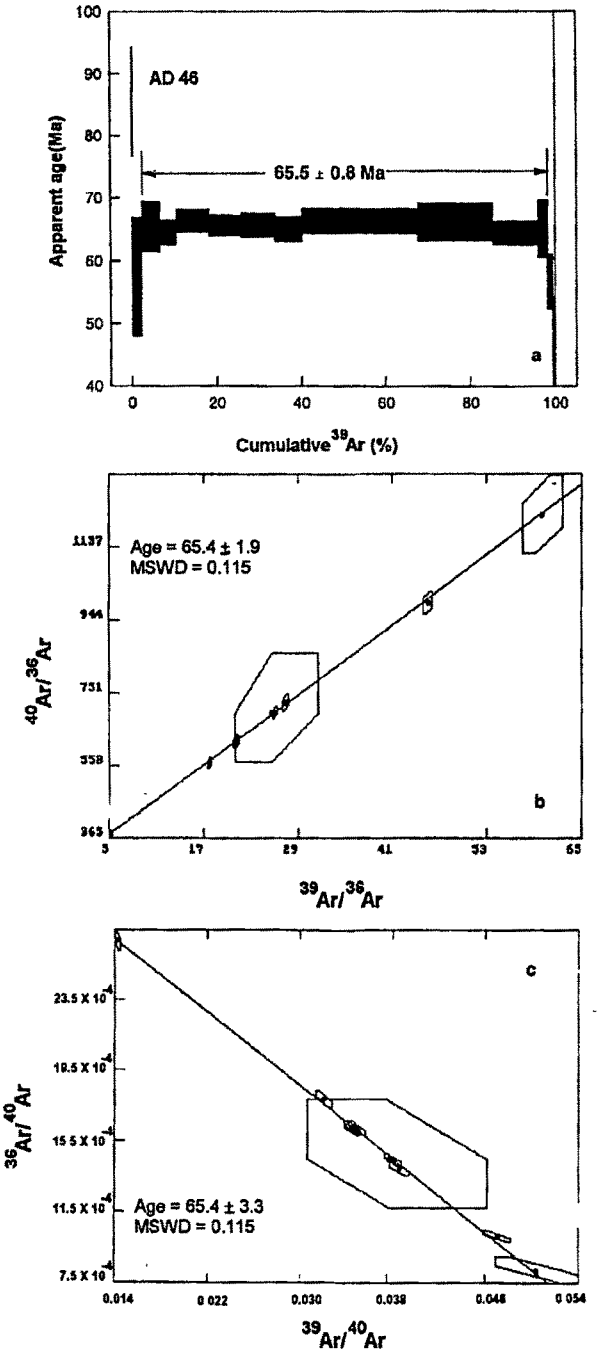

Fig. 4.3. *(a) Step heating $^{40}Ar/^{39}Ar$ apparent age spectrum for AD-46 (Phlogopite separate from a carbonatite of Amba Dongar) with the plateau age. (b) $^{40}Ar/^{36}Ar$ vs. $^{39}Ar/^{36}Ar$ correlation diagram of AD-46 with isochron age and MSWD value. (c) $^{36}Ar/^{40}Ar$ vs. $^{39}Ar/^{40}Ar$ correlation diagram of AD-46 with inverse isochron age and MSWD value. Please also see the caption of Fig. 4.1.*

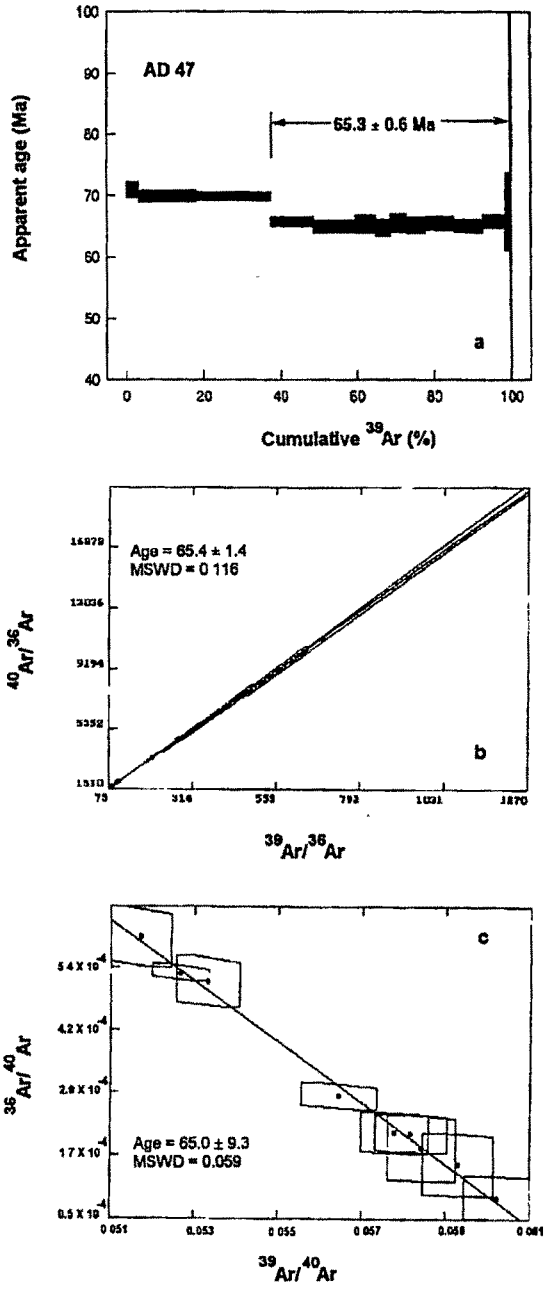

Fig. 4.4. *(a) Step heating $^{40}Ar/^{39}Ar$ apparent age spectrum for AD-47 (Amba Dongar Tinguaite) with the plateau age. First three steps of the spectrum are not included in the plateau (See text for discussion). (b) $^{40}Ar/^{36}Ar$ vs. $^{39}Ar/^{36}Ar$ correlation diagram of AD-47 with isochron age and MSWD value. (c) $^{36}Ar/^{40}Ar$ vs. $^{39}Ar/^{40}Ar$ correlation diagram of AD-47 with inverse isochron age and MSWD value. Please also see the caption of Fig. 4.1.*

of radiogenic argon since their crystallization. The undisturbed nature of these samples is also reflected in the total ages, which are indistinguishable from the plateau ages within the 2σ level of error. In the isotope correlation plots of the plateau steps of all these samples showed atmospheric trapped argon composition (i.e. $(^{40}Ar/^{36}Ar)_i = 295.5$) within the limits of uncertainties (2σ errors) implying that the plateau ages are true ages of the samples.

Table 4.5. Summary of results of ^{40}Ar-^{39}Ar dating of Amba Dongar samples.

Sample	Plateau			Isochron			Inverse Isochron			Integrated Age
	steps	% ^{39}Ar	Age (Ma)	Age (Ma)	Trap	MSWD	Age (Ma)	Trap	MSWD	(Ma)
AD-16	13	97.88	64.8 ±0.6	64.5 ±1.7	297.4 ±13.2	0.064	65.0 ±4.3	292.7 ±11.5	0.047	64.5 ±1.5
AD-45	14	98.27	64.7 ±0.5	65.0 ±1.4	297.7 ±12.8	0.282	64.5 ±4.2	306.7 ±13.2	0.069	65.5 ±1.4
AD-46	10	98.27	65.5 ±0.8	65.4 ±1.9	295.9 ±6.5	0.115	65.4 ±3.3	295.9 ±6.5	0.115	65.4 ±1.6
AD-47	9	61.05	65.3 ±0.6	65.4 ±1.4	296.9 ±23.4	0.116	65.0 ±9.3	310.6 ±29.9	0.059	67.2 ±1.4

Note: Trap: Initial $^{40}Ar/^{36}Ar$ (trapped argon); MSWD: Mean Square Weighted Deviate.
Errors are 2σ.

Indistinguishable ages of alkaline silicate rocks and carbonatites indicate that these two rock types of Amba Dongar complex are contemporaneous. The weighted mean (determined following Bevington (1969)'s procedures) of all plateau ages is 65.0±0.3 Ma, which is the age of emplacement of the Amba Dongar complex.

4.1.2. Discussion

The contemporarity of alkaline silicate rocks and carbonatites of Amba Dongar complex probably indicates a genetic relationship between these two. The 65.0±0.3 Ma age of this complex suggests that the complex got emplaced towards the end phase of Deccan Trap magmatism and it is ~2.0 Ma younger than the main pulse of Deccan (67.0 Ma, Pande et al, in preparation). As mentioned in Chapter-II, the Amba Dongar complex intrudes into the Deccan tholeiites of this region. Therefore, the Traps of this region are older than 65.0 Ma.

This age of Amba Dongar complex along with the two northern most 68.5 Ma old alkaline complexes at Sarnu-Dandali and Mundwara fits well in the plume theory for the generation of Deccan flood basalts and is consistent with the idea of 10-15 cm/year northward motion of the Indian plate over nascent Reunion hotspot (Basu et al., 1993). In this plume model, Amba Dongar complex would represent a late stage alkaline magmatism on the southern end side of the plume head.

Amba Dongar is part of the Chhota Udaipur carbonatite-alkaline district of Gujarat, which covers an area of ~1200 km^2 (Viladkar, 1996) and consists of several alkaline complexes. Phenai Mata carbonatite-alkaline complex (present to the northeast of Amba Dongar), which is also a part of this district, has been dated to 64.96±0.11 Ma by Basu et al. (1993). This probably indicates that the carbonatite-alkaline magmatism of this district occurred at 65.0 Ma, which happens to be just at the K/T boundary (Izett et al., 1991). This coincidence makes these carbonatite alkaline magmatisms very important in the ongoing debate on the K/T mass-extinctions. Alkaline and carbonatite magmatism are associated with the release of very high amount of CO_2 + CO + SO_2 gases (Bailey and Hampton, 1990). Owing to their very low viscosity and density these melts get emplaced/erupted very fast which obviously results in a lot of volatile input into the atmosphere in a very short interval of time. A conservative calculation shows that the total CO_2 flux from just carbonatites of Chhota Udaipur district was 2.67 x 10^{14} moles, which came out in a very short period of time (in a few years). Workers who believe in the internal cause (i.e. Deccan Volcanism) to be responsible for the mass-extinctions at K/T boundary suggest that the high amount of CO_2 released due to the Deccan volcanism (~5 x 10^{17} moles in ~1 Ma ; McLean et al., 1985) is one of the major reasons for the catastrophism. In this context the carbonatite-alkaline magmatism of Chhota Udaipur district would have enhanced the catastrophic effects due to addition of a very significant amount of CO_2 in a very short time into the already disturbed atmosphere.

4.1.3. Summary

The age of Amba Dongar carbonatite-alkaline complex is 65 Ma. This age is consistent with the plume hypothesis proposed for the origin of this complex (Sen, 1995) and also confirms the genetic relationship of Amba Dongar with the Deccan flood basalts. Being

emplaced just at the K/T boundary it could have enhanced the catastrophic effects leading to mass extinctions, by rapidly adding a substantial amount of CO_2 into the atmosphere.

4.2 Sr ISOTOPIC STUDIES OF AMBA DONGAR COMPLEX

4.2.1. Results

Sr isotope ratio and concentration were measured in samples of carbonatites, alkaline rocks and different country rocks from Amba Dongar complex. The aim of this study was to assess the role of different magmatic processes, particularly the crustal contamination, in the evolution of this complex and to characterize the isotopic composition of the source region. Table 4.6 summarizes the results of this study. It gives concentrations of Rb and Sr, measured $^{87}Sr/^{86}Sr$ and $^{87}Rb/^{86}Sr$ ratios with 2σ error and initial $^{87}Sr/^{86}Sr$ ratios calculated using the age of 65 Ma for Amba Dongar. As mentioned in Chapter-III, the 2σ errors in the $^{87}Sr/^{86}Sr$ measurements were higher in the samples analyzed at Physical Research Laboratory compared to the errors in the samples analyzed at National Geophysical Research Institute. The initial $^{87}Sr/^{86}Sr$ ratios of alkaline rocks and carbonatites are plotted against Sr concentration in Fig. 4.5.

Table 4.6. Results of Sr isotopic measurements in samples from Amba Dongar.

Sample	Rb (ppm)	Sr (ppm)	$(^{87}Sr/^{86}Sr)_m$ (atomic)	$(^{87}Rb/^{86}Sr)_m$ (atomic)	$(^{87}Sr/^{86}Sr)_i$
Alkaline Rocks					
AD-14	27	1998	0.7062±3	0.0391	0.7062
AD-16*	14	3511	0.70633±4	0.0115	0.70632
AD-17*	51	1854	0.70621±4	0.0796	0.70614
AD-18	80	1551	0.7069±2	0.1492	0.7068
AD-45*	103	1172	0.70678±4	0.2543	0.70655
AD-47*	95	93	0.71562±4	2.9579	0.71289
AD-65*	21	2535	0.70706±6	0.02397	0.70704
AD-66*	18	3278	0.70660±6	0.01589	0.70658

AD-67*	85	237	0.71154±3	1.03089	0.71058
Calcite Carbonatites					
AD-1	0.5	6176	0.7066±3	0.0023	0.7066
AD-10/1	0.7	5413	0.7059±3	0.00037	0.7059
AD-38	1.4	3710	0.7060±4	0.00109	0.7060
AD-49	bdl	3594	0.7055±2	bdl	0.7055
AD-52*	5.0	2705	0.7060±2	0.0053	0.70605
Ferro-carbonatites					
AD-19	0.8	3248	0.7065±2	0.0007	0.7065
AD-36	bdl	4920	0.7061±2	bdl	0.7061
AD-55	bdl	8477	0.7061±1	bdl	0.7061
Sandstone					
AD-6	56	68	0.7590±7	2.3947	0.7568
Limestones					
AD-59/1	bdl	676	0.7087±2	bdl	0.7087
AD-62	4	4558	0.7109±2	0.00254	0.7109

* = Samples analyzed at National Geophysical Research Institute, Hyderabad. 'm' stands for measured isotopic ratio and 'i' for initial ratio (at 65 Ma). bdl = below detection limit. Errors are 2σ.

The initial $^{87}Sr/^{86}Sr$ ratios of alkaline rocks are highly variable (0.70614-0.71289) compared to those of carbonatites (0.7055-0.7066). The Sr isotopic ratios of carbonatites fall within the range of values given by Deans and Powell (1968) and overlap with the range given by Simonetti et al. (1995). Sr concentration in carbonatites (2705-8477 ppm) are higher than the alkaline silicate rocks (93-3511 ppm) (Table 4.6 and Fig. 4.5). Initial $^{87}Sr/^{86}Sr$ and Sr concentrations of ferrocarbonatites are similar to those of calcite carbonatites.

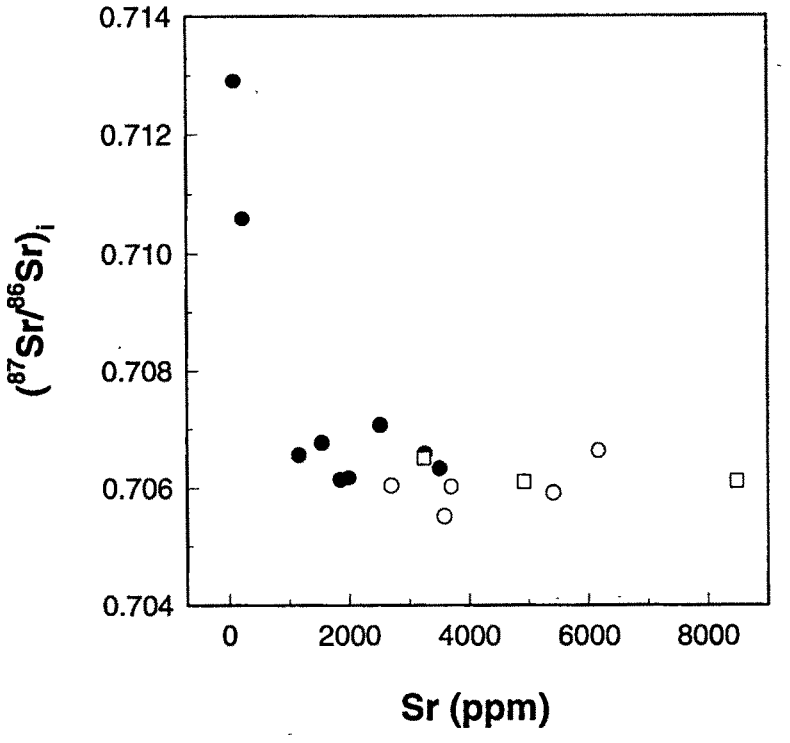

Fig. 4.5. Plot of initial $^{87}Sr/^{86}Sr$ vs. Sr content for the whole-rock samples of Amba Dongar complex. Filled circle = alkaline rocks; open circles = calcite carbonatites; and open squares = ferrocarbonatites.

4.2.2. Discussion

As seen in Fig.4.5, the alkaline rocks show higher initial $^{87}Sr/^{86}Sr$ ratios and lower Sr concentrations compared to the carbonatites. Whereas, the initial ratios of carbonatites are homogeneous within the experimental error. The trend of decreasing Sr concentration with increasing isotopic ratio shown by the alkaline rocks suggests that probably the rocks have been contaminated by some crustal material having high $^{87}Sr/^{86}Sr$ and lower Sr concentration during their crystallization. The country rocks, sandstone (Table 4.6) and Precambrian granitic gneiss (Gopalan et al., 1979), are likely candidates for contaminant. Limestones do not qualify to be the contaminant as the Sr ratios of these (0.7087 and 0.7109) are smaller than the highest initial ratio (0.71289) observed in alkaline rocks. Hence, to find out the contaminant and the amount of contamination simple binary mixing

and assimilation fractional crystallization (AFC) (DePaolo, 1981) models were applied to the observed data. The following section discusses the results of these models.

4.2.2a. Simple Binary Mixing and AFC for Alkaline Rocks

A simple binary mixing curve was generated (Fig.4.6) taking an unfenitized sandstone [$(^{87}Sr/^{86}Sr)_i$ = 0.7568 and Sr = 68 ppm] as one end-member and an alkaline rock [$(^{87}Sr/^{86}Sr)_i$ = 0.70632 and Sr = 3511 ppm] with highest Sr concentration as the second end-member. As seen in Fig.4.6, the binary mixing curve does not coincide with the observe alkaline rock trend.

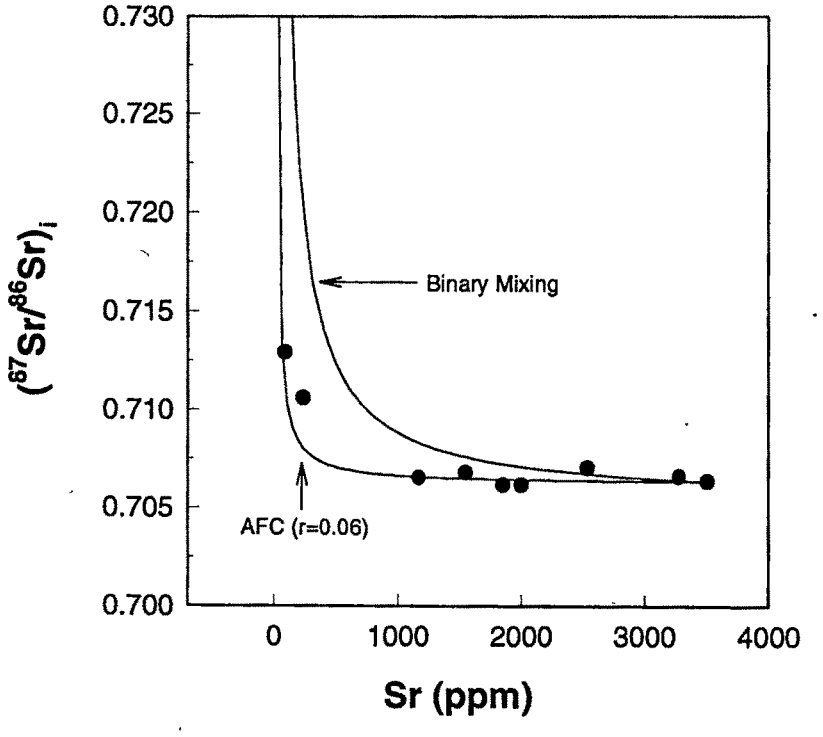

Fig. 4.6. *Plot of initial $^{87}Sr/^{86}Sr$ vs. Sr content for alkaline rocks of Amba Dongar complex. Binary mixing curve represents results of simple binary mixing between alkaline silicate magma with Bagh sandstone and the AFC curve represents results of AFC modelling (DePaolo, 1981), when Bagh sandstone gets assimilated in the alkaline silicate magma for a r (rate of assimilation/rate of crystallization) value of 0.06. See section 4.2.2a for discussion.*

The AFC model (DePaolo, 1981) was tried out with the above sandstone as the assimilant and the alkaline magma with Sr ratio of 0.70632 and concentration of 1951 ppm. The Sr concentration in the magma was determined assuming a rock-melt bulk distribution coefficient of 1.8. This distribution coefficient was calculated considering an average alkaline rock (nepheline = 25%, K-feldspar = 10%, aegirine augite = 12%, melanite = 5%, calcite = 7%, apatite = 4% and matrix = 37%) and mineral-alkaline melt partition coefficients K_d (neph.) = 2.7 [assumed to be same as K_d (K-spar-melt)], K_d (K-spar) = 2.7 [Long (1978)], K_d (aug.) = 0.1, K_d (melanite) = 0.001 [Jones (1995)], K_d (calcite) = 4.0 [assumed to be same as K_d (carbonate liquid-silicate liquid), Green et al., 1992] and K_d (apatite) = 14.5 [assumed to be same as K_d (apatite-basaltic melt), Nagasawa (1970)]. Using the above end-members AFC curves were generated for different r (rate of assimilation/rate of crystallization) values and it was found that the model curve with r = 0.06 (i.e. 6% assimilation) explained the observed alkaline rock trend (Fig.4.6).

A similar exercise was carried out taking the Precambrian basement gneisses, which are exposed near Chhota Udaipur, as the assimilant. The Sr isotopic composition and concentration of gneiss (0.7690, 145 ppm) were taken from Gopalan et al. (1979). Like sandstone, in this case the binary mixing hyperbola did not explain the observed trend (Fig.4.7), whereas the AFC curve for r = 0.03 (i.e. 3% assimilation) explained the observed variation.

In summary, combined wall-rock assimilation fractional crystallization process is probably the cause of observed isotopic and concentration variation in alkaline rocks. However, as both sandstone and gneiss assimilation explain this, it is difficult to find out the true assimilant/contaminant unequivocally.

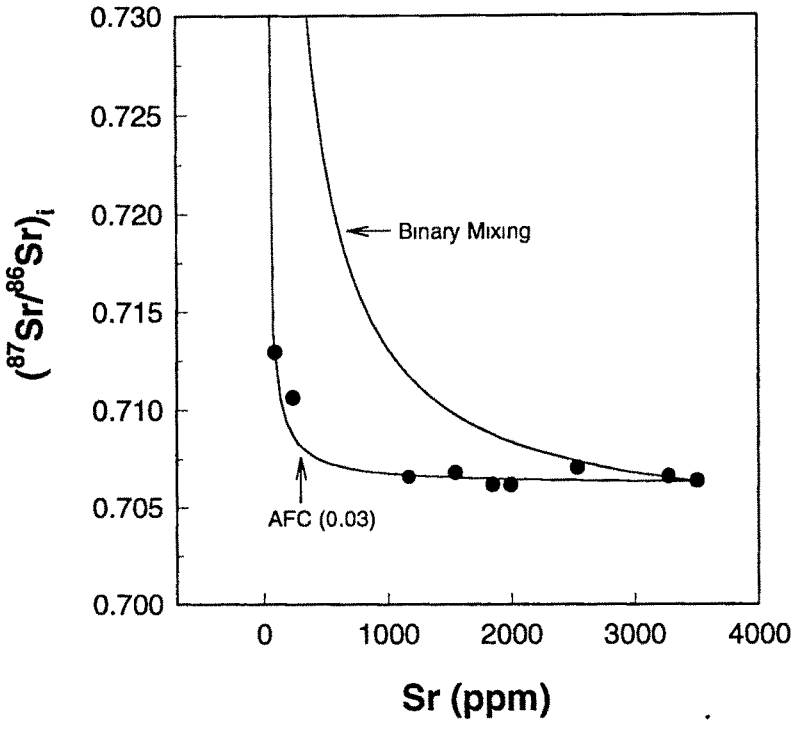

Fig. 4.7. Plot of initial $^{87}Sr/^{86}Sr$ vs. Sr content for alkaline rocks of Amba Dongar complex. Binary mixing curve represents results of simple binary mixing between alkaline silicate magma with a Precambrian gneiss (basement rock) from Chhota Udaipur (Gopalan et al., 1979) and the AFC curve represents results of AFC modelling (DePaolo, 1981), when the above gneiss gets assimilated in the alkaline silicate magma for a r value of 0.03 (see section 4.2.2a for details).

4.2.2b. An Alternative Explanation

Liquid immiscibility has been proposed to be the underlying process in the formation of alkaline silicates and carbonatites (LeBas, 1977; Kjarsgaard and Hamilton, 1989). In Amba Dongar, these two types of rocks are temporally and spatially related, which indicates a possible involvement of liquid immiscibility in their generation. Secondly, the alkaline rocks, as discussed in the above section, show crustal contamination. Hence, an attempt was made to include liquid immiscibility in the AFC process. For this a model was developed for trace element and isotopic effects by modifying the AFC model of DePaolo (1981) and then the model was applied to the observed data. In the following paragraphs, I discuss the model in general and its application to Sr-isotope systematics of alkaline rocks of Amba Dongar.

A. Assimilation Fractional Crystallization coupled with Liquid Immiscibility (AFCLI).

In this model it is assumed that the wall-rock assimilation, fractional crystallization of alkaline rock and the separation of immiscible carbonate melt occur simultaneously and the immiscibility is a fractional process like crystallization. Other assumptions are same as those considered by DePaolo (1981) for the simple AFC model.

(i) *Element Concentrations*

Consider a parent magma body, whose mass is M_m at any time t, which is assimilating wall rock at a rate dM_a/dt, removing carbonate liquid at a rate dM_l/dt and crystallizing silicate phases at a rate dM_c/dt. dM_a, dM_l and dM_c stand for mass at any instant of assimilated material, carbonate melt and crystallized solids, respectively. Let us define $D_c = C_c/C_m$, the silicate rock-melt distribution coefficient of a particular element and $D_l = C_l/C_m$, the carbonate melt-silicate melt distribution coefficient of the same element, where C_c, C_l and C_m, respectively stand for concentrations in crystallizing phase, carbonate melt and parent magma. Now the change of mass of the magma can be written (following the procedure given by DePaolo (1981)) as:

$$d(C_m M_m) = C_a\, dM_a - D_l\, C_m\, dM_l - D_c\, C_m\, dM_c \quad (1)$$

$$\text{or, } dC_m = \frac{dM_a}{M_m}(C_a - C_m) - \frac{dM_l}{M_m}(D_l - 1)C_m - \frac{dM_c}{M_m}(D_c - 1)C_m \quad (2)$$

Defining the parameters $a = dM_a/dM_c$ (rate of assimilation/rate of crystallization) and $b = dM_l/dM_c$ (rate of carbonate immiscibility/rate of crystallization) and replacing dM_a and dM_l by $(a.dM_c)$ and $(b.dM_c)$ in equation (2) we have:

$$dC_m = \frac{dM_c}{M_m}[a(C_a - C_m) - b(D_l - 1)C_m - (D_l - 1)C_m]$$

$$= \frac{dM_c}{M_m}[aC_a - C_m(a + bD_l - b + D_c - 1)] \quad (3)$$

If $F = M_m/M_m^{\circ}$ (fraction of remaining parent magma where M_m° is the initial mass of the parent magma) then

$$\frac{dF}{F} = \frac{dM_c}{M_m}(a - b - 1) \quad (4)$$

$$\text{or, } \frac{dM_c}{M_m} = \frac{dF}{F}\left(\frac{1}{a - b - 1}\right) \quad (5)$$

Now substituting the value of dM_c/M_m in equation (3), we have

$$\frac{dC_m}{dF/F} = \left(\frac{a}{a-b-1}\right)C_a - \left(\frac{a-b+bD_l+D_c-1}{a-b-1}\right)C_m \quad (6)$$

$$\text{or, } \frac{dC_m}{dF/F} = \left(\frac{a}{a-b-1}\right)C_a - zC_m \quad (7)$$

where $z = (a - b + bD_l + D_c - 1) / (a - b - 1)$ (8)

The transformation (7) is valid only when $(a - b) \neq 1$, that means when $dM_a \neq dM_c + dM_l$. This is the most general case of the equation (7). Rearranging equation (7) we get

$$\frac{dC_m}{\left(\frac{a}{a-b-1}\right)C_a - zC_m} = \frac{dF}{F} \quad (9)$$

Now integrating equation (9) with the initial conditions; at t = 0, F=1 and $C_m = C_m^\circ$ (initial concentration of the element in magma to start with), we get the equation for concentration variation in the parent magma:

$$C_m = C_m^\circ F^{-z} + \left(\frac{a}{a-b-1}\right)\frac{C_a}{z}(1-F^{-z}) \quad (10)$$

which is similar to equation (6a) of DePaolo (1981). Equation (10) is the most general case of concentration variation in AFCLI model. When there is no liquid immiscibility (b=0) then equation (10) reduces to simple AFC equation (6a) of DePaolo (1981): $C_m = C_m^\circ F^{-z} + \left(\frac{a}{a-1}\right)\frac{C_a}{z}(1-F^{-z})$, where z = (a + D_c-1)/(a-1) and a is r of DePaolo (1981).

(ii) *Isotopic Ratios*

For heavier isotopes, there is no isotopic fractionation during any of the magmatic processes, hence the isotopic ratios E_m, E_c and E_l are equal at any instant during AFCLI. The differential equation involving isotopic ratios in this model can be written as:

$$d(M_mC_mE_m) = C_aE_adM_a - C_cE_cdM_c - C_lE_ldM_l \quad (11)$$

Now expanding this equation and substituting the value of dCm from equation (3), we get:

$$C_mE_m(dM_a - dM_c - dM_l) + M_mC_mdE_m + M_mE_m[(dM_c/M_m)\{a(C_a - C_m) - b(D_l - 1)C_m\}] =$$

$$C_aE_adM_a - C_cE_cdM_c - C_lE_ldM_l \quad (12)$$

Simplifying equation (12) we get:

$$dE_m = \frac{dM_aC_a}{M_mC_m}(E_a - E_m) \quad (13)$$

for the most general case ($dM_a \neq dM_l + dM_c$) equation (13) will be:

$$\frac{dE_m}{(\frac{a}{a-b-1})\frac{C_a}{C_m}(E_a - E_m)} = \frac{dF}{F} \qquad (14)$$

Integrating equation (14) we get the isotopic ratio evolution equation:

$$\frac{E_m - E_m^o}{Ea - E_m^o} = 1 - (\frac{C_m^o}{C_m})F^{-z} \qquad (15)$$

Where E_m^o is the initial ratio of the parent magma. This equation is same as the evolution equation (15b) of DePaolo (1981), but here z is different (see equation (8)).

The AFCLI model equations (10) and (15) may be applied to situations where both wall-rock assimilation and liquid immiscibility are important. Like any other model this model also has certain limitations, which arise from the basic assumption of simultaneity of fractional crystallization and liquid immiscibility. The application of this model is also limited to magmas in which liquid immiscibility occurs within the crust so that the contamination effects are readily observed in the final products. In the case of alkaline rocks and carbonatites this model probably is the best model to explain isotopic variations resulted from wall rock assimilation as the silicate-carbonate liquid immiscibility has been experimentally observed to occur within the crust (Wyllie, 1989).

Fig.4.8 shows the application of AFCLI model to Sr isotope systematics and the model curves are compared with the simple binary mixing curve. In this figure the model calculations are done when a magma with initial $^{87}Sr/^{86}Sr$ of 0.705 and Sr concentration of 400 ppm assimilates a wall rock having ratio 0.72 and concentration 200 ppm. The model curves are generated for different D_c (rock-melt distribution coefficient of Sr) at a constant D_l of 4.0 (carbonate-silicate distribution coefficient of Sr). Fig.4.8a shows the model evolution curves for a=0.2 and b=0.2 and Fig.4.8b shows these for a=1.0 and b=0.02.

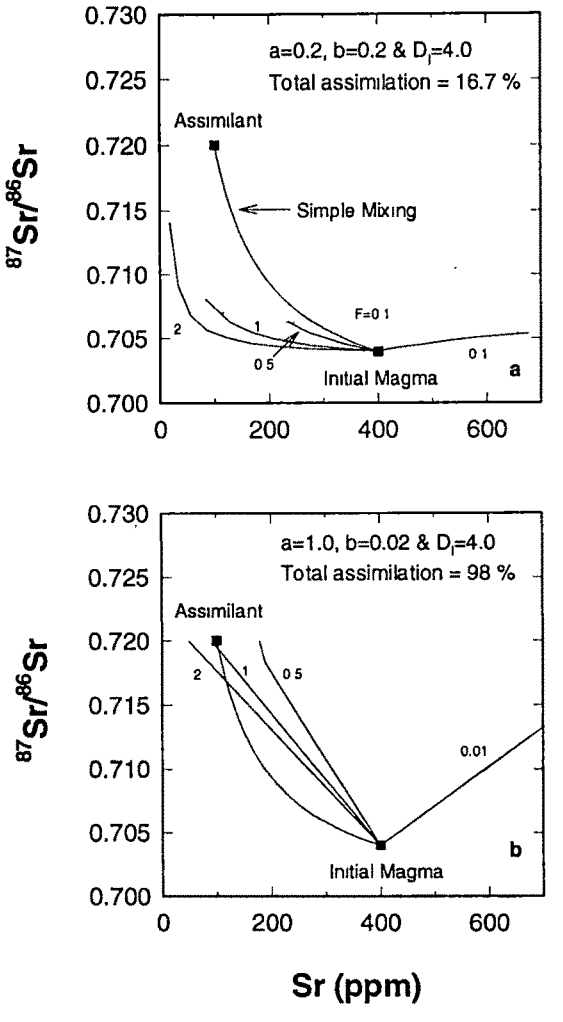

Fig. 4.8. *$^{87}Sr/^{86}Sr$ and Sr concentration evolution in a carbonated silicate magma affected by simultaneous wall rock assimilation, fractional crystallization of alkaline silicate rocks and separation of a carbonate magma by liquid immiscibility for different values of a (rate of assimilation/rate of crystallization) and b (rate of immiscibility/rate of crystallization). Numbers on model curves represent D_c (bulk distribution coefficient for Sr between alkaline rock and magma). In plot (a) evolution is done up to F (fraction of remaining magma) = 0.1 and in (b) up to F= 1.0. The total assimilation percent was calculated using equation (16). The D_i (bulk distribution coefficient for Sr between carbonate melt and silicate melt) is taken as 4.0 in both the cases. See section 4.2.2b for discussion.*

In Fig.4.8a, calculations are done up to F=0.1, whereas in Fig.4.8b, calculations are done up to F=0 (i.e., process completed). Most of the properties of AFCLI model curves are very similar to AFC curves (Fig.3 of DePaolo (1981)), however, the most striking

difference of this model is that even for a small amount of contamination a significant change in the isotopic ratio and concentration can be achieved in a short time (i.e. for a larger F) compared to AFC model.

(iii) ***Amount of Assimilation***

The amount of assimilation in AFCLI model, expressed in percentage is :

% assimilation = [mass of assimilated material/(mass of alkaline rock + mass of carbonatite)] ×100

$$= [M_a/(M_c+M_l)] \times 100$$

$$= [(M_a/M_c)/(1+(M_l/M_c)] \times 100$$

$$= [a/(1+b)] \times 100 \qquad (16)$$

(iv) ***Composition of the Carbonate Melt***

As the crystallization temperatures of carbonates are lower than the silicates, carbonate melt is expected not to crystallize during AFCLI process. Most likely the carbonate melt which fractionally gets removed from the parent melt slowly accumulates and after the liquid immiscibility is over it comes out of the system and travels up ward as a single homogeneous melt before it crystallizes. In such a situation the concentration of an element and isotopic ratio of the carbonate melt will be averages of those of all the fractional melts separated out during AFCLI. If $\bar{C}_c$ and $\bar{C}_m$ are average concentrations in the crystallized phase and carbonate magma, respectively then we can write a mass balance equation:

$$C_a M_a + C_m^o M_m^o = \bar{C}_c M_c + \bar{C}_l M_l \qquad (17)$$

Equation (17) can be rewritten as

$$C_a M_a + C_m^o M_m^o = D_c \bar{C}_m M_c + D_l \bar{C}_m M_l \qquad (18)$$

where $\bar{C}_m$ is the time average concentration of the element in the evolving parent magma. Simplifying (18) we get

$$\bar{C}_m = \frac{C_a M_a + C_m^o M_m^o}{D_c M_c + D_l M_l} \qquad (19)$$

Hence,

$$\bar{C}_l = D_l \bar{C}_m = D_l \left[\frac{C_a M_a + C_m^o M_m^o}{D_c M_c + D_l M_l}\right] \qquad (20)$$

$$\text{or, } \bar{C}_l = D_l\left[\frac{aC_a + (1+b-a)C_m^o}{D_c + bD_l}\right] \quad (21)$$

Equation (21) gives the required concentration of the element in the accumulated carbonate melt. Doing similar mass balance for isotopic ratio we get:

$$\bar{E}_l = \bar{E}_m = E_m^0\left(\frac{C_m^o M_m^0}{C_a M_a + C_m^o M_m^o}\right) + \left(\frac{E_a C_a M_a}{C_a M_a + C_m^o M_m^o}\right) \quad (22)$$

Alkaline and carbonate melts get emplaced very rapidly owing to their low viscosity and density, which may lead to a very small amount of contamination/assimilation of wall-rocks in such melts (i.e. $M_a << M_m^o$). In the case of Sr isotopic ratio and concentrations, most of the crustal rocks, which are likely candidates for assimilant have very low concentrations of Sr (i.e. $C_a << C_m^o$). So for Sr systematics, one can safely make the following approximations:

$$\frac{C_m^o M_m^o}{C_a M_a + C_m^o M_m^o} \approx 1 \quad (23)$$

and

$$\frac{E_a C_a M_a}{C_a M_a + C_m^o M_m^o} \approx 0 \quad (24)$$

Hence, equation (22) becomes:

$$\bar{E}_l = \bar{E}_m = E_m^o \quad (25)$$

This essentially means that even if there is a crustal contamination of the parent magma, due to very high content of Sr in this melt, the $^{87}Sr/^{86}Sr$ of the carbonate melt (which is an average of evolving E_m values) formed by liquid immiscibility retains the initial value of the parent magma (i.e. $= E_m^o$).

B. Application of AFCLI model to Amba Dongar Complex

In Amba Dongar, out of all the country rocks only the Precambrian gneiss qualifies to be an assimilant for the parent magma, as other rocks such as sandstone, limestone and basalt are surficial rocks, which probably do not occur at depths, where liquid immiscibility takes place. Hence, considering gneisses ($^{87}Sr/^{86}Sr$ = 0.7690 and Sr = 145 ppm) as an assimilant AFCLI model curves were generated using D_c = 1.8 (assumed, see section 4.2.2a) and D_l = 4.0 (from Green et al., 1992). It was found that the evolution curve with a = 0.05 and b = 0.15 (Fig.4.9) explained the observed alkaline rock trend which suggests that the parent

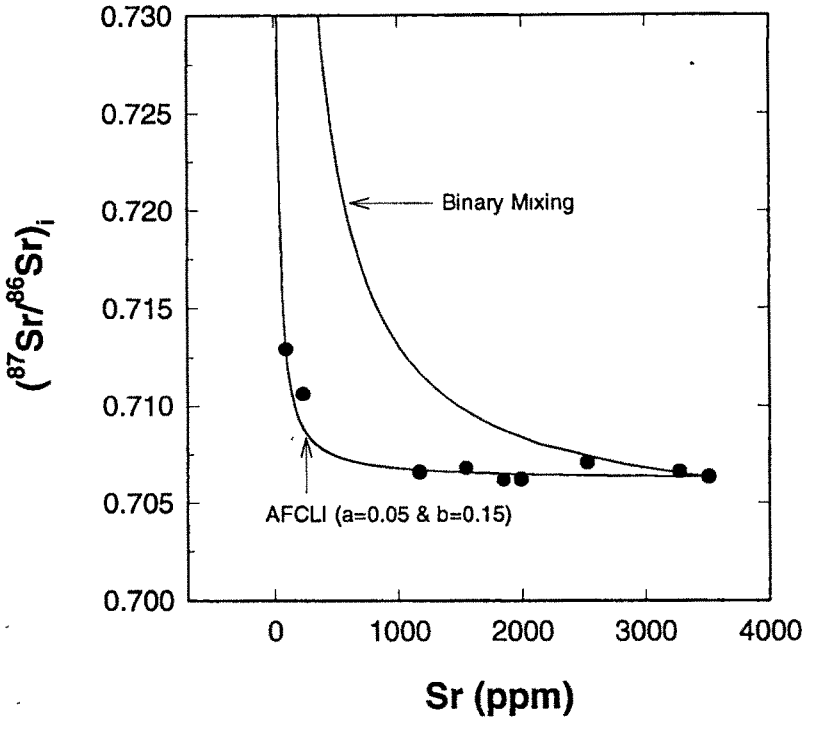

Fig. 4.9. *Plot of initial $^{87}Sr/^{86}Sr$ vs. Sr concentration for alkaline rocks of Amba Dongar complex. Top curve represents results of binary mixing between an alkaline silicate magma and Precambrian gneiss. Bottom curve represents results of AFCLI modelling (see section 4.2.2b.) with a carbonated silicate magma and the gneiss as two end-members at a = 0.05 and b = 0.15. For the model the bulk distribution coefficients for Sr, D_c and D_l are taken to be 1.8 and 4.0, respectively. Please see the caption of Fig. 4.8 and text in section 4.2.2b for discussion.*

magma of this complex have evolved through AFCLI by assimilating ~4% of basement gneisses. In such a case the carbonate magma generated by means of liquid immiscibility will have initial $^{87}Sr/^{86}Sr$ of 0.70632 (same as the parent magma) and Sr concentration of 4306 ppm (calculated using equation (21)). However, the lowest initial $^{87}Sr/^{86}Sr$ of carbonatites of Amba Dongar (Table 4.6) is 0.7055±2. This discrepancy may be due to the lack of data of the most primitive or uncontaminated alkaline rock, which could be used as the magmatic end-member in the AFCLI model.

The Sr isotopic evolution of Amba Dongar alkaline rocks are explained by both the AFC and the AFCLI model. This is because the distribution coefficient of Sr for alkaline rock is assumed to be more than 1.0, which masks the effects of liquid immiscibility in a simple AFC model. If the above distribution coefficient is less than 1.0 then the AFC model cannot explain the observed alkaline rock trend of Amba Dongar complex (Fig.4.5), whereas AFCLI can explain (this is evident in Fig.4.8a). Hence, the AFCLI process is believed to be the most probable magmatic process that have generated the alkaline rocks and carbonatites of Amba Dongar.

4.2.3. Sr Isotopic Evolution of Carbonatites of Amba Dongar

After its removal from the parent magma, carbonate magma rises rapidly within the crust and crystallizes on or close the surface. During its ascent, like the parent magma, it may get contaminated by the wall-rocks. However, because of its rapid ascent and very different composition, carbonate melt may not be able to assimilate silicate wall-rocks but can get contaminated by compositionally similar rocks such as limestones. In Amba Dongar complex, to check for such contamination Sr isotopes were used.

Fig.4.10 shows the binary mixing curve for Amba Dongar limestone ($^{87}Sr/^{86}Sr$) = 0.7087 and Sr = 676 ppm) and carbonatite ($^{87}Sr/^{86}Sr$ = 0.70549 and Sr = 6810 ppm, taken from Simonetti et al., (1995)). The figure 4.10 also shows AFC evolution curves for different D values. As one can see neither the simple binary mixing nor the AFC of limestones explains the observed variations of $^{87}Sr/^{86}Sr$ and Sr concentration in carbonatites. Hence, carbonatites are not contaminated by any of the country rocks. The probable explanation for the Sr concentration variation in carbonatites is the fractional crystallization of the carbonate parent magma. Considering the high errors associated with the $^{87}Sr/^{86}Sr$ measurements in the carbonatites (measured at Physical Research Laboratory, see section 3.4.5 of Chapter-III), the variation in initial $^{87}Sr/^{86}Sr$ is too small to be a result of any magmatic or secondary process.

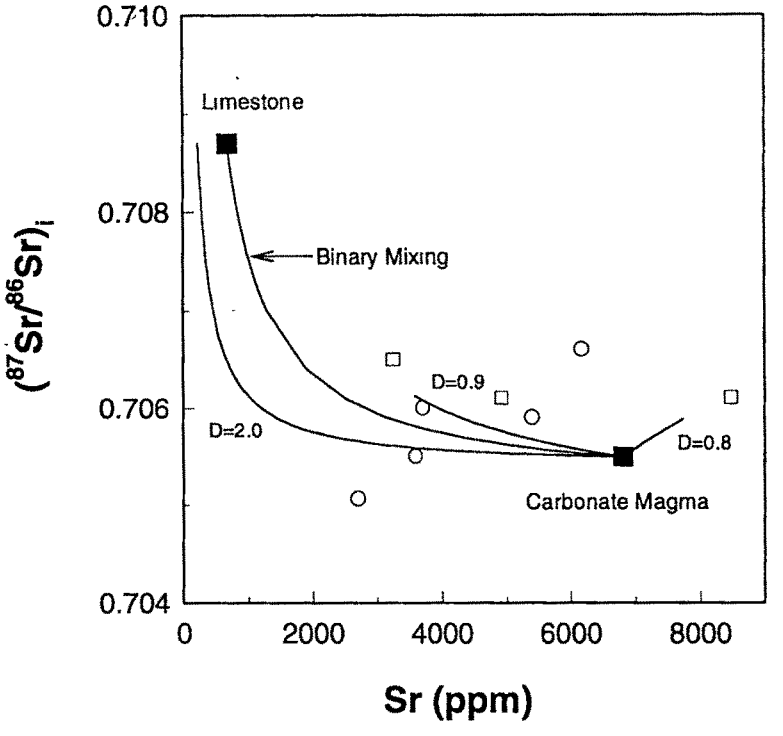

Fig. 4.10. *Plot of initial $^{87}Sr/^{86}Sr$ vs. Sr content for Amba Dongar carbonatites. Open circles = calcite carbonatites,; open squares = ferrocarbonatites. Binary mixing curve represents results of simple binary mixing between carbonate magma and Bagh limestone. Other curves are AFC curves generated with the same end end-members for different values of D (bulk distribution coefficient for Sr between carbonatite and carbonate magma). See section 4.2.3 for discussion.*

4.2.4. Mantle Source Regions

The range of initial strontium isotopic ratios of Amba Dongar carbonatites observed in the present study and those observed by other workers (Deans et al., 1968; Simonetti et al., 1995) overlap with the observed range of Mundwara complex (0.7038 - 0.7055; Rathore et al., 1996). The only available initial Sr ratio from Sarnu-Dandali complex (0.70449; Basu et al., 1993) also falls within the range of Mundwara. This observation probably suggests a similarity in the mantle source regions of these complexes. Although the Sr ratios of Mundwara and Sarnu-Dandali complexes are higher than that of the Reunion-basalts (0.7033 - 0.7044; White et al., 1990), He-isotopic evidence (Basu et al., 1993) suggests a plume origin for these complexes. As the carbonatites and the least contaminated alkaline

rocks from Amba Dongar have similar Sr ratios like those of rocks from Mundwara , I believe that Amba Dongar too was derived from a plume source. The difference in the ratios in the alkaline complexes and the present day basalts from Reunion island can be attributed either to the involvement of enriched subcontinental lithosphere in the generation of these complexes (mixing of plume material with the material from subcontinental lithosphere) or to the complex evolutionary history of the Reunion hotspot (White et al., 1990).

4.2.5. Summary

Strontium isotopic study of Amba Dongar revealed that the silicate rocks and carbonatite of this complex ware generated by liquid immiscibility and the parent magma of this complex was contaminated by the basement gneisses (up to ~4%). The model which gives the above results also suggests that the carbonate melt does not retain any isotopic signature of this contamination process rather retains the isotopic ratio of the primary magma if it does not get contaminated during its later evolution after immiscibility, which is true for Amba Dongar carbonatites. The overlapping of initial strontium isotopic ratios of Amba Dongar, Mundwara and Sarnu-Dandali probably suggests a similarity of their source regions and possibly all these complexes were derived from the Reunion plume.

4.3. TRACE-ELEMENT STUDIES ON AMBA DONGAR COMPLEX

Trace element variations were studied in carbonatites and alkaline rocks of Amba Dongar complex to understand the major magmatic processes involved in the evolution of this complex. The abundances of Zr, Ba, Hf and nine rare earth elements (REE) (La, Ce, Sm, Eu, Gd, Tb, Yb, and Lu) were measured in samples of calcite carbonatites, ferrocarbonatites and alkaline rocks by INAA following the procedures described in Chapter-III.

4.3.1. Results

The REE, Zr, Ba and Hf concentrations of four calcite carbonatites, three ferrocarbonatites and three alkaline rocks are given in Table 4.7. Chondrite normalized REE concentrations are plotted in Fig. 4.11 and chondrite normalized concentrations of some selective trace elements (which also includes Sr concentrations taken from the previous section) are shown

in Fig. 4.12. In both the figures the concentration patterns are grouped according to the rock types. As seen in Fig. 4.11, carbonatites are enriched in lighter REE compared to the alkaline rocks and within carbonatites, ferrocarbonatites are enriched in these elements compared to calcite carbonatites. Heavier REE abundance patterns of both types of carbonatites overlap (Fig. 4.11). Enrichment of other incompatible trace elements also follows the same trend; i.e., ferrocarbonatites > calcite carbonatites > alkaline silicate rocks (Fig. 4.12).

Table 4.7. Trace element abundances in the whole-rock samples from Amba Dongar.

Sample	AD 10	AD 12	AD 17	AD 19	AD 31	AD 36	AD 38	AD 43	AD 45	AD 47
Conc. (ppm)										
Zr	258	448	741	1165	905	472	216	446	683	197
Ba	1736	114630	552	8553	8779	28684	2663	8974	1623	573
La	325	3464	161	2084	1372	5620	356	971	139	34
Ce	581	5528	227	4276	2465	6241	615	1794	264	61
Nd	209	778	69	1583	938	935	215	640	120	25
Sm	26.4	82.2	10.4	180	137.5	95.1	16.4	63.0	18.4	4.6
Eu	7.0	17.0	2.8	42.3	29.5	19.9	7.0	17.1	5.0	1.1
Gd	14.6	61.7	9.5	96.1	110.5	72.7	17.5	51.8	13.4	4.0
Tb	1.6	3.6	1.2	10.2	7.9	5.0	2.1	4.1	1.9	0.6
Yb	3.1	13.1	3.5	10.2	23.2	20.5	4.3	6.9	4.8	2.5
Lu	0.44	0.84	0.51	0.96	1.64	1.2	0.55	0.54	0.65	0.40
Hf	0.25	0.47	10.2	0.64	0.77	0.32	0.34	0.62	9.4	3.0

Note: AD-10, AD-31, AD-38 and AD-43 are calcite carbonatites. AD-12, AD-19 and AD-36 are ferrocarbonatites. AD-17, AD-45 and AD-47 are alkaline rocks.

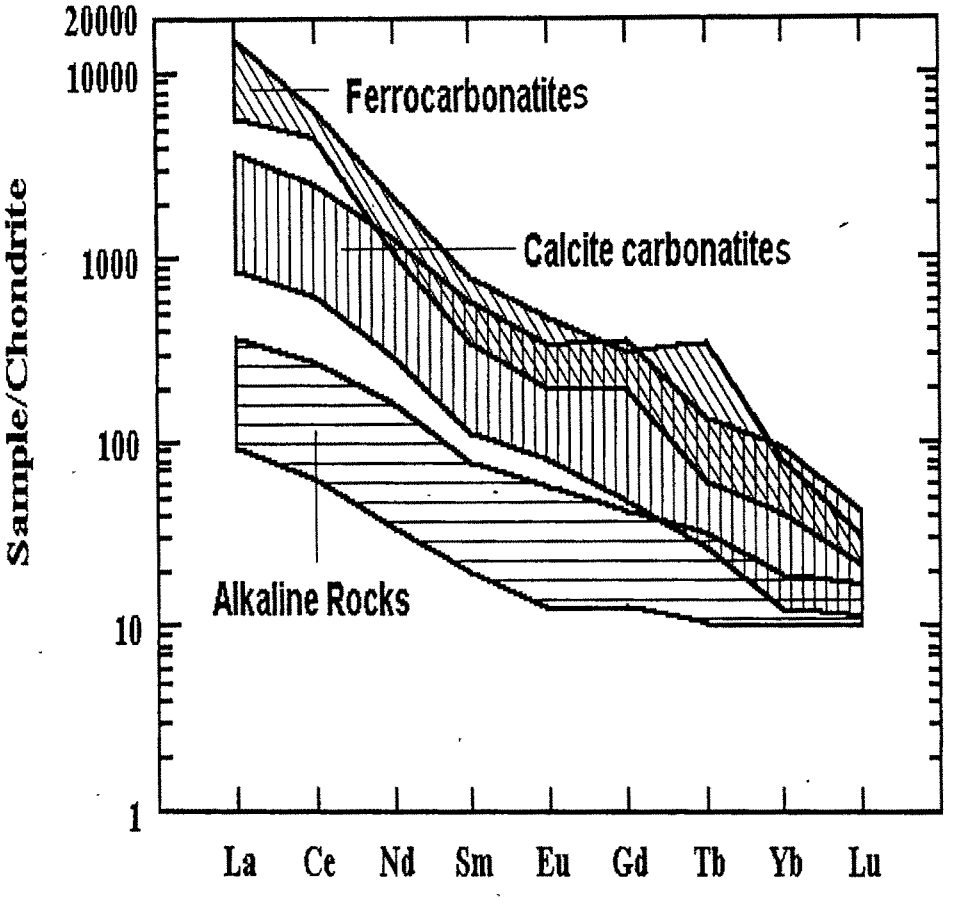

Fig. 4.11. Chondrite normalized concentrations of nine rare earth elements in different lithological units of Amba Dongar complex are shown in groups. Chondrite values are those of Taylor and McLennan (1985).

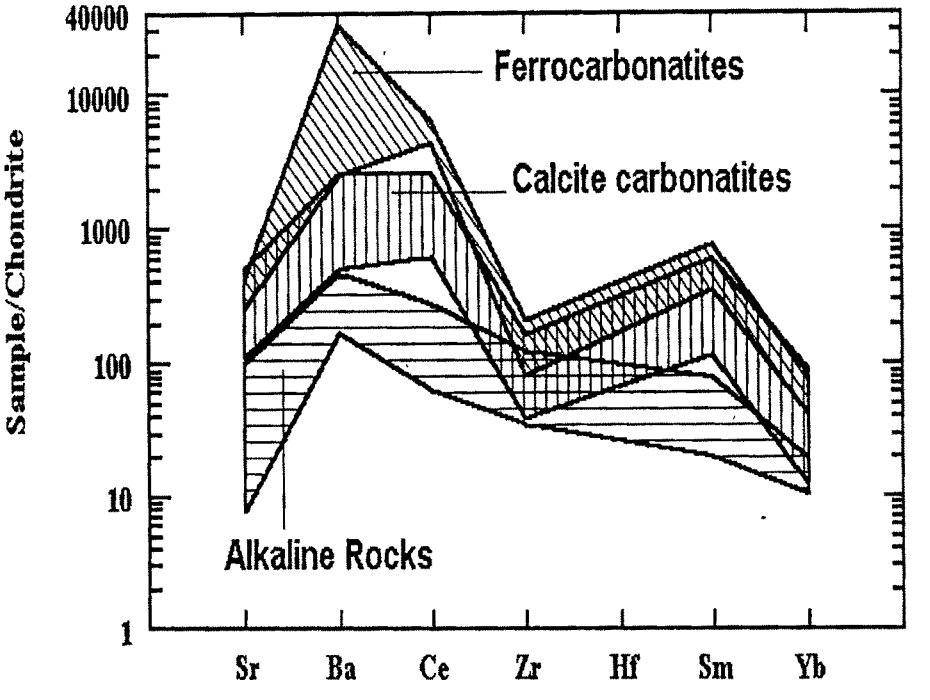

Fig. 4.12. Trace-element abundances in different lithological units of Amba Dongar Complex normalized to Chondrite abundances. Chondrite values are from Taylor and McLennan (1985).

4.3.2. Discussion

Amba Dongar carbonatites, like most of the carbonatites of the world, are highly enriched in LREE, a feature usually attributed to the generation of the parent magma of these rocks by extremely low degree of partial melting of a carbonated peridotite or eclogitic source (Nelson et al., 1988). The higher abundance of these elements in carbonatites compared to the alkaline rocks probably is a result of fractional crystallization or liquid immiscibility process involved in the formation of these rocks. Similarly the higher LREE and Ba content in ferrocarbonatites compared to calcite carbonatites indicates their derivation from a carbonate parent magma at a later stage by fractional crystallization. The negative anomalies of Zr in carbonatites (Fig. 4.12) may be attributed to the early removal of zircon from the parent magma.

The main purpose of the present trace element studies in Amba Dongar complex is to establish whether alkaline silicate rocks and carbonatites of this complex have a common genetic link through liquid immiscibility or not. For this a simple conservative calculation is done assuming that the carbonatites of Amba Dongar have crystallized fractionally from a carbonate magma after its separation from a carbonated silicate parent magma through liquid immiscibility. In a fractional crystallization process concentration of a particular element in the crystallizing solid (C_s) evolves as:

$$C_s = C_o D f^{(D-1)} \quad (26)$$

where C_o is the original concentration in the carbonate magma, D is the rock-magma distribution coefficient of the element under consideration and f is the fraction of remaining parent melt. To find out the concentration of the element in the silicate melt, we need to know C_o. For this, it was assumed that the observed minimum and maximum concentrations of different elements represent the carbonatites formed from the carbonate parent melt at f = 1 and f = 0.001, we get two simultaneous equations for two unknowns C_o and D.

$$C_s^i = C_o D \quad (27)$$

$$C_s^f = C_o D (0.001)^{D-1} \quad (28)$$

where C_s^i and C_s^f stand for minimum and maximum concentration of the element in carbonatites, respectively. Then solving for D and C_o, we get:

$$D = 1 + [\ln(C_s^f / C_s^i)] / [\ln(0.001)] \quad (29)$$

and

$$C_o = C_s^i / D \quad (30)$$

Using equations (29) and (30), the D and C_o values for different rare earth elements (La, Ce, Sm, Eu, Yb and Lu) were calculated. Table 4.8 summarizes these values. As the measured concentrations (C_s^i and C_s^f) have some analytical errors and also the rocks analyzed for this work do not represent the whole carbonatite intrusion, a conservative error of 10 % was assigned to the estimated C_o values. Then using nephelinitic melt-carbonate melt partition coefficients (at 1150° C and 6 Kb) of Hamilton et al. (1989), the expected concentrations in the silicate melt (C_{sm}) were calculated from the relation;

$$C_{sm} = C_o K_d \quad (31)$$

The error in this estimated concentration was calculated using the equation:

$$\sigma_{sm} = C_{sm}\sqrt{(\frac{\sigma_{K_d}}{K_d})^2 + (\frac{\sigma_{C_o}}{C_o})^2} \quad (32)$$

where σ_{K_d} and σ_{C_o} represent the errors in the K_d values and C_o values (10 %), respectively. The estimated concentration with their errors are given in Table 4.9. the chondrite normalized pattern of these estimated concentrations (with their errors) are plotted in Fig. 4.13 (silicate melt-1) and compared with the alkaline rock field. The alkaline rock field of Fig. 4.13 also includes data from Viladkar and Dulski (1986) apart from the data from the present study. The estimated concentration in the carbonate melt (C_o) is also shown in this figure. The estimated concentration field for silicate magma overlaps with the observed field. Similar estimations were made using the carbonate melt-silicate melt partition coefficients given by Wendlandt and Harrison (1979) for Ce and Sm (silicate melt-2 and silicate melt-3 of Fig. 4.13) and it was found that these model melts fell well within the observed alkaline rock field of Amba Dongar. The above observations, though have many limitations which arise from the choice of K_d values and initial melt compositions, suggest that the carbonatites and alkaline rocks of Amba Dongar were derived by liquid immiscibility.

Table 4.8. Modelled Distribution coefficients (Carbonatite-Carbonate Melt) of some REE and their estimated concentrations in the carbonate melt.

Elements	$D_{rock\text{-}melt}$	C_o (ppm)
La	0.59	551
Ce	0.66	880
Sm	0.72	37
Eu	0.74	9.5
Yb	0.71	4.4
Lu	0.81	0.54

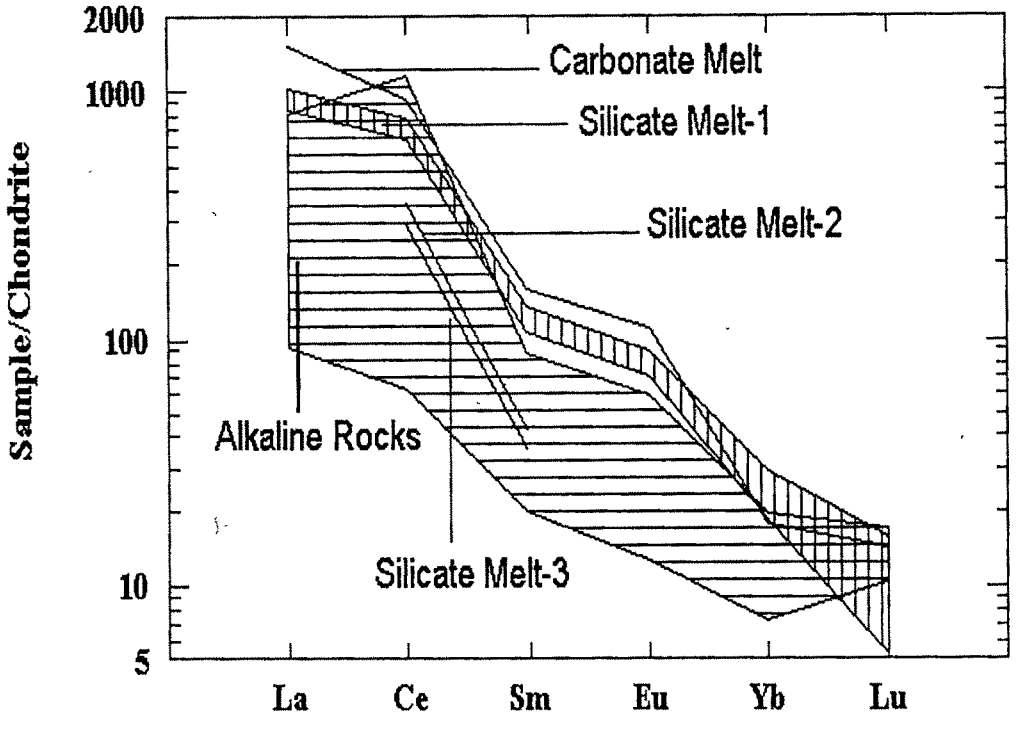

Fig. 4.13. Chondrite normalized REE diagram, illustrating potential silicate parent melts for the Amba Dongar carbonate melt, calculated on the basis of available experimental carbonate melt-silicate melt partition coefficients (K_d values). Silicate melt-1 field is calculated using K_d values from Hamilton et al. (1989). Silicate melt-2 and 3 are calculated using K_d values respectively for 20 kbar & 1200°C and 5 kbar & 1200°C from Wendlandt and Harrison (1979). The alkaline rock field is the observed data, which also includes data from Viladkar & Dulski (1986). See section 4.3.2 for discussion.

Table 4.9. Estimated concentrations of some REE in the silicate melt with their errors.

Elements	C_{SM} (ppm)	1σ (ppm)
La	342	33 5
Ce	678	62 2
Sm	28.5	3.4
Eu	6.9	0 8
Yb	5.9	1 4
Lu	0.4	0.2

SM stands for silicate melt

4.3.3. Summary

The rare earth elemental abundances in different rocks of Amba Dongar complex show an enrichment pattern in the order; alkaline rocks < calcite carbonatites < ferrocarbonatites. Ferrocarbonatites were probably generated from the magma at a later stage by fractional crystallization. Model calculations suggest that the carbonate magma of this complex was derived by liquid immiscibility from the silicate magma.

4.4. STABLE CARBON AND OXYGEN ISOTOPES

Study of stable carbon isotopic variations in carbonatites may provide important clues to the nature of carbon in the mantle, in particular to the carbon isotopic heterogeneity and possibly to the fate of recycled carbon. The combined study of carbon and oxygen isotopes in carbonatites and associated alkaline rocks helps in characterizing their source regions, understanding the processes involved in their formation and the isotopic evolution during and after their emplacement. Stable carbon and oxygen isotopes were analyzed in samples from the three carbonatite-alkaline complexes of Deccan province in order to understand the isotopic evolution of these complexes and to characterize the stable isotopic compositions of their mantle source regions. Before discussing the results of the present work, at this juncture, it will be appropriate to discuss briefly the earlier stable isotopic studies on carbonatites in general.

4.4.1. Stable Carbon and Oxygen Isotopic Variations in Carbonatites: A Brief Review

In one of the earliest stable isotopic studies on carbonatites, Taylor et al. (1967) suggested that the carbon and oxygen isotopic compositions of carbonatites were homogeneous and defined a field (Taylor Box) for carbonatites in a $\delta^{13}C$ versus $\delta^{18}O$ plot (Fig.4.14). But later studies (Pineau et al., 1973; Deines and Gold, 1973; Nelson et al., 1988; Deines, 1989) showed a considerable range of $\delta^{13}C$ and $\delta^{18}O$ compositions

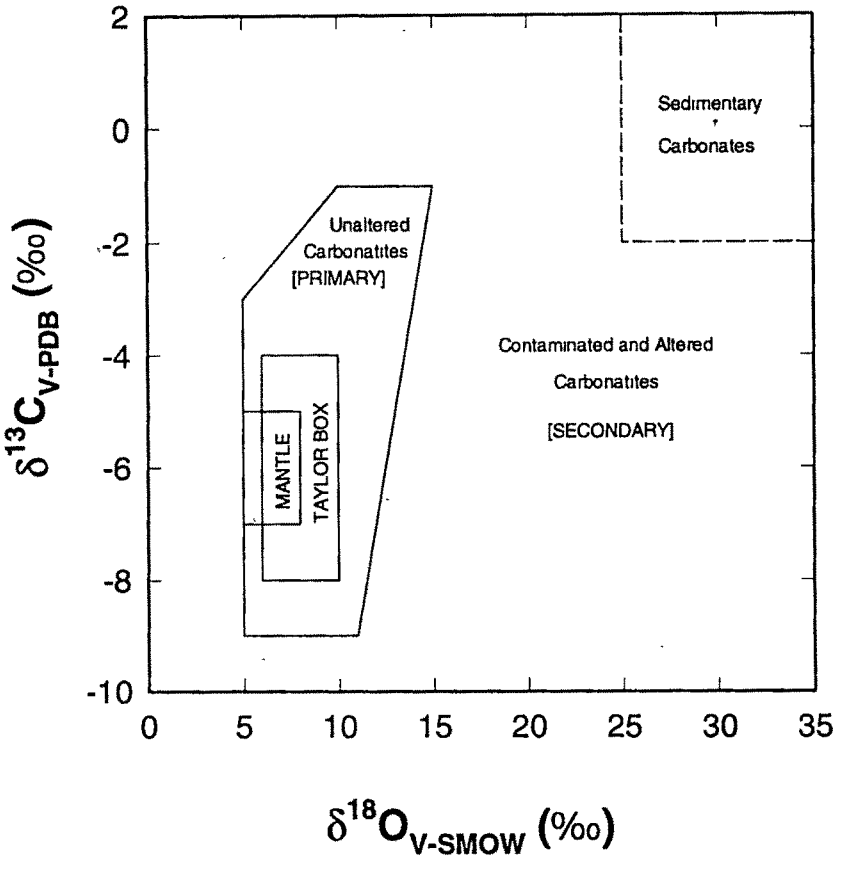

Fig. 4.14. *Plot of $\delta^{13}C$ vs. $\delta^{18}O$ showing different carbonatite and sedimentary carbonate fields. Mantle box is after Nelson et al. (1988), Taylor box represents the primary carbonatites studied by Taylor et al. (1967) and the unaltered (primary) carbonatite field is inferred from studies of Plyusnin et al. (1980) and Deines (1989). Crustally contaminated and altered carbonatites (secondary) plot between the primary carbonatite and the sedimentary carbonate fields.*

which partly overlap with the mantle compositions inferred from studies of mid-oceanic ridge basalts and meteorites. The variations in $\delta^{13}C$ and $\delta^{18}O$ in carbonatites have been interpreted in different ways by earlier workers. Deines and Gold (1973) related these variations to the emplacement levels of carbonatites and suggested that the deep-seated complexes have narrower ranges of isotopic compositions (primary variations) compared to the shallower ones, which they attributed to secondary near-surface processes. Pineau et al. (1973) observed three different groups of $\delta^{13}C$ and

$\delta^{18}O$ variations. The first group showed typical mantle values; the second showed correlated variation of $\delta^{13}C$ and $\delta^{18}O$, which they attributed to Rayleigh fractionation during late stage carbonatite crystallization and the third showed no correlation of $\delta^{13}C$ and $\delta^{18}O$, which was explained by fluid related secondary processes. In another study, Deines (1989) suggested that the correlated variation could be explained by simultaneous crystallization of carbonates and silicates from a parent magma.

In general, carbonatites can be grouped into two: (1) those which are not affected by secondary processes and show either mantle values or some kind of correlated variation of $\delta^{13}C$ and $\delta^{18}O$ (Primary variations) (2) those which show extreme variations, probably as a result of alteration by secondary processes (Secondary variations). Considering $\delta^{13}C$ and $\delta^{18}O$ variations of carbonatites of the world (Plyusnin et al., 1980; Deines 1989), it is possible to define two different fields for the above described groups of carbonatites in a $\delta^{13}C$ versus $\delta^{18}O$ diagram. Group-1 variety (Fig. 4.14) encompasses the fields of mantle rocks (Nelson et al., 1988) and the primary carbonatite field defined by Taylor (1967). Group-2 variety of carbonatites generally fall outside the Group-1 field (Fig.4.14). In order to evaluate the isotopic compositions of the mantle source regions, for a given complex, it is important to distinguish the primary variation (which bears the magmatic signatures) from the secondary.

4.4.1a. Primary Carbonatites

Primary carbonatites, according to the general belief, are purely magmatic and whose $\delta^{13}C$ and $\delta^{18}O$ variations overlap with the mantle values. These are unaltered rocks (belong to Group-1, as defined above), whose isotopic variations are either results of magmatic isotope fractionation processes or reflect the source heterogeneity (Deines,1989). In the following paragraphs, I briefly discuss different models which have been proposed by different workers to explain these variations.

The magmatic processes which are expected to cause $\delta^{13}C$ and $\delta^{18}O$ variations in carbonatites include, extraction of carbonatite melt from the mantle, liquid immiscibility, crustal contamination and fractional crystallization. Deines (1989)

suggested that $\delta^{13}C$ and $\delta^{18}O$ variations in carbonatites could be related partly to the extraction of carbonate melt from a heterogeneous source region. Liquid immiscibility has been suggested as an important process in the formation of carbonatites (Wyllie, 1989; Kjarsgaard and Hamilton, 1989). Mattey et al. (1990) found from experimental studies that the carbon isotopic fractionation between carbonate melt and silicate melt is very small (0.4‰) in the temperature pressure range of 1200-1400°C and 5-30 kbars, which led them to suggest that carbon isotopes do not fractionate during liquid immiscibility. However, such an inference may not be correct, if fractionation of ^{13}C during liquid immiscibility is of Rayleigh type. Isotopic fractionation during liquid immiscibility will be discussed in detail in the next section.

Contamination of carbonate magma by crustal rocks is another magmatic process which can affect their isotopic composition. Carbon being a trace element in most of the crustal rocks, except limestones, contamination of these rocks may not generate large variations in $\delta^{13}C$ composition of carbonatites. $\delta^{18}O$ value of crustal rocks (excluding limestones) are not very different from the carbonatites, hence, contamination effects may not be detected. Contamination due to limestones can generate isotopic compositions which are likely to fall between mantle field and sedimentary carbonate field in a $\delta^{13}C$ vs. $\delta^{18}O$ plot (Fig. 4.14). In such a case it is difficult to extract information about the source regions. Therefore, in such situations it is important to assess the extent of contamination using other isotope systematics (e.g., Sr).

Fractional crystallization of carbonatite from a carbonate melt is another magmatic process which may generate variations in $\delta^{13}C$ and $\delta^{18}O$. Lack of knowledge about the fractionation factors between the minerals and the carbonate melt makes the modelling of isotopic variations during fractional crystallization difficult. With certain assumptions and considering the involvement of magmatic fluids and silicate phases, earlier workers (Pineau et al., 1973; Deines, 1989) modelled the effects of fractional crystallization. Pineau et al. (1973) gave an approximate equation for isotopic fractionation from a two component source and suggested that the late stage calcite (calcite carbonatite) crystallization from a CO_2 enriched, H_2O bearing magmatic fluid

at 700°C could explain the correlated variation of $\delta^{13}C$ and $\delta^{18}O$ in some primary carbonatites. To explain the observed slope (of 0.4) of the $\delta^{13}C$ - $\delta^{18}O$ plot, they restricted the oxygen contribution from H_2O and silicates present in the magma to less than 30%. Later this was challenged by Deines (1989) on the ground of their unrealistic assumption. Deines (1989) proposed a Rayleigh isotopic fractionation model to treat simultaneous fractional crystallization of carbonates and silicates (or carbonate-silicate immiscibility) from a parent melt and suggested that probably such a process could explain the observed slope of $\delta^{13}C$ versus $\delta^{18}O$ plot. However, the model required unrealistic fractionation factors ($\alpha^{18}O$(silicate rock-magma) = 0.9978, which is too low and $\alpha^{13}C$(carbonatite-magma) = 0.9993, which in fact should be more than 1.0) and unrealistic molar ratios of carbon between carbonatite and silicates (=1000, which is too high considering the fact that the volume of carbonatites is much smaller than the volume of silicate rocks in a given complex).

4.4.1b. Altered Carbonatites

Altered carbonatites generally do not fall in the primary carbonatite box of Fig.4.14 because of their higher $\delta^{18}O$ values. These rocks sometimes also show widely different $\delta^{13}C$ values compared to primary carbonatites. Many models have been proposed (Deines, 1989; Santos and Clayton, 1995) to explain these variations. These models propose different fluid related processes as responsible mechanisms for alteration of magmatic isotopic signatures of carbonatites. As fluid activity during and after the carbonatite magmatism is very common in carbonatite complexes (this is evident from the fenitization of host rocks, formation of hydrothermal mineral deposits, presence of alteration products in carbonatites, recrystallization textures and above all the extreme variation of $\delta^{13}C$ and $\delta^{18}O$ of carbonatites and the host rocks affected by fluid activities), it is likely that isotopic compositions of some of the carbonatites are likely to get affected by this.

Fluids can be magmatic, hydrothermal or meteoric water of varying isotopic compositions. The $\delta^{13}C$ variations in altered carbonatites (though smaller compared to $\delta^{18}O$) suggest for a CO_2 bearing aqueous fluid activity being responsible for the isotopic alteration. To understand the effect of such fluid activity on the C and O

isotopic composition of carbonatites, a simple closed system fluid-rock interaction model was developed by Santos and Clayton (1995). However, this model had some flaws in the derivations, which have been rectified in this work (this will be discussed in the section 4.4.3).

4.4.2. Results

The carbon and oxygen isotopic compositions of carbonates from carbonatites, alkaline rocks and metasomatic rocks from Amba Dongar, Mundwara and Sarnu-Dandali complexes were measured following the procedures described in Chapter-III. Isotopic compositions of coexisting calcites and ankerites were measured following the selective CO_2 extraction procedures developed by me (see Section 3.2.2b of Chapter-III). Table 4.10 summarizes the results. $\delta^{13}C$ and $\delta^{18}O$ of calcites of samples from Amba Dongar, Mundwara and Sarnu-Dandali are plotted in Fig.4.15a, b and c, respectively. Some calcite carbonatites of Mundwara and Sarnu-Dandali fall within the mantle box defined by Nelson et al. (1988) (Figures 4.15b and 4.15c). But most of the calcite carbonatites do not show mantle values and have higher $\delta^{13}C$ and $\delta^{18}O$ values compared to those of the mantle. The $\delta^{13}C$ and $\delta^{18}O$ ranges of calcites from different rocks are very similar in all the three complexes. The highest $\delta^{18}O$ values in each complex are observed in calcites from metasomatic rocks and ferrocarbonatites. Calcites from alkaline rocks of Amba Dongar show two groups in a $\delta^{13}C$ vs $\delta^{18}O$ plot (Fig.4.15a).

Table 4.10. Carbon and Oxygen isotopic compositions of samples from carbonatite-alkaline complexes of Deccan Province.

Sample	$\delta^{13}C_{calcite}$ (‰)	$\delta^{18}O_{calcite}$ (‰)	$\delta^{13}C_{ankerite}$ (‰)	$\delta^{18}O_{ankerite}$ (‰)
Amba Dongar				
AD-1	-2.9	7.4		
AD-2/x	-3.3	14.9		
AD-2/y	-3.1	14.3		
AD-3	-3.3	20.8		
AD-4	0.1	10.5		
AD-8	-3.6	6.1		

AD9/2	-2.4	10.9		
AD-10/1x	-4.4	8.6		
AD-10/1y	-4.2	9.2		
AD-10/2x	-3.9	11.1		
AD-10/2y	-4.4	9.6		
AD-12	-4.3	25.8	-1.8	15.2
AD-13/1	-3.7	17.3		
AD-14	-3.8	11.3		
AD-17/1	-6.3	13.9		
AD-18	-5.9	13.0		
AD-19	-2.7	12.1	-4.7	7.3
AD-20	-3.4	15.7		
AD-24	-1.5	29.0		
AD-25	---	---	-4.2	8.6
AD-26	-2.6	29.5		
AD-27	-3.5	8.0		
AD-28	-3.4	28.6		
AD-29	-4.0	18.7		
AD-30	-6.9	22.3		
AD-31	-2.9	12.1		
AD-32	-3.4	10.4		
AD-33	-5.4	27.4	-2.3	13.0
AD-34	---	---	-1.8	16.3
AD-35	-3.3	27.2	-2.7	15.5
AD-38	-4.4	10.2		
AD-39	-3.6	12.7		
AD-40	-3.2	12.1		
AD-41	-3.2	14.7		
AD-43	-1.9	13.0		
AD-44/1	-4.8	18.2		
AD-45	-6.3	10.9		
AD-47	-5.7	10.7		
AD-49	-3.1	9.0		
AD-51	-4.3	15.0		
AD-52	-4.8	13.1		
AD-54	-3.6	11.2		
AD-55	-3.8	27.6	-1.1	18.2
AD-58	-6.7	25.9		

AD-59/1	0.1	10.6
AD-60	-0.1	14.2
AD-62	0.9	24.6
AD-63	-4.2	10.2
AD-64	-4.0	10.5
NS-2	-3.3	12.2
NS-3	-3.5	11.3
NS-20/2	-4.5	9.9
NS-20/O/2	-4.8	9.2
NS-20/O/3	-4.5	10.6
NS-20/O/4	-4.2	10.2
NS-20/6	-4.3	9.6
NS-20/8	-4.6	9.5
NS-20/9	-4.2	10.6
NS-20/10	-3.8	10.2
NS-20/11	-3.8	7.6
NS-20/13	-5.1	9.5
Mundwara		
M-1	-5.2	7.9
M-2	-6.4	6 1
M-3	-3.8	21.6
M-15	-3.7	9.4
M-39	-3.9	10.1
M-40	1.1	16.7
M-121	-1.2	16.2
Sarnu-Dandali		
C-94	-2.7	18.7
C-119	-4.9	9.3
C-142	-2.0	16.7
C-143	-5.4	8.2
C-149	-5.3	25.2
C-177	-1.4	28.2
C-254	-4.4	10.9
C-255	-3.6	16.3
C-290	-5.9	13.9
C-291	-6.1	22.9
A-18	-3.6	24.3
A-161	-1.6	21.2

A-800	-2.1	24.6
A-805	-1.6	25.4
A-807	-1.1	27.5
A-808	-4.5	23.5
A-841	-1.6	17.0

Note: x and y are two different parts of a single whole rock sample (were taken out by drilling). $\delta^{13}C$ is expressed with respect to V-PDB and $\delta^{18}O$ with respect to V-SMOW.

Fig. 4.15a shows carbon and oxygen isotopic composition of calcites from different types of carbonatites and metasomatic rocks from Amba Dongar complex. It was found that the two major variety of calcite carbonatites show two different kind of isotopic variations in Fig.4.15a. The first variety (massive, coarse to medium grained and unaltered calcite carbonatites) shows some kind of correlated variation of $\delta^{13}C$ and $\delta^{18}O$ (open circles in Fig. 4.15a) starting from inside the primary carbonatite box (modified after Taylor, (1967); Keller and Hoefs, (1995)). The second variety of calcite carbonatite (fine grained, brown coloured and altered late stage calcite carbonatite veins) shows higher $\delta^{18}O$ values but similar $\delta^{13}C$ values (open triangles in Fig.4.15a) compared to the first variety. Some of the massive calcite carbonatites, which are found to be altered have also been included with the second variety. The altered nature of calcite carbonatites was detected by the presence of secondary microcrystalline silica, recrystallization texture hematization of magnetites and fluorite mineralization in these. Calcites from metasomatic rocks and ferrocarbonatites clearly plot as a separate group with very high $\delta^{18}O$ (~28 ‰) in Fig. 4.15a. Fig. 4.16 shows the $\delta^{13}C$ and $\delta^{18}O$ values of coexisting calcite and ankerites of ferrocarbonatites from Amba Dongar. In all ferrocarbonatites $\delta^{18}O$ of calcite is substantially higher compared to that of the coexisting ankerite. $\delta^{13}C$ of ankerites are higher compared to calcites as well, except in one case. A hydrothermal vein calcite associated with fluorite deposit was also analyzed; $\delta^{13}C$ and $\delta^{18}O$ compositions were -6.7 ‰ and 25.9 ‰, respectively.

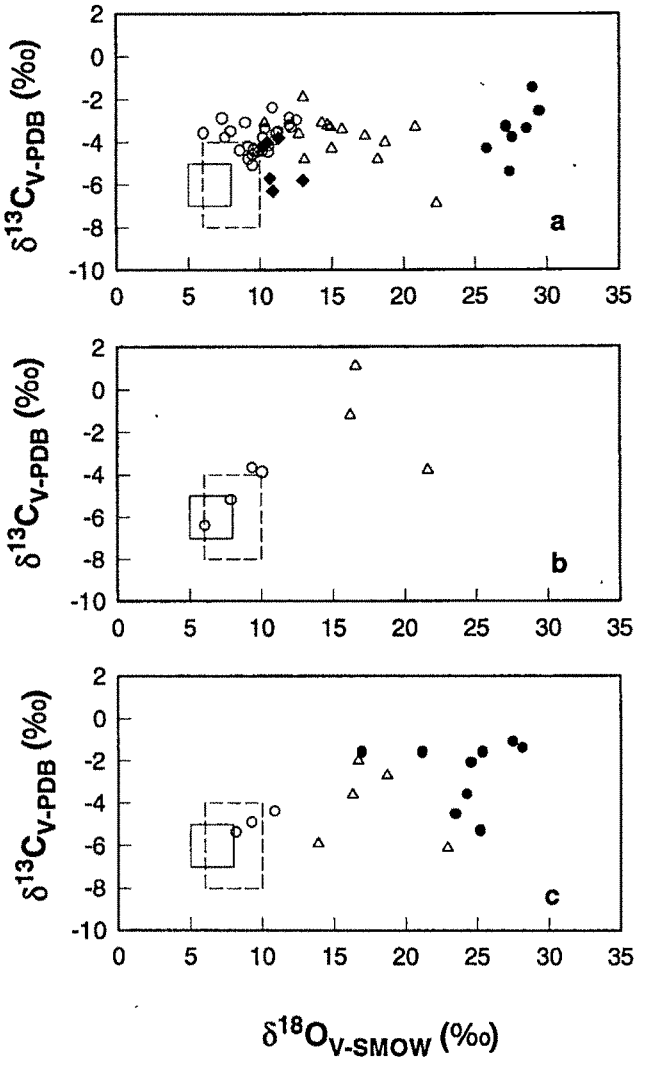

Fig. 4.15. (a) $\delta^{13}C$ and $\delta^{18}O$ compositions of calcite from carbonatites, alkaline rocks and metasomatic rocks of Amba Dongar. (b) $\delta^{13}C$ and $\delta^{18}O$ of calcite from calcite carbonatites of Mundwara. (c) $\delta^{13}C$ and $\delta^{18}O$ of calcite from calcite carbonatites, ferrocarbonatites and metasomatic rocks of Sarnu-Dandali. Symbols: ○ = unaltered calcite carbonatites; △ = altered calcite carbonatites and late stage calcite carbonatite veins; ● = ferrocarbonatites and metasomatic rocks; ◆ = alkaline rocks. The small box with solid outline is the mantle box of Nelson et al. (1988) and the large box with dashed outline is for primary carbonatites (modified after Taylor, 1967 and Keller and Hoefs, 1995).

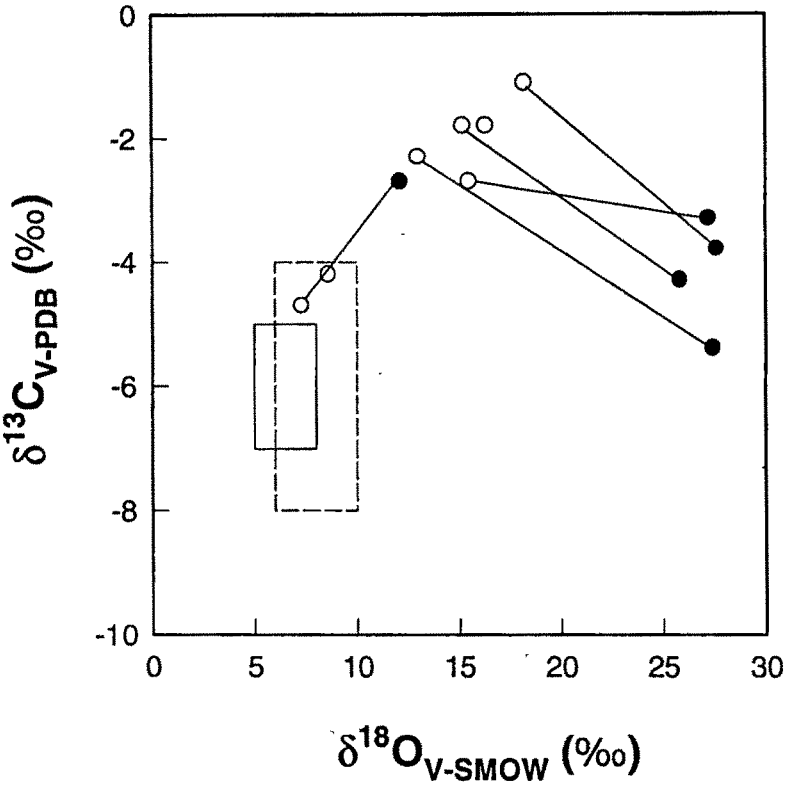

Fig. 4.16. *$\delta^{13}C$ and $\delta^{18}O$ of coexisting calcites (filled circles) and ankerite (open circles) joined by tie lines, from ferrocarbonatites of Amba Dongar. Boxes are mantle box (solid outline) and primary carbonatite box (dashed outline) as defined in Fig. 4.15.*

Calcite carbonatites from Mundwara show the widest range of $\delta^{13}C$ compared to those of calcite carbonatites from other two complexes. $\delta^{13}C$ of calcites from calcite carbonatites varies from -6.4 ‰ to 1.0 ‰ (Fig. 4.15b). Four of these samples show correlated variation of $\delta^{13}C$ and $\delta^{18}O$. Other samples plot away from the mantle and primary carbonatite box with very high $\delta^{18}O$ values.

In Sarnu-Dandali, $\delta^{13}C$ values of calcite from calcite carbonatites vary from -6.1 ‰ to -2.0 ‰, and $\delta^{18}O$ from 8.0 ‰ to 22.9 ‰ (Fig. 4.15c). Three calcite carbonatite samples show correlated variation of $\delta^{13}C$ and $\delta^{18}O$ and all others in this complex, which are found to be altered, show high $\delta^{18}O$ values. Metasomatic rocks and ferrocarbonatites also show higher $\delta^{18}O$ values compared to that of the calcite carbonatites.

4.4.3. Discussion

As described above, the isotopic compositions of calcite carbonatites from all the three complexes clearly form two groups in $\delta^{13}C$ versus $\delta^{18}O$ covariation diagrams (unaltered calcite carbonatites and altered calcite carbonatites). Ferrocarbonatites and metasomatic rocks from all the complexes, generally fall in the altered carbonatite field of such diagrams with very high $\delta^{18}O$ values. The $\delta^{13}C$ and $\delta^{18}O$ of unaltered calcite carbonatites from all three complexes (Fig.4.15) clearly show some kind of correlated variation, which is likely to a be result of one/more magmatic processes involved in the formation of carbonatites. As the limestone-contamination is already ruled out in the case of Amba Dongar (from Sr isotopic study) and there is no limestone in the vicinity of carbonatites in other two complexes, it is unlikely that crustal contamination could have contributed towards the observed isotopic variations in carbonatites in all the three complexes. Hence, the magmatic processes such as liquid immiscibility and fractional crystallization are probably responsible for the $\delta^{13}C$ and $\delta^{18}O$ variation in unaltered calcite carbonatites of the complexes. In the following sub-section (4.4.3a). I discuss the isotopic effects that could be generated by the silicate-carbonate liquid immiscibility. In the sub-section (4.4.3b) the isotopic effects generated by fractional crystallization are modelled and the results of unaltered rocks from the complexes under consideration are interpreted. As discussed in the section 4.4.1, the extreme $\delta^{13}C$ and $\delta^{18}O$ variations (shown by altered calcite carbonatites, calcite from ferrocarbonatites and metasomatic rocks) are probably results of fluid activities in these complexes. In sub-section 4.4.3c a model developed for fluid-rock interaction is given and the observed isotopic variation are interpreted using this model.

4.4.3a. Liquid Immiscibility

It is generally believed that carbonate-silicate immiscibility has insignificant effect on the isotope distributions in these melts (Mattey et al., 1990; Santos and Clayton, 1995). However such an inference is valid only when the immiscibility process is an equilibrium process. It has been suggested that carbonate-silicate liquid immiscibility is a very rapid process (Wyllie, 1989) and after their separation, these two liquids are unlikely to interact (Kjarsgaard and Hamilton, 1989). In such a process the isotopic fractionation is likely to be of Rayleigh type. If the parent magma (PM) is a carbonated silicate magma from which carbonate melt separates out continuously then the carbon isotopic composition in the remaining silicate melt (SM) is be given by

$$\delta^{13}C_{SM} = (1000+\delta^{13}C^{i}_{PM})f^{\alpha-1} - 1000 \quad (33)$$

where f is the fraction of the source melt remaining; and the average carbon composition of the carbonate melt (CM) separated out after the completion of liquid immiscibility is given by

$$(\delta^{13}C_{CM})_{avg} = \frac{\delta^{13}C^{i}_{PM} - f\delta^{13}C_{SM}}{1-f} \quad (34)$$

where α stands for carbon isotope fractionation factor between carbonate melt and silicate melt (=1.0004; Mattey et al., 1990) and $\delta^{13}C^{i}_{PM}$ denotes the initial primary magma composition. With decreasing f, $\delta^{13}C_{SM}$ goes on depleting; however, the accumulated carbonate magma which comes out of the magma chamber upon completion of liquid immiscibility has an average $\delta^{13}C$ composition given by equation (34). The final value of f can be determined independently for a give complex using

$$f = 1/(1+N_{CM}/N_{SM}) \quad (35)$$

where N_{CM}/N_{SM} is the molar ratio of carbon in the carbonate melt (CM) to the silicate melt (SM). In one example, for f = 0.308 (a conservative value) and $\delta^{13}C^{i}_{PM}$ = -5.5‰, we find $\delta^{13}C_{SM}$ = -6‰ and ($\delta^{13}C_{CM})_{avg}$ = -5.3‰. Clearly a Rayleigh carbon isotopic fractionation during liquid immiscibility enhances the $\delta^{13}C$ of the carbonate melt relative to the parent melt. If carbonate melt comes out of the magma chamber in batches during immiscibility, contrary to what is assumed in the above model, then it may generate a series of isotopically heterogeneous melts and which in turn can generate the observed isotopic variations upon crystallization. However, Sr isotopic studies do not support this batch separation (as discussed in Section 4.3, carbonatites

do not show $^{87}Sr/^{86}Sr$ ratio heterogeneity even when the parent magma gets contaminated during liquid immiscibility). A similar evaluation can also be made for oxygen isotopes with the knowledge of oxygen isotope fractionation factor between silicate and carbonate melt.

In summary, liquid immiscibility can only decide the initial isotopic composition of the primary carbonate melt prior to its crystallization, not the variation observed in the ultimate product (i.e. the carbonatites). Hence, the only process which probably can explain the correlated variation observed in unaltered calcite carbonatites is fractional crystallization. In the next section, I discuss a model developed to treat fractional crystallization of carbonatites.

4.4.3b. Fractional Crystallization

To model the isotopic effects generated during fractional crystallization of a carbonate magma Rayleigh isotopic fractionation process was assumed. Carbonatite magmas are rich in CO_2 and H_2O fluids, which are likely to affect the isotopic composition of the rock during crystallization. If calcite represents the crystallizing primary carbonatite (which is mainly calcite carbonatite) then its oxygen isotopic evolution will be controlled by three source components (i.e. melt, CO_2 and H_2O), whereas carbon isotopic evolution will be controlled by two source components (melt and CO_2). To treat isotopic fractionation in such cases where the isotopic evolution of the product depends on multiple source components, a model (called Rayleigh isotopic fractionation from a multicomponent source) was developed. In the following subsection I discuss the model in general and next I apply this model to explain the carbon and oxygen isotopic variations in some primary carbonatites.

A. Rayleigh Isotopic Fractionation from a Multicomponent Source

Here a Rayleigh fractionation equation is derived to evaluate the isotopic evolution of a reservoir which has many discrete components, with distinctly different isotopic ratios, each contributing isotopes of an element to a phase forming and separating out of the reservoir. For this we assume that (a) the different components of the source are in isotopic equilibrium with each other always (i.e., the isotopic composition of the

source reservoir at any time can be expressed as a product of isotopic composition of the most abundant component of the source and a linear combination of the fractionation factors between the rest of the components with the major one), (b) the product that forms is in instant isotopic equilibrium with the source before being removed, (c) the process is isothermal, and (d) the abundance of the heavier isotope is much smaller than that of the lighter isotope of the element under consideration (e.g. $[^{12}C] >> [^{13}C]$).

(i) ***Notations***

n, n_o	Number of atoms of the element under consideration in the whole source reservoir at the time $t > 0$ and at $t = 0$ respectively.
N, N_o	Number of molecules of the i^{th} component of the source at $t > 0$ and at $t = 0$, respectively.
r_{j1}	Ratio of the initial number of moles of the j^{th} component to the 1^{st} component (N_j/N_1). The latter is chosen to be the biggest component so that $r_{j1} \leq 1$ for all j.
L	Total number of components in the reservoir at $t = 0$.
p_i	Number of atoms contributed by the i^{th} source component to the phase(s) formed (e.g. in the case of calcite precipitation from CO_2 and H_2O mixture, CO_2 contributes 2 atoms of oxygen and H_2O, one).
P	A constant for given L; $P = \sum_1^L p_i$
R	Isotopic ratio of the element under consideration; subscripts s, c, i denote the source reservoir, phase formed and the i^{th} source component; o denotes the value at $t = 0$.
α_{ij}	Fractionation factor between the i^{th} and j^{th} component ($=R/R_j$). Note that $\alpha_{ii} = 1$ for all the values of i.
A	Overall fractionation factor between the phase(s) formed and the multicomponent source reservoir ($= R_c / R_s$).
f	Fraction of atoms of the element under consideration left in the source ($= n / n_o$).
f_j	j^{th} critical value of f, when the j^{th} reservoir gets exhausted.
δ	Isotopic composition expressed in permil $[(R / R_{std} - 1) .10^3]$.

Δ Deviation of isotopic composition from its initial value (δ-δ_o).

In addition to these variables g, a and b are defined below.

(ii) ***Equations***

By definition we have

$$n_o = \sum_1^L p_j N_{oj} \tag{36}$$

$$n = \sum_1^L p_j N_j \tag{37}$$

and

$$R_s = \frac{\sum_1^L p_j N_j R_j}{\sum_1^L p_j N_j} \tag{38}$$

Using $\alpha_{j1} = R_j/R_1$ and $f = n/n_o$ we get

$$R_s = \frac{R_1 \sum_1^L p_j N_j \alpha_{j1}}{n_o f} \tag{39}$$

Also, the number of atoms removed from the j^{th} component and the total number of atoms removed from the reservoir are related by

$$p_j N_{oj} - p_j N_j = \frac{p_j}{P} n_o (1-f) \tag{40}$$

Therefore,

$$p_j N_j = \frac{p_j}{P}[n_o f - n_o (1 - \frac{PN_{oj}}{n_o})] \tag{41}$$

or,

$$p_j N_j = \frac{p_j}{P}[n_o f - n_o (1 - \frac{Pr_{j1}}{\sum_1^L p_i r_{i1}})] \tag{42}$$

By defining f_j, the j^{th} critical value of f, when the j^{th} source component exhausts (i.e., $N_j = 0$). This is given by (from equation 42):

$$f_j = 1 - \frac{Pr_{j1}}{\sum_1^L p_i r_{i1}} \tag{43}$$

Defining

$$a = \frac{1}{P} \sum_1^L p_j \alpha_{j1} \tag{44}$$

and

$$b = \frac{1}{P}\sum_{1}^{L} p_j \alpha_{j1} f_j \qquad (45)$$

And using equations (41) to (45) in (39) we obtain

$$R_s = R_1 (a - \frac{b}{f}) \qquad (46)$$

The physical significance of the variables a and b is that they are weighted mean values of the equilibrium fractionation factors between the different source components and the major (first) component. In the case of a, the weights are the numbers of atoms of the element under consideration contributed by various source components. In the case of b, besides this, the weight factor includes the critical values of f (i.e., the values of f when each of the source component exhausts).

Treating the mixed reservoir as a single unit, the Rayleigh fractionation equation in differential form can be written as:

$$\frac{dR_s}{R_s} = (A - 1)\frac{df}{f} \qquad (47)$$

where

$$A = \frac{R_c}{R_s} = \frac{\alpha_{c1}}{(a - b/f)} \qquad (48)$$

using (46).

Hence,

$$A - 1 = \frac{(\alpha_{c1} - a + b/f)}{(a - b/f)} \qquad (49)$$

Defining $g = \alpha_{c1}$-a, we have

$$\frac{dR_s}{R_s} = (\frac{g + b/f}{a - b/f})\frac{df}{f} \qquad (50)$$

or

$$\frac{dR_s}{R_s} = g(\frac{df}{af - b}) + b(\frac{df}{af^2 - bf}) \qquad (51)$$

Expanding the second term into partial fractions we obtain,

$$\frac{dR_s}{R_s} = (\frac{g}{a})[\frac{d(af - b)}{(af - b)}] + [\frac{d(af - b)}{(af - b)}] - [\frac{df}{f}] \qquad (52)$$

Integrating and applying the initial condition that at f= 1, $R_s = R_{os}$, we get

$$\ln(\frac{R_s}{R_{os}}) = (\frac{g}{a} + 1)\ln[\frac{d(af-b)}{(af-b)}] - \ln f \tag{53}$$

$\ln(R/R_{os})$ can be approximated to $(\delta-\delta_o)10^{-3}$ for small values of δ.

Therefore,

$$(\delta - \delta_o) = 10^3(\frac{\alpha_{c1}}{a})\ln(\frac{af-b}{a-b}) - \ln f \tag{54}$$

Equation (54) describes the isotopic evolution of the multicomponent source reservoir. As the product and the source are related by A (eq. 48) the isotopic composition of the product as a function of f will be:

$$(\delta - \delta_o)_{product} = (\frac{\alpha_{c1}}{a-b/f})\delta_{source} - (\frac{\alpha_{c1}}{a-b})(\delta_o)_{source} + 10^3[(\frac{\alpha_{c1}}{a-b/f}) - (\frac{\alpha_{c1}}{a-b})] \tag{55}$$

I now show that equation (54) can be reduced to a single component Rayleigh equation ($P = p_1$ and $\alpha_{11} = 1$; $r_{11} = 1$ and $r_{21} = 0$; $f_1 = 0$). Now, $a = 1$ and $b = 0$; therefore, $\delta-\delta_o = 10^3\ (\alpha_{c1}-1)\ln(f)$. In the case of initial molar quantities of different source components being equal (i.e., $N_1 = N_2 = N_3 \ldots N_L$), r_{j1} is unity for all value of j (=1 to L) and $f_j = 0$ for all j. From (45) we see that $b = 0$ and (54) reduces to $(\delta-\delta_o) = 10^3\ [(\alpha_{c1}/a) - 1]\ln(f)$, similar to the equation for a single component case, but with an effective fractionation factor given by (α_{c1}/a). For a two component case (calcite precipitation: $Ca^{2+} + CO_2 + H_2O \rightarrow CaCO_3 + 2H^+$) Pineau et al. (1973) had derived an approximate equation:

$$\delta - \delta_o = 10^3\{[(\alpha_{c1}-1) - \frac{(\alpha_{21}-1)}{3}]\ln f + \frac{2}{3}[(\frac{1-r_{21}}{2+r_{21}})(\alpha_{21}-1)(1-\frac{1}{f})]\} \tag{56}$$

where the subscripts c, 1 and 2 denote $CaCO_3$, CO_2 and H_2O, respectively. Under some approximations, the above described multicomponent Rayleigh equation (54) reduces to this equation. This can be readily seen by doing the integration (52) with an approximated value of A in equation (48): $A \sim (\alpha_{c1}/a)(1+b/f) \sim (\alpha_{c1}/a)+(b/f)$, as both α_{c1} and a are close to unity. Therefore, equation (51) becomes:

$$\frac{dR_s}{R_s} = (\frac{\alpha_{c1}}{a} - 1)\frac{df}{f} + b(\frac{df}{f^2}) \tag{57}$$

and the solution yields:

$$\delta - \delta_o = 10^3[(\frac{\alpha_{c1}}{a} - 1)\ln f + b(1-\frac{1}{f}) \tag{58}$$

For the two component case, $a = (1/3)(2+\alpha_{21})$ from (44) , $b = (1/3)(2f_1+\alpha_{21}f_2)$ from (45) and $f_1 = 1-[3/(2+r_{21})]$; $f_2 = 1-[3r_21/(2+r_{21})]$. Hence $b = (2/3)(2f_1+\alpha_{21}f_2)[(1-r_{21})/(2+r_{21})]$. Again $[(\alpha_{c1}/a)-1]$ can be approximated to be $(\alpha_{c1}-1)$ as a~1. Using this, and the relation for b in (57), I obtain Pineau et al's approximate equation (56).

However, when the initial molar quantities of different source components are different, the least of them will get exhausted first (this is why we chose index 1 for the largest source component). This happens when $f = f_j$, the j^{th} critical value of f when j^{th} source component gets exhausted. Subsequent isotopic evolution of the system can be still obtained from equation (54) by redefining P, a, b for the remaining L-1 components, δ_o taken as the δ value of the reservoir at the point when $f = f_j$, and replacing f by f/f_j . Similar calculations can be made as more and more components get exhausted. Finally, when all but the largest reservoir get exhausted, the isotopic evolution will be given by: $(\delta'-\delta_o) = 10^3(\alpha_{c1}-1) \ln f'$, where δ' is the δ value of the source at the point when L-1 reservoirs got exhausted, and $f' = f / f_{L-1}$. The above arguments show that there will be L-1 discontinuities in the δ versus f plot.

The above described model is a closed system generalized model which treats Rayleigh isotopic fractionation from a multicomponent source. This model can be applied to many geological processes like calcite precipitation from a fluid, hydrothermal graphite formation, metamorphic decarbonation, serpentinization etc., to understand the isotopic evolution of the source during such processes. In the present work, only the application of this model to the formation of carbonatites is discussed.

(iii) *Primary carbonatites*

Unaltered carbonatites whose carbon and oxygen isotopic composition is considered to be primary are generally calcite carbonatites. In calcite carbonatites it is the calcite which is the major mineral. Hence, isotopic composition of calcite can be treated as that of the calcite carbonatite. Probably the C and O isotopic fractionation behaviours of a carbonate melt and calcite are very similar (Deines, 1989), hence, it is safe to assume the fractionation factors of C and O between calcite and the carbonate melt as unity. Which means that the crystallization of calcite from a pure carbonate melt may

not cause any isotopic fractionation. However, if calcite crystallizes in equilibrium with the associated magmatic fluids then fractionation will occur. It is known that carbonate magmas carry a large amount of CO_2-H_2O fluids along with them. If calcite fractionally crystallizes from such a melt-fluid system then its formation reaction will probably be:

$$Ca^{2+} + CO_2 + H_2O \rightarrow CaCO_3 + 2H^+$$

as proposed by Pineau et al. (1973). Isotopically, CO_2 is the only source of carbon for calcite, while oxygen is contributed by CO_2 and H_2O. So the carbon isotopic evolution will follow a single component Rayleigh fractionation process, whereas, that of oxygen will follow a two component Rayleigh process.

Carbon isotopic evolution of the source and carbonatite then will be given by :

$$\delta^{13}C_s = (1000+\delta^{13}C_s^1)f_c^{(\alpha^c-1)} - 1000 \quad (59)$$

and

$$\delta^{13}C_{cal} = \alpha^c(1000+\delta^{13}C_s^1)f_c^{(\alpha^c-1)} - 1000 \quad (60)$$

where α^c is the fractionation factor of carbon between calcite and CO_2, f_c is the fraction of remaining carbon in the source and $\delta^{13}C_s^1$ is the initial carbon isotopic composition of the source. For oxygen isotope evolution of the source and the carbonatite, the multicomponent Rayleigh fractionation model for a two component case was used. In such a case oxygen isotopic evolution equation for calcite of carbonatite derived from (55), will be :

$$\delta^{18}O_{cal} = 10^3\left(\frac{\alpha_{c1}^o}{a-b/f_o} - 1\right) + \left(\frac{\alpha_{c1}^o}{a-b/f_o}\right)\delta^{18}O_s \quad (61)$$

where α_{c1}^o is the fractionation factor of oxygen between calcite and the largest source component. f_o is the fraction of remaining oxygen in the reservoir. a, b and $\delta^{18}O_s$ are to be determined from equations (44), (45) and (54) respectively. To determine these parameters we need the values of p_j, s, P, α_{j1}, r_{i1} and f_j. In this calcite crystallization process, $p_1 = 2$, $p_2 = 1$, $P = 3$, α_{j1} is either $\alpha_{H_2O-CO_2}$ or $\alpha_{CO_2-H_2O}$ depending on which one of the two source components is the largest. f_j value, the j^{th} critical value of f_o, will depend on the smallest component. r_{i1} is the initial molar ratio of the i^{th} source component and the major (or first) source component. Here I discuss the isotopic

evolution of the source and calcite in two different cases: (I) when CO_2 is the largest source component, (II) H_2O is the largest source component.

Case-I

First I consider a case when CO_2 is the largest source component. Hence, subscript 1 will be used for CO_2 and 2 for H_2O. The initial molar ratio r_{11} is r_{21} (i.e. H_2O/CO_2). The value of f_o at which H_2O will be completely used up in the calcite formation is given by:

$$f_{H_2O} = 1 - \frac{3r_{21}}{2 + r_{21}} \tag{62}$$

The other parameters are :

$$a = \frac{1}{3}(2 + \alpha_{21}) \tag{63}$$

$$b = \frac{2}{3}(\alpha_{21} - 1)\left(\frac{1 - r_{21}}{2 + r_{21}}\right) \tag{64}$$

To calculate $\delta^{13}C$ and $\delta^{18}O$ of calcite at the same time of formation, I relate f_c and f_o by:

$$f_c = \left(\frac{1 - r_{21}}{3}\right) + f_o\left(\frac{2 + r_{21}}{3}\right) \tag{65}$$

The carbon and oxygen isotope composition of the source can then be calculated putting the values of above parameters for appropriate r_{21} values in equations (56) and (54), respectively. Fig. 4.17 shows the evolution of ($\delta^{18}O$-$\delta^{18}O_o$) of the source as a function of f_o for different r_{21} values and Fig. 4.18 shows the covariation of ($\delta^{13}C$-$\delta^{13}C_o$) and ($\delta^{18}O$-$\delta^{18}O_o$) of the source for different r_{21} values. The end of each evolution curve marks the exhaustion of the smallest source component (i.e., H_2O). Similarly the carbon and oxygen isotope composition of the calcite can be found out from equations (60) and (61), respectively as a function of fraction of remaining source. Fig. 4.19a shows isotopic evolution curves of calcite, in a $\delta^{13}C$ vs. $\delta^{18}O$ space, for different r_{21} values. In this example the temperature of calcite formation is taken to be 700°C and the initial source $\delta^{13}C$ and $\delta^{18}O$ values are -5.5 ‰ and 8.5 ‰, respectively. Here the fractionation factors used are taken from Ritchet et al. (1977) and Chacko et al. (1991).

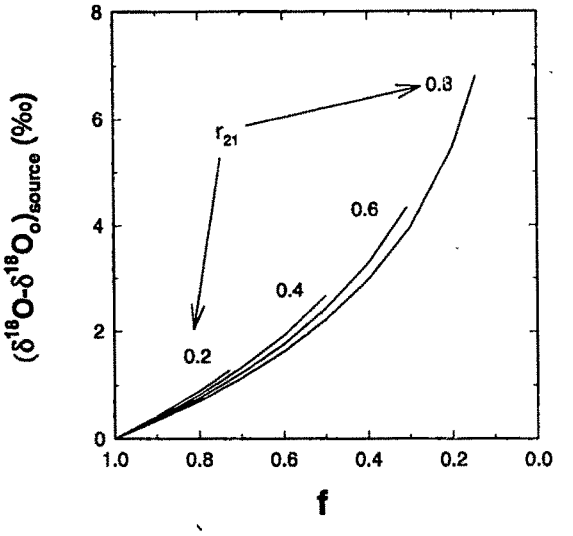

Fig. 4.17. *Oxygen isotopic evolution curves of a two component source (CO_2+H_2O), relative to the initial source composition, from which calcite is fractionally crystallizing as a function of f (fraction of remaining oxygen atoms in the source) for different r_{21} (initial molar ratio of H_2O to CO_2) values. End of each curve marks the exhaustion of H_2O reservoir (Case-I of the multicomponent Rayleigh fractionation model for carbonatites). See section 4.4.3b for discussion.*

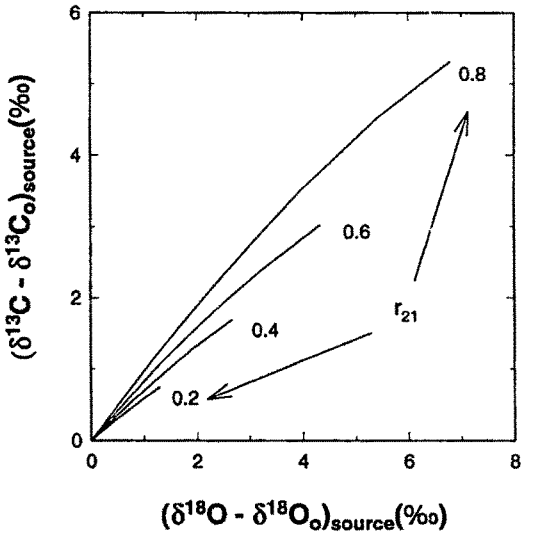

Fig. 4.18. *Covariation of oxygen and carbon isotopic compositions of the source relative to the initial values in the same cases as in Fig. 4.17.*

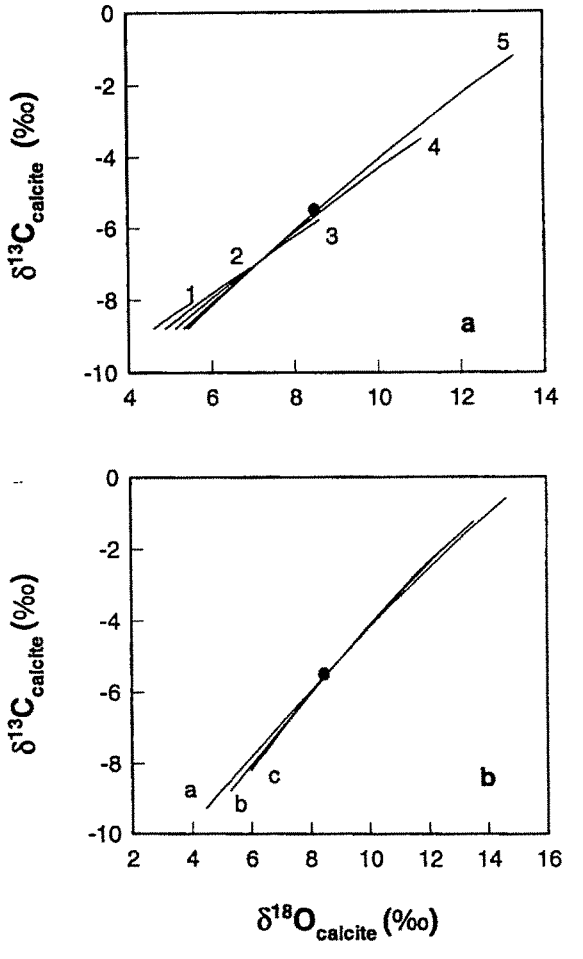

Fig. 4.19 (a) Plot of $\delta^{13}C$ vs. $\delta^{18}O$ showing isotopic evolution curves for the calcite (at 700°C) generated by the multicomponent Rayleigh fractionation model in Case-I (CO_2 is the largest source component). Filled circle represents the initial composition of the carbonate magma. Curves 1 to 5 are for r_{2l} values of 0.2, 0.4, 0.6, 0.8 and 0.9, respectively. (b) Isotopic evolution curves for calcite at r_{2l} = 0.95 at three different temperatures a = 500°C, b = 700°C and c = 900°C. Filled circles = initial magma. See section 4.4.3b (Case-I) for discussion.

The most striking feature of isotopic evolution curves (Fig. 4.19a) is that at the beginning of crystallization, isotopic compositions of calcite are lower than those of the initial source and then as the crystallization proceeds calcite becomes more and

more enriched and its isotopic compositions become higher than the initial source. Model calculations also showed that the slope of the isotopic evolution curves is not very sensitive to the temperature variation (Fig. 4.19b), however, it is sensitive to r_{21} values (Fig. 4.19a.). In fact, a particular range of variation of $\delta^{13}C$ and $\delta^{18}O$ of calcite can be explained by fractional crystallization at different temperatures. Hence, the isotopic evolution of fractionally crystallizing calcites in such a case is mainly controlled by the initial source compositions and the initial molar ratio of H_2O to CO_2.

Case-II

In the second case, I consider H_2O to be the largest source component. Then subscript 1 will be used for H_2O and 2 for CO_2 in all the equations. Here the value of f_o at which CO_2 finished is:

$$f_{CO_2} = (1 - r_{21}) / (1 + 2r_{21}) \tag{66}$$

and other parameter are:

$$a = 1 + \frac{2}{3}(\alpha_{21} - 1) \tag{67}$$

$$b = \frac{2}{3}(\alpha_{21} - 1)\left(\frac{1 - r_{21}}{1 + 2r_{21}}\right) \tag{68}$$

f_o and f_c are related by

$$f_c = \frac{1}{3}\left(1 - \frac{1}{r_{21}}\right) + \frac{1}{3}\left(2 + \frac{1}{r_{21}}\right) f_o \tag{69}$$

Using these parameters, $\delta^{13}C$ and $\delta^{18}O$ values at different f_o were calculated from equations (60) and (61), respectively for similar source compositions as used in Case-I. Fig. 4.20 shows the isotopic evolution curves at 700°C for different r_{21} values. Calculations were done up to $f_c = 0.001$ and at these points $f_o > f_{critical}$ ($=f_{CO_2}$). That is why the end points of all evolution curves have same $\delta^{13}C$ value. In this example the effect of change in r_{21} is much larger on the slope of the evolution curve compared to the Case-I. However, the variation in $\delta^{18}O$ generated by the model, here, is much smaller than what is observed when CO_2 is the largest source component (Case-I).

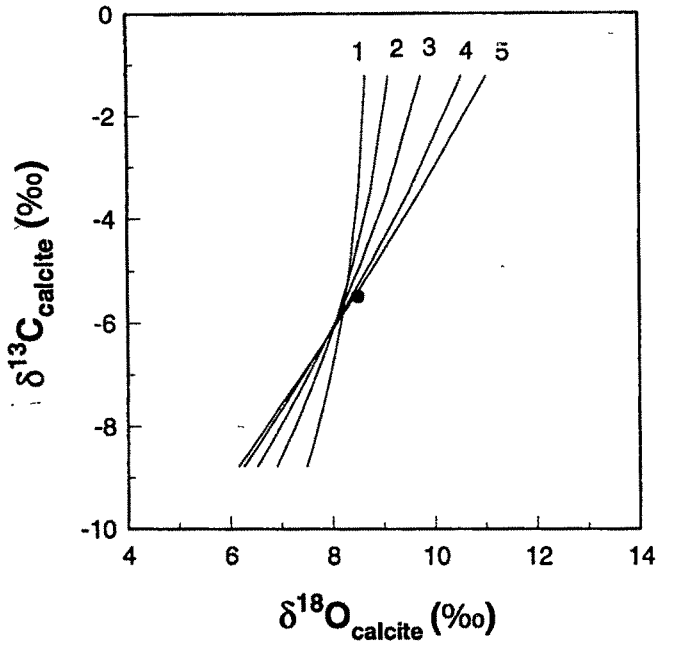

Fig. 4.20. *Plot of $\delta^{13}C$ vs. $\delta^{18}O$ showing isotopic evolution curves for calcite generated by Case-II (H_2O is the largest source component) of the multicomponent Rayleigh fractionation model at 700°C. Different curves (numbered) are for different r_{21} values (same as in Fig. 4.19a). Filled circle = initial magma. Here the calculations are done up to f_c (fraction of remaining carbon in the source) of 0.001. See section 4.4.3b (Case-II) for discussion.*

The above proposed multicomponent Rayleigh fractionation model probably can explain the $\delta^{13}C$ and $\delta^{18}O$ variations observed in primary carbonatites of different complexes of the world. It has been observed in many complexes that the observed correlated variation of $\delta^{13}C$ and $\delta^{18}O$, if fitted with straight lines give slopes whose values are less than 1 (Pineau et al., 1973; Deines, 1989). This can be explained if we consider Case-I of our model as slopes of evolution curves in this case are less than 1. It has been suggested that CO_2 is probably the major fluid associated with primary carbonate magmas (Kjarsgaard and Hamilton, 1989), which again supports the isotopic evolution of carbonatites following Case-I. If water were considered to be the major fluid component in the primary magma, then also Case-I of the model can be applied if

it is assumed that most of this water rich fluids go out of the magma as fenitizing fluids before the crystallization starts making the remaining fluid CO_2 enriched.

Primary carbonatites (mainly calcite carbonatites) also contain other minerals like magnetite, apatite, phlogopite, fluorite and other silicates and oxides. Although abundance of these minerals is very small compared to calcite, their crystallization may affect the oxygen isotope composition of the source magma. However, non-availability of fractionation factors between these minerals and melt creates difficulty in evaluating the exact isotopic effects. Using Chiba et al. (1989)'s fractionation factor for calcite-magnetite and calcite-water (Friedman and O'Neil, 1977) fractionation factors, it was found that fractional crystallization (Rayleigh type) enriches the $\delta^{18}O$ (by ~1‰) of the melt. The crystallization of apatite probably depletes the $\delta^{18}O$ of the melt at magmatic temperatures [this was found out assuming that $\alpha^{18}O$ (apatite-water) = $\alpha^{18}O$ (calcite-water)]. In all these calculations it was assumed that the carbonate melt and calcite have similar oxygen fractionation properties. Hence, in our model curves a range of ±1‰ in initial $\delta^{18}O$ composition of the source can be considered to accommodate the possible variation from crystallization of minerals other than calcite.

B. Unaltered Calcite Carbonatites from Carbonatite complexes of Deccan Province

(i) *Amba Dongar Complex*

Very coarse to medium grained unaltered calcite carbonatites of Amba Dongar show correlated variation of $\delta^{13}C$ and $\delta^{18}O$ values (Fig.4.15a). It was found that there are two such correlation trends, separated by at least 3‰ in $\delta^{18}O$. From field relations, it was found that the group having lower $\delta^{18}O$ values (Group-II) are relatively finer grained calcite carbonatites (alvikites of Viladkar, 1981) and these intrude into the coarse grained variety, which have higher $\delta^{18}O$ values (Group-I). The study Sr isotopes in these rocks and limestones (Section 4.2) revealed that these rocks were not contaminated by limestones. Hence, the observed slope of $\delta^{13}C$- $\delta^{18}O$ plot cannot be due to contamination from country rocks (limestones). As discussed earlier this kind of isotopic variation is a result of fractional crystallization and can be explained by Rayleigh fractionation from a CO_2 rich fluid-magma system (Case-I of the

multicomponent Rayleigh fractionation model). In such a case the $\delta^{13}C$ and $\delta^{18}O$ evolution of the calcite (of calcite carbonatite) can be calculated using equations (60) and (61), respectively, with proper substitution of the parameters a and b (equations 63 and 64). However, to apply this model, we need the initial $\delta^{13}C$ and $\delta^{18}O$ values of the parent carbonate magma. These can be assumed in different ways so that the model evolution curves fit the observed data. However, there is an independent way of estimating these for Amba Dongar complex, particularly the initial $\delta^{13}C$ value, with the help of liquid immiscibility model described in the section 4.4.3a, which is discussed in the following paragraph.

Many of the alkaline rocks of Amba Dongar contains calcite as an accessory phase. Calcites from unaltered alkaline rocks show two groups in $\delta^{13}C$ vs $\delta^{18}O$ plot (Fig.4.15a), which probably indicate that there are two different generations of alkaline rocks, though mineralogically these two groups are not very different. The average $\delta^{13}C$ of Group-I is -6‰, while of Group-II is -4‰. Assuming that these two groups were derived from two isotopically different primary carbonated silicate magmas by liquid immiscibility, the $\delta^{13}C$ compositions of corresponding two carbonate magmas were determined using equation (34) of section 4.4.3a. For this calculation the value of the fraction of remaining carbon in the source is taken as 0.238 [equation (35)], which is derived using carbon atom ratio in carbonatite to silicate rocks of 3.2 (in Amba Dongar, calcite carbonatites comprise 20% of the complex and average carbonate amount in these is 90%, while silicates have around 7% carbonate in them). The calculations yielded two different initial $\delta^{13}C$ compositions for two different carbonate magmas, one having $\delta^{13}C$ of -5.3‰ and the other -3.2‰. It is likely that these two isotopically different carbonate magmas have crystallized to give the two groups of calcite carbonatites observed in this complex. As the fractionation factor for oxygen between carbonate melt and silicate melt is not known, it is not possible to evaluate the $\delta^{18}O$ composition of the carbonate magma using liquid immiscibility model. However, it can be assumed to be in the range of 7 ‰ to 9 ‰, 2 ‰ enriched than the mantle peridotites (Deines, 1989). Using the above initial values of $\delta^{13}C$ and $\delta^{18}O$, the model calculations were done and it was found that the model curve at 800°C crystallization temperature and r_{21} value (initial H_2O/CO_2) of 0.9 explained the observed enrichment

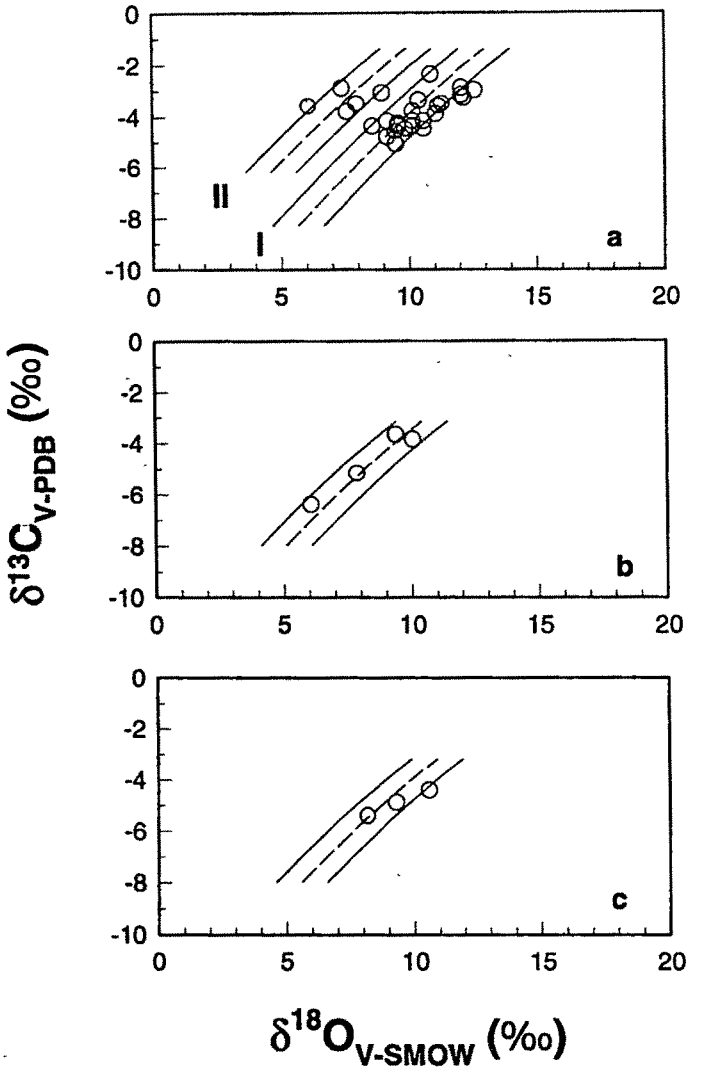

Fig. 4.21. *Observed data (open circles) for unaltered calcite carbonatites and two component Rayleigh fractionation model curves (dashed) for Amba Dongar (a), Mundwara (b) and Sarnu-Dandali (c). The solid curves represent model curves, which encompasses the ±1 ‰ variation of the initial $\delta^{18}O$ of the magma. In Fig. 4.21a, I and II represent the two groups of calcite carbonatites from Amba Dongar. See section 4.4.3b (B) for discussion.*

trend of Group-I calcite carbonatites when the initial $\delta^{18}O$ of magma was 8.5 ‰ (Fig.4.21a). However, the entire variation of $\delta^{13}C$ and $\delta^{18}O$ of these rocks could be explained by the model curves when the initial $\delta^{18}O$ of the carbonate magma varied from 7.5 ‰ to 9.5 ‰. This ±1 ‰ variation in initial $\delta^{18}O$ takes care of other factors,

particularly the crystallization of accessory minerals, which affect only the $\delta^{18}O$ of the crystallizing carbonate magma. Similar calculations for Group-II showed (Fig.4.21a) that their isotopic variations could be explained by their crystallization from a carbonate magma having r_{21} value of 0.8 and a smaller $\delta^{18}O$ initial value of 7.5 ‰. The two component Rayleigh fractionation model also generates $\delta^{13}C$ and $\delta^{18}O$ values which are beyond the range of observed values. Most likely, the rocks falling in the lower range of values are present below the present level of erosion and these were crystallized at an early stage. Similarly, the model generated values which fall in a higher range than the observed values either have been altered by secondary processes or the rocks which had them have been eroded out. In summary, uncontaminated and unaltered calcite carbonatites of Amba Dongar were found to have crystallized from two isotopically different primary carbonate melts (with $\delta^{13}C$ values of -5.3 ‰ and -3.2 ‰) which were enriched in CO_2 compared to H_2O.

It is usually believed that the carbon isotopic composition of a primary carbonate melt reflects its mantle source composition. The initial $\delta^{13}C$ of the primary melt of Group-I calcite carbonatites (-5.3 ‰) falls within the mantle $\delta^{13}C$ range suggested by Nelson et al. (1988), whereas the initial $\delta^{13}C$ of primary melt for Group-II calcite carbonatites (-3.2 ‰) is higher by at least 1.8 ‰ than the highest $\delta^{13}C$ values suggested for an average mantle (i.e. -5 ‰) (Nelson et al., 1988). This carbon isotopic enrichment in Group-II melt could be due to its generation from an isotopically different source than Group-I which essentially means that the source region of Amba Dongar complex was isotopically heterogeneous. However, it is difficult to explain the generation of compositionally similar magmas of a given complex from different source regions. But, if such a process was possible in Amba Dongar then the $\delta^{13}C$ enrichment of the source region for Group-II calcite carbonatites probably reflects mixing its juvenile carbon ($\delta^{13}C$ = -5 ‰) with the enriched recycled crustal carbon ($\delta^{13}C$ = 0-2 ‰) (Nelson et al., 1988). This means that the Group-II calcite carbonatites of Amba Dongar bear signatures of recycled crustal carbon. Alternatively, the $\delta^{13}C$ enrichment of the primary melt of Group-II can as well be explained by its removal from Group-I melt some time late in the crystallization history and subsequent mixing with water rich magmatic fluids of lower $\delta^{18}O$. We propose this late stage mixing with magmatic water in order

to maintain the required H_2O/CO_2 ratio of the magma for fractional crystallization and to bring down the $\delta^{18}O$ value from ≥10 ‰ to 7.5 ‰. However, such a mechanism does not explain the presence of the Group-II variety of alkaline rocks in this complex. Hence, the most appropriate explanation for the ^{13}C enrichment of Group-II melt is the incorporation of recycled carbon, which probably can be attributed to the metasomatic fluid activity in the source region.

Mundwara Complex

The unaltered calcite carbonatites of Mundwara also showed correlated $\delta^{13}C$ and $\delta^{18}O$ variations (Fig. 4.15b). Application of the two component Rayleigh fractionation model revealed that these rocks ere crystallized at 800°C from a primary carbonate magma whose initial $\delta^{13}C$ and $\delta^{18}O$ were -5 ‰ and 8 ‰, respectively and H_2O/CO_2 ratio in the magma was 0.8 (Fig.4.21b). Like Amba Dongar, here also we needed ±1 ‰ variation of initial $\delta^{18}O$ variation to explain the entire observed values (Fig. 4.21b), which suggests that the crystallization minerals other than carbonates had affected the $\delta^{13}C$ and $\delta^{18}O$ evolution of these rocks.

Sarnu-Dandali Complex

Like other two complexes, unaltered calcite carbonatites of Sarnu-Dandali also showed correlated $\delta^{13}C$ and $\delta^{18}O$ variation (Fig. 4.15c) indicating the involvement of fractional crystallization in their formation. We applied the two component Rayleigh model and found that the fractional crystallization of calcite at 800°C from a magma having H_2O/CO_2 ratio of 0.8 and initial values of $\delta^{13}C$ and $\delta^{18}O$, -5 ‰ and 8.5 ‰, respectively, could explain the observed variation (Fig. 4.21c).

In summary, the primary carbonate melts of all the three completed show average mantle $\delta^{13}C$ compositions and $\delta^{18}O$ compositions in the range of 7-9 ‰. These isotopic compositions are consistent with their origin from the mantle (Nelson et al., 1988 and Deines, 1989). The enrichment trend shown by the unaltered calcite carbonatites from these complexes in $\delta^{13}C$ vs $\delta^{18}O$ plot are interpreted here as product of fractional crystallization of these rocks from CO_2 rich carbonate melts. A two

component Rayleigh fractionation model successfully explains the correlated variation of $\delta^{13}C$ and $\delta^{18}O$ of these calcite carbonatites.

4.4.3c. A Fluid-Rock Interaction Model to Explain Secondary Isotopic Effects

A. The Model

To explain the $\delta^{13}C$ and $\delta^{18}O$ variations in altered rocks (altered calcite carbonatites, ferrocarbonatites and metasomatic rocks) a fluid-rock interaction model was developed by modifying an earlier model proposed by Santos and Clayton (1995). In a closed system condition the fluid-rock isotopic exchange of carbon and oxygen can be written as following to simple mass balance equations:

$$F_c\delta^{13}C^i_{fluid} + R_c\delta^{13}C^i_{rock} = F_c\delta^{13}C^f_{fluid} + R_c\delta^{13}C^f_{rock} \quad (70)$$

$$F_o\delta^{18}O^i_{fluid} + R_o\delta^{18}O^i_{rock} = F_o\delta^{18}O^f_{fluid} + R_o\delta^{18}O^f_{rock} \quad (71)$$

where F_c and F_o are amounts of carbon and oxygen, respectively; in the fluid expressed in moles. R_c and R_o are those for the rock. Superscripts i and f stand for initial and final, respectively. From these two equations final rock compositions can be found out. The relations for the final rock compositions are:

$$\delta^{13}C^f_{rock} = \frac{(F_c/R_c)(\delta^{13}C^i_{fluid} + \Delta^c_{rock-fluid}) + \delta^{13}C^i_{rock}}{1+(F_c/R_c)} \quad (72)$$

$$\delta^{18}O^f_{rock} = \frac{(F_o/R_o)(\delta^{18}O^i_{fluid} + \Delta^o_{rock-fluid}) + \delta^{18}O^i_{rock}}{1+(F_o/R_o)} \quad (73)$$

where $\Delta^c_{rock\text{-}fluid}$ and $\Delta^o_{rock\text{-}fluid}$ stand for the isotopic fractionation of oxygen and carbon, respectively, between rock and fluid. As the fluids are CO_2 containing aqueous fluids, the oxygen fractionation between the rock (i.e., calcite) and the fluid will depend on CO_2/H_2O ratio in the fluid. Defining r as the molar ratio of CO_2 to H_2O in the fluid, it was found the relation for $\Delta^o_{rock\text{-}fluid}$:

$$\Delta^o_{rock-fluid} = 10^3 \ln\alpha^{18}O_{cal-CO_2} + 10^3 \ln(1+2r) - 10^3(2r + \alpha^{18}O_{H2O-CO2}) \quad (74)$$

where $\alpha^{18}O_{cal\text{-}CO2}$ and $\alpha^{18}O_{H2O\text{-}CO2}$ are oxygen fractionation factors between calcite and CO_2 and H_2O and CO_2 respectively. For a covariance ($\delta^{13}C$-$\delta^{18}O$) plot, we require values corresponding to same time of formation/interaction. Therefore we relate F_o/R_o and F_c/R_c as:

$$F_o/R_o = [(2r+1)/3r][F_c/R_c] \quad (75)$$

Hence, in the final form the fluid-rock interaction equations are:

$$\delta^{13}C^{f}_{rock} = \frac{(F_c / R_c)(\delta^{13}C^{i}_{fluid} + \Delta^{c}_{rock-fluid}) + \delta^{13}C^{i}_{rock}}{1 + (F_c / R_c)} \quad (76)$$

$$\delta^{18}O^{f}_{rock} = \frac{(\frac{2r+1}{3r})(F_c / R_c)(\delta^{18}O^{i}_{fluid} + \Delta^{o}_{rock-fluid}) + \delta^{18}O^{i}_{rock}}{1 + (\frac{2r+1}{3r})(F_o / R_o)} \quad (77)$$

The value of $\Delta^{o}_{rock-fluid}$ is substituted from equation (74).

This model again is a simple closed system fluid-rock interaction model which assumes that the isotopic behaviour of CO_2-H_2O fluid is the same as a separate mixture of CO_2 and H_2O and it does not consider the isotopic effects generated by other carbon bearing species (like H_2CO_3, CO_3^{2-} and HCO_3^-) which are likely to be present in such fluids. However, such a simple model is reasonably a good model to interpret the extreme variations of $\delta^{13}C$ and $\delta^{18}O$ in altered carbonatites.

Fig. 4.22a illustrates the model and shows the evolution of the isotopic compositions of calcite with initial $\delta^{13}C$ and $\delta^{18}O$ values -6 ‰ and 6 ‰, respectively, which interacts with a fluid having similar initial compositions and CO_2/H_2O ratio of 0.001. Fig. 4.22b shows similar evolution when calcite interacts with a fluid having CO_2/H_2O ratio of 10. The calculations are done for F_c/R_c values ranging from 0 to infinity and temperatures varying from 100°C to 400°C. Fractionation factors are taken from Ritchet et al. (1977) and Chacko et al. (1991). It can be seen in these two figures that, CO_2 rich fluids do not generate very high enrichment in $\delta^{18}O$. Hence, to get extreme enrichments in $\delta^{18}O$, the interacting fluids have to be H_2O rich. This effect of CO_2/H_2O ratio of the fluid on the isotopic evolution is clearly demonstrated in Fig. 4.23. Physically the F_c/R_c characterizes the extent of fluid-rock interaction (e.g., $F_c/R_c = \infty$ implies that the fluid has completely altered the rock).

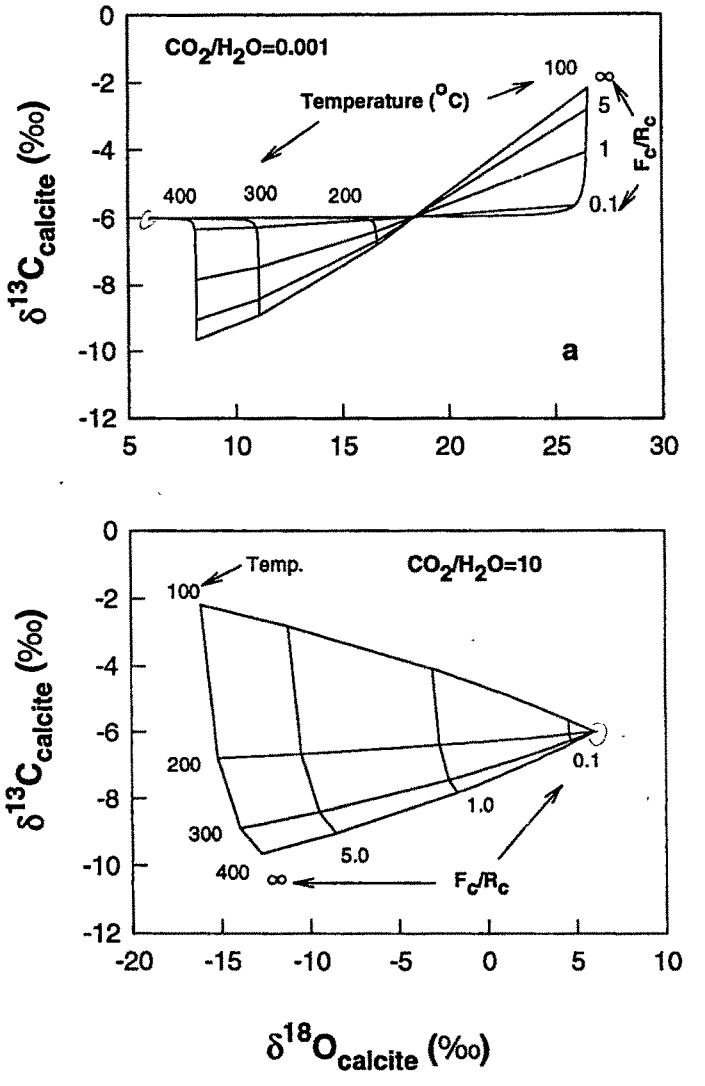

Fig. 4.22. *(a) Evolution of carbon and oxygen isotopic compositions of calcite (initial $\delta^{13}C$ = -6 ‰ and $\delta^{18}O$ = 6 ‰) which interacts with a H_2O-CO_2 fluid (initial $\delta^{13}C$ = -6 ‰ and $\delta^{18}O$ = 6 ‰) having CO_2/H_2O = 0.001. The fluid/rock ratios (F_c/R_c) varies from 1 to infinity and temperature from 100°C to 400°C. (b) In this figure the fluid CO_2/H_2O ratio is 10, whereas other parameters are same as in (a).*

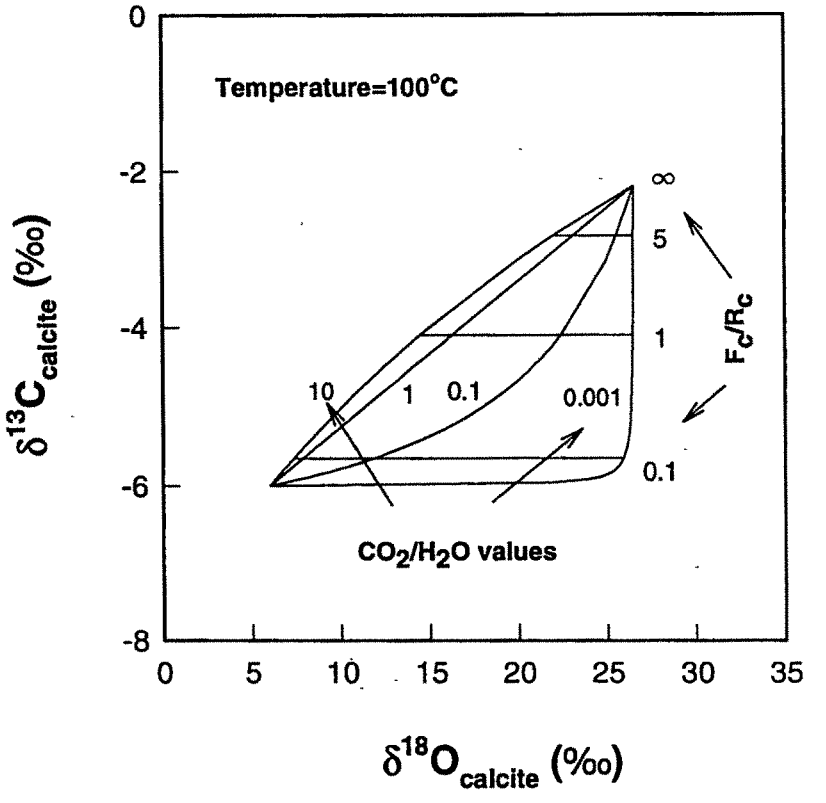

Fig. 4.23. Evolution of carbon and oxygen isotopic compositions of the same calcite as in Fig. 4.22 through fluid-rock interaction at a constant temperature of 100°C and varying fluid CO_2/H_2O ratio from 0.001 to 10. Fluid initial compositions are same as in Fig. 4.22.

B. Altered Rocks from Carbonatite Complexes of Deccan Province

$\delta^{13}C$ and $\delta^{18}O$ compositions of calcites of altered carbonatites and metasomatic rocks from all the three complexes show extreme variations and they neither plot in the mantle box nor show any kind of correlation as observed in the case of unaltered calcite carbonatites. As discussed earlier such isotopic variation is a result of secondary processes, particularly those related to post-crystallization fluid activities. In the following discussion, I explain the observed isotopic variations in these rocks using the fluid-rock interaction model described above.

(i) ***Amba Dongar Complex***

The altered calcite carbonatites, late stage calcite carbonatite veins, calcites from ferrocarbonatites and metasomatic rocks from Amba Dongar show wide range of $\delta^{13}C$ and $\delta^{18}O$ values (Fig.4.15a). As Amba Dongar is a shallow seated complex, one would expect a lot of fluid action in this complex. In addition to its shallow emplacement level, the carbonatites of this complex hosts a massive fluorite deposit which is known to be a hydrothermal deposit (Simonetti and Bell, 1995). This suggests that a large scale fluid activity took place in this complex after the carbonatite emplacement and probably this was responsible for wide spread alteration observed. The carbon isotopic variations in altered carbonatites indicate that the fluids which were responsible for the alteration were CO_2 bearing aqueous fluids. Fluid inclusion study of Roedder (1973) also suggests similar post magmatic fluid activity in this complex.

To understand the nature of alteration and the kind of fluids involved in the alteration process, the fluid-rock interaction model was applied. For the model calculations, the initial $\delta^{13}C$ and $\delta^{18}O$ compositions of the calcite carbonatites were taken to be -2.5 ‰ and 12 ‰, respectively (representative of a late stage calcite carbonatite) and for ferrocarbonatites and metasomatic rocks the initial values of $\delta^{13}C$ = -2 ‰ and $\delta^{18}O$ = 13 ‰ were taken. Three different initial fluid compositions were considered for the model (1) $\delta^{13}C$ = -7.7 ‰ and $\delta^{18}O$ = 10.7 ‰ (a hydrothermal fluid, whose compositions were derived using those of the hydrothermally precipitated pure calcites associated with fluorite deposits and assuming an equilibrium precipitation of these calcites from the fluid at 150°C), (2) $\delta^{13}C$ = -4 ‰ and $\delta^{18}O$ = 0 ‰ (a meteoric fluid), and (3) $\delta^{13}C$ = -6 ‰ and $\delta^{18}O$ = 7 ‰ (a pure magmatic fluid). Model calculations were done for fluid CO_2/H_2O ratio of 0.001 and 0.1. Figures 4.24, 4.25 and 4.26 show the model calculations with the observed data for altered calcite carbonatites and late stage calcite carbonatite veins, while figures 4.27, 4.28 and 4.29 are for ferrocarbonatite and metasomatic rocks. It was found that the variations in calcite carbonatites could either be explained by interaction with the hydrothermal fluid (Fig. 4.24) or with the magmatic fluid (Fig. 4.26), but ferrocarbonatites and metasomatic rocks show alteration by the hydrothermal fluid alone (Fig. 4.27a) and have not been affected by magmatic waters like calcite carbonatites (Fig. 4.29).

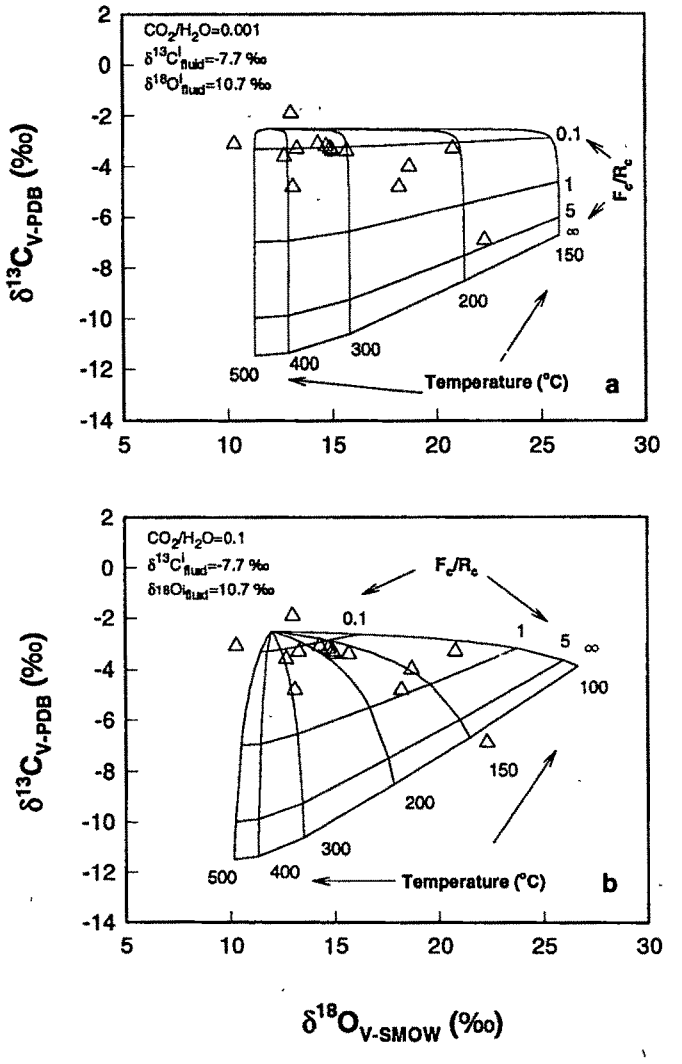

Fig. 4.24. Comparison of $\delta^{13}C$ and $\delta^{18}O$ values of altered calcite carbonatites from Amba Dongar with the fluid-rock interaction model curves for two different conditions (a) CO_2/H_2O of the fluid = 0.001 and (b) CO_2/H_2O of fluid = 0.1, for a hydrothermal fluid having initial $\delta^{13}C$ and $\delta^{18}O$ of -7.7‰ and 10.7‰, respectively. The initial values for the rock: $\delta^{13}C$ = -2.5‰ and $\delta^{18}O$ = 12.0‰.

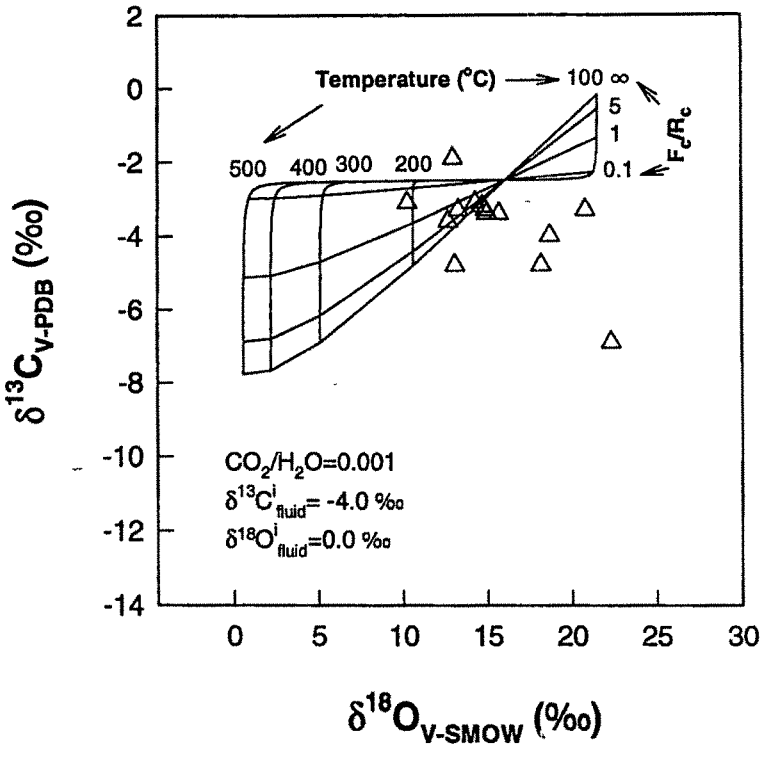

Fig. 4.25. *Comparison of observed data of Amba Dongar altered calcite carbonatites with a fluid-rock interaction model curves when the fluid has* $\delta^{13}C^i$ *= -4‰,* $\delta^{18}O^i$ *= 0‰ (meteoric-hydrothermal) and* CO_2/H_2O *= 0.001.*

None of the rocks seemed to have been affected by meteoric water alteration (Figs. 4.25 and 4.28). It was also found that the fluids having CO_2/H_2O ratio of 0.001 and 0.1 both could explain the variation in case of calcite carbonatites at temperatures between 100 and 400°C (Fig. 4.24a and b) whereas ferrocarbonatites and metasomatic rocks seemed to have interacted with fluid having CO_2/H_2O ratio of 0.001 at lower temperatures between 100 and 200°C (Fig. 4.27a). In summary, it is inferred that the isotopic composition of some calcite carbonatites (massive and veins) of Amba Dongar have been affected by a magmatic fluid and a hydrothermal fluid (which was responsible for fluorite mineralization) at different temperatures, whereas ferrocarbonatites and metasomatic rocks show alteration at lower temperature by the fluorite mineralizing hydrothermal fluid. However, it should be noted that the observed

isotopic variation may not be a result of one stage interaction process rather it could be a result of superimposed alteration effects generated by interaction of different fluids having different isotopic compositions and CO_2/H_2O ratios at different temperatures.

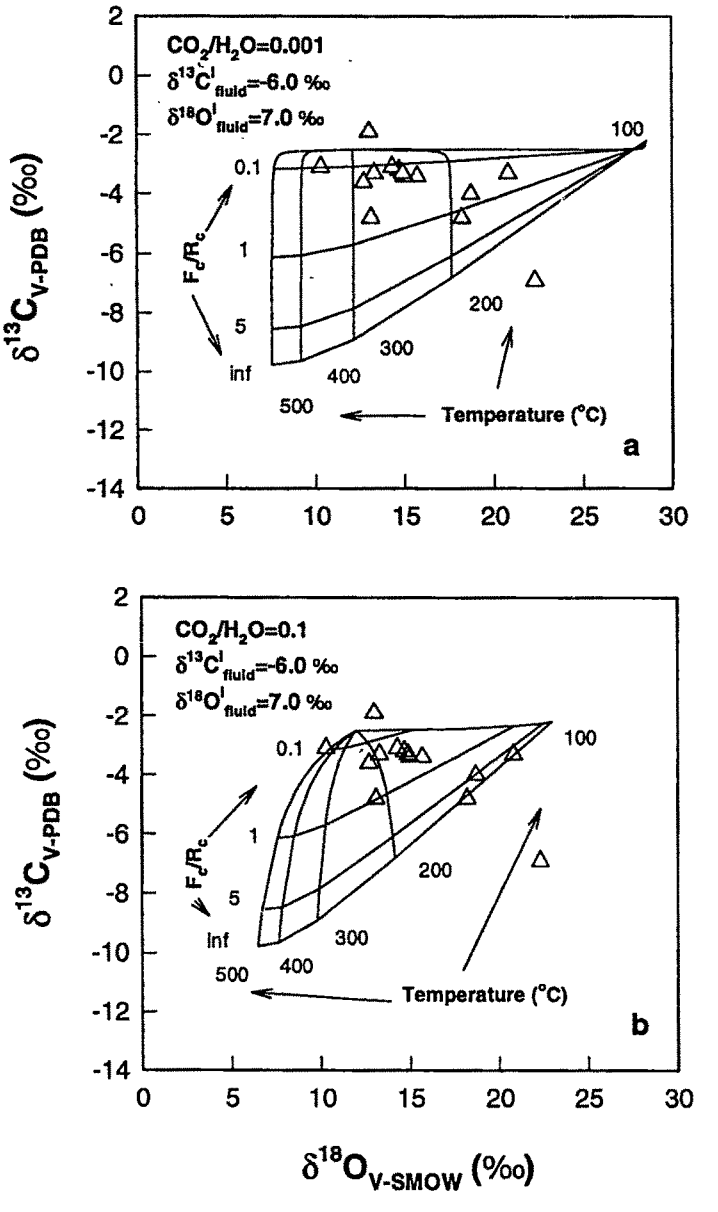

Fig. 4.26. Comparison of $\delta^{13}C$ and $\delta^{18}O$ values of altered calcite carbonatites from Amba Dongar with fluid-rock interaction model curves when the fluid is a magmatic fluid with (a) CO_2/H_2O = 0.001 and (b) CO_2/H_2O = 0.1.

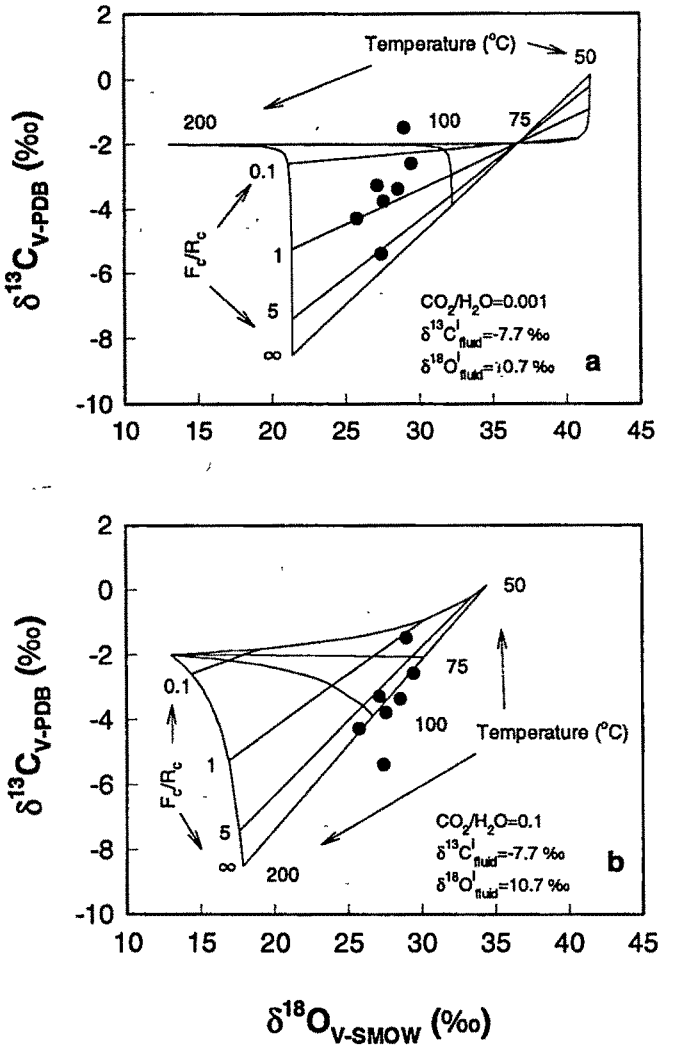

Fig. 4.27. *Comparison of $\delta^{13}C$ and $\delta^{18}O$ values of the ferrocarbonatites and metasomatic rocks from Amba Dongar with the fluid-rock interaction model curves when the fluid (hydrothermal) has (a) CO_2/H_2O = 0.001 and (b) CO_2/H_2O = 0.1. The initial rock: $\delta^{13}C$ = -2.0‰ and $\delta^{18}O$ = 13‰.*

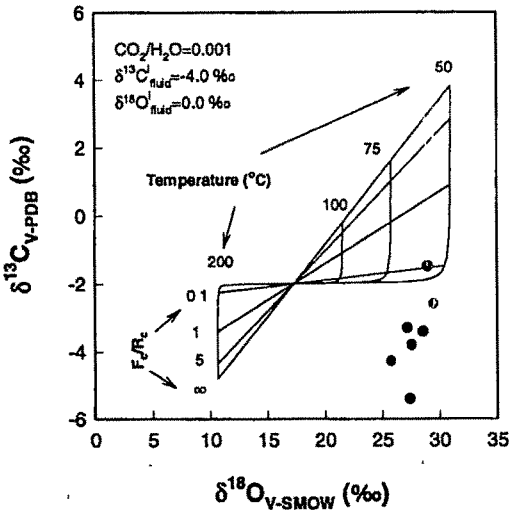

Fig. 4.28. Comparison of the $\delta^{13}C$ and $\delta^{18}O$ ferrocarbonatites and metasomatic rocks of Amba Dongar complex with the fluid-rock interaction model curves when the fluid is meteoric. Initial rock compositions are same as in Fig. 4.27.

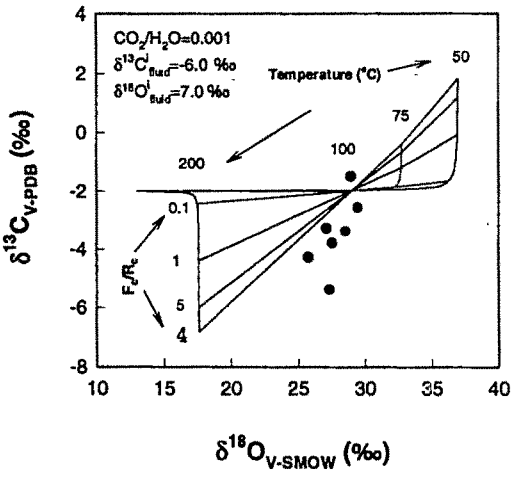

Fig. 4.29. Comparison of $\delta^{13}C$ and $\delta^{18}O$ of ferrocarbonatites and metasomatic rocks of Amba Dongar with the fluid-rock interaction model curves when the fluid is magmatic. Initial rock compositions are same as in Fig. 4.27.

Mundwara Complex

Application of fluid-rock interaction model to altered calcite carbonatites of Mundwara complex revealed that these rocks were altered by a low temperature meteoric-

hydrothermal fluid (Fig. 4.30). The fluid was found to be a CO_2 bearing aqueous fluid with initial $\delta^{13}C$ and $\delta^{18}O$ isotopic compositions of -1 ‰ and -4 ‰, respectively and having CO_2/H_2O ratio of 0.001. The $\delta^{13}C$ and $\delta^{18}O$ compositions of the rock was assumed to be -5 ‰ and 8 ‰, respectively. The temperature of fluid-rock interaction was found to be between 75°C to 150°C.

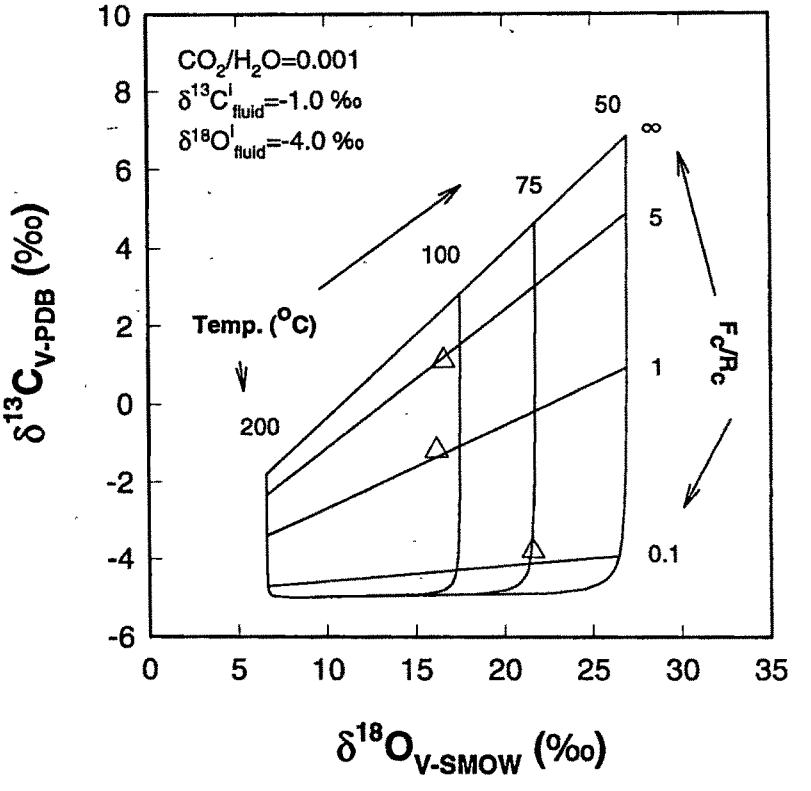

Fig. 4.30. *Comparison of $\delta^{13}C$ and $\delta^{18}O$ of altered calcite carbonatites of Mundwara complex with the fluid-rock interaction model curves when the fluid is meteoric-hydrothermal. The initial rock compositions are assumed to be: $\delta^{13}C$ = -5.0 ‰ and $\delta^{18}O$ = 8.0 ‰.*

Sarnu-Dandali Complex

Like, Mundwara, the extreme isotopic variation shown by altered calcite carbonatites, calcites from ferrocarbonatites and metasomatic rocks of Sarnu-Dandali complex was found to be a result of low temperature (50-150°C) fluid-rock interactions involving a

meteoric-hydrothermal fluid (Fig. 4.31). The fluid initial $\delta^{13}C$ and $\delta^{18}O$ compositions of -1.0 ‰ and -3 ‰, respectively, were used for the model calculations.

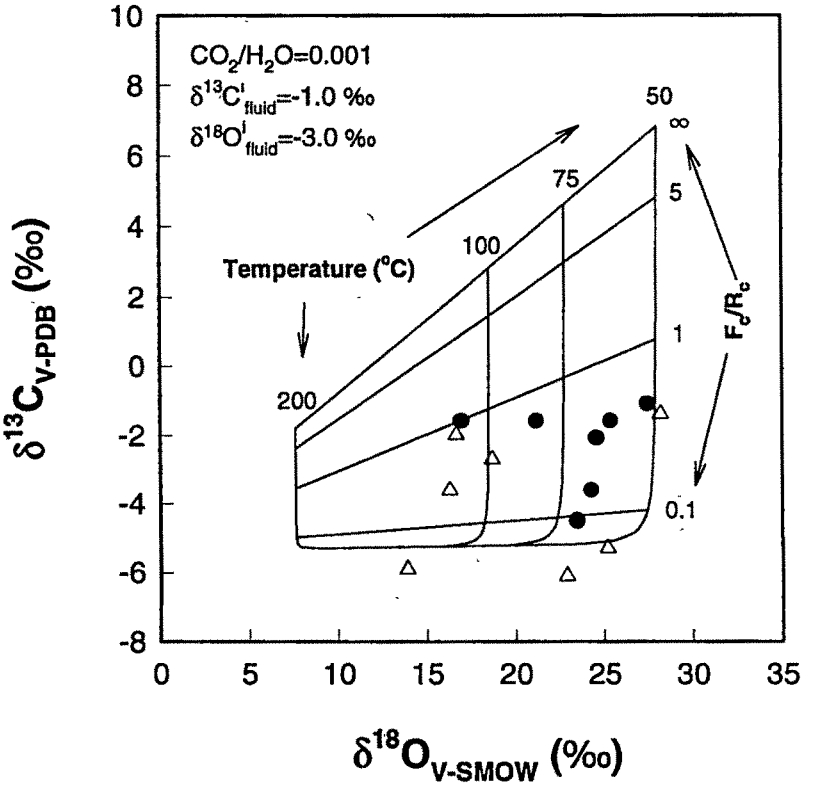

Fig. 4.31. *Comparison of the observed $\delta^{13}C$ and $\delta^{18}O$ variation of altered calcite carbonatites, ferrocarbonatites and metasomatic rocks of Sarnu-Dandali with the fluid-rock interaction model curves when the fluid is meteoric-hydrothermal. Initial rock compositions: $\delta^{13}C$ = -5.0 ‰ and $\delta^{18}O$ = 8.0 ‰.*

In summary, the extreme variations of $\delta^{13}C$ and $\delta^{18}O$ in carbonatites and metasomatic rocks from Amba Dongar, Mundwara and Sarnu-Dandali are found to have been generated by interaction of CO_2 bearing aqueous fluids with the rocks at temperatures between 50° and 400°C. In the case of Amba Dongar the calcite carbonatites have probably been affected by both magmatic and fluorite mineralizing hydrothermal fluids, whereas ferrocarbonatites and metasomatic rocks by only the fluorite mineralizing

fluid. In the case of Mundwara and Sarnu-Dandali, low temperature alteration by meteoric-hydrothermal fluid is observed.

4.4.3d. Ferrocarbonatites from Amba Dongar

Fig. 4.16 shows the $\delta^{13}C$ and $\delta^{18}O$ values of coexisting calcite and ankerite from different ferrocarbonatite samples of Amba Dongar complex. Calcites are depleted in $\delta^{13}C$ but highly enriched in $\delta^{18}O$ compared to the coexisting ankerites, except in one sample, in which calcite shows higher $\delta^{13}C$ and $\delta^{18}O$ values. Except for this sample, in all other samples there is a clear indication of disequilibrium between calcites and ankerites (inferred from the negative value of $\Delta^{18}O_{dol\text{-}cal}$, Northrop and Clayton, (1966)). The sample which showed isotopic equilibrium gave a temperature of equilibration of ~380°C, which was calculated based on the carbon isotope fractionation equation of Sheppard and Schwartz (1970). The temperature of equilibration of 380°C indicates that the crystallization temperature of these rocks was ≥380°C. The higher values of $\delta^{18}O$ of calcites are due to hydrothermal alteration, this has already been discussed in the previous section.

4.4.4. Summary

The carbon and oxygen isotopic compositions of the carbonatites of Deccan Province show mantle signatures. All the three complexes studied here show similar isotopic variations. The correlated $\delta^{13}C$ and $\delta^{18}O$ variations observed in unaltered calcite carbonatites of these complexes are successfully explained here by a multicomponent Rayleigh fractionation model (Section 4.4.3b) which reveals that the variations are results of fractional crystallization of these carbonatites from CO_2 rich carbonate magmas. Model calculations also indicate that the carbon isotopic composition of the primary melts for these complexes essentially show average mantle values, except a particular batch of primary melt at Amba Dongar. This batch of primary melt has higher $\delta^{13}C$ composition (by at least 1.8‰) than the average mantle. Such an enrichment probably indicates the incorporation of recycled crustal carbon into this batch of carbonate magma.

Most of the extreme variations of $\delta^{13}C$ and $\delta^{18}O$ in carbonatites and metasomatic rocks studied here are explained by a fluid-rock interaction model (section 4.4.3c). Application of this model reveals that some Amba Dongar rocks have been altered by magmatic and fluorite mineralizing hydrothermal fluids, whereas in other two complexes, evidence of low temperature meteoric-hydrothermal alteration is found. In most of the ferrocarbonatites studied here, coexisting calcites and ankerites show isotopic disequilibrium and calcites are highly altered compared to ankerites. A temperature estimation in Amba Dongar based on carbon isotopes reveals that the crystallization temperature of ferrocarbonatites was >380°C.

PART-B: CARBONATITE-ALKALINE COMPLEXES OF ASSAM-MEGHALAYA PLATEAU

In this part, the results of different isotopic studies of three carbonatites-alkaline complexes (Sung Valley, Samchampi and Swangkre) are presented and discussed. This part is divided into three sections, discussing the results of ^{40}Ar-^{39}Ar chronology and strontium isotopic study of Sung Valley complex and stable isotopic study of all the three complexes, respectively.

4.5. ^{40}Ar-^{39}Ar CHRONOLOGY OF SUNG VALLEY COMPLEX

The formation of a large igneous province during Early Cretaceous at the continental margins of eastern Antarctica, western Australia and eastern India is generally believed to be related to the Kerguelen plume activity (Storey et al., 1992). This activity started around 116 Ma ago with the extrusion of Rajmahal Traps on the Indian subcontinent (Baksi, 1986; Ghose et al., 1996). Other magmatic activities of eastern India, which are considered to be members of the above large igneous province include Sylhet Traps; lamprophyres, dolerites and basalts of Bengal basin; and carbonatite-alkaline complexes of Assam-Meghalaya plateau (Ghose et al., 1996). The available geochronological data on Sung Valley complex give ages varying from 90 Ma to 150 Ma (Chattopadhay and Hashimi, 1984; Krishna et al., 1991; Kent et al., 1992). Hence, to precisely determine the age of these carbonatite-alkaline activities and to establish their temporal relationship with the Rajmahal Traps, precise ^{40}Ar-^{39}Ar dating of

samples from Sung Valley complex was undertaken in this work following the procedures described in Chapter-III.

4.5.1. Results

Three samples, one whole rock sample of alkali pyroxenite (SV-4) and two phlogopite mineral separates from carbonatites (SV-7 and SV-12) were dated. The argon isotopic compositions, fraction of ^{39}Ar released, apparent ages and percent radiogenic argon ($^{40}Ar^*$) released, for each temperature step are given in Tables 4.11-4.13. Modified J factors are also given in these tables. The age spectra along with isotope correlation diagrams are shown in Figures 4.11-4.13. The plateau ages along with percent ^{39}Ar included in the plateaus; isochron and inverse isochron ages of plateau steps along with ratios of trapped argon and MSWD values; and integrated (total) ages are summarized in Table 4.14. The two phlogopite separates (SV-7 and SV-12) yielded good plateaus in the age spectra (Fig. 4.32a and Fig. 4.33a) giving ages of 106.4±1.3 (2σ) Ma and 107.5±1.4 (2σ) Ma respectively, which are indistinguishable within the assigned errors. The pyroxenite (SV-4), a monomineralic rock yielded a four high temperature steps (1000°C 1150°C) plateau (Fig. 4.34a) with an age of 108.0±2.0 (2σ) Ma, agreeing with the phlogopite ages within 2σ level of error. However, the saddle shaped age spectrum (Fig.4.34a) and non-atmospheric trapped argon component (i.e., y-intercept >295.5; Table 4.14) of this sample suggest the presence of a small amount of inherited argon. Therefore, only the phlogopite ages are considered for the age calculation and the weighted mean of these, 106.9±0.9 (2σ) Ma, is the age of emplacement of Sung Valley complex.

Table 4.11. Step heating argon isotopic compositions and apparent ages of sample SV-4 (Sung Valley Pyroxenite). Errors on age are without and with (bracketed) error on J. Errors quoted are at 1σ .

(J = 0.00220 ± 0.00004)

Temp. (°C)	$^{36}Ar/^{39}Ar$ ±1σ	$^{37}Ar/^{39}Ar$ ±1σ	$^{40}Ar/^{39}Ar$ ±1σ	AGE (Ma) ±1σ	^{39}Ar (%)	$^{40}Ar^*$ (%)
500	3.53	10.06	2288.0	2380	0.01	54.43
	0.51	0.27	203.0	166 (168)		
600	2.04	3.33	1692.0	2208	0.02	64.45
	0.19	0.69	76.0	61 (65)		
650	0.815	10.23	489.8	788	0.10	50.84
	0.026	0.20	4.3	22 (25)		
700	0.991	35.67	664.3	1078	0.06	55.92
	0.043	0.35	6.7	31 (34)		
750	2.276	26.70	1039.0	1066	0.12	35.25
	0.028	0.51	11.0	21 (25)		
800	0.305	2.78	233.5	495	0.37	61.42
	0.034	0.18	2.1	31 (32)		
850	0.080	0.420	80.7	214	0.71	70.76
	0.022	0.075	1.0	23 (24)		
900	0.0497	0.439	50.65	137.5	1.35	71.0
	0.0019	0.017	0.58	2.9 (3.7)		
950	0.02279	0.4942	41.39	132.6	2.69	83.73
	0.00095	0.0089	0.99	3.8 (4.4)		
1000	0.01382	1.648	32.69	110.2	4.14	87.51
	0.00049	0.023	0.37	1.4 (2.4)		
1050	0.00275	2.977	29.04	108.73	17.72	97.20
	0.00022	0.023	0.21	0.62 (1.96)		

1100	0.000884	3.0930	28.17	107.58	57.37	99.07
	0.000062	0.0062	0.16	0.53 (1.91)		
1150	0.00661	6.127	30.29	109.17	12.61	93.55
	0.00022	0.012	0.22	0.78 (2.02)		
1200	0.0253	129.4	70.9	236	0.97	89.44
	0.0049	2.1	2.7	10 (11)		
1250	0.0176	101.76	60.1	205.6	0.77	91.34
	0.0049	0.24	1.3	7.8 (8.5)		
1300	0.039	69.39	69.6	217	0.45	83.47
	0.011	0.33	2.3	14 (15)		
1400	0.071	33.15	73.0	196	0.54	71.25
	0.015	0.11	3.2	20 (20)		
Integrated Values	0.01117	5.776	34.23	118.82	100.0	90.35
	0.00025	0.021	0.12	0.47 (2.08)		

Table 4.12. Step heating argon isotopic compositions and apparent ages of sample SV-7 (Phlogopite from Sung Valley Carbonatite). Errors on age are without and with (bracketed) error on J. Errors quoted are at 1σ .

(J = 0.00230 ± 0.00004)

Temp. (°C)	$^{36}Ar/^{39}Ar$ ±1 σ	$^{37}Ar/^{39}Ar$ ±1 σ	$^{40}Ar/^{39}Ar$ ±1 σ	AGE (Ma) ±1 σ	^{39}Ar (%)	$^{40}Ar^*$ (%)
600	0.1429	3.0	98.9	222	0.07	57.33
	0.0088	1.1	1.7	11 (11)		
650	0.0775	1.53	63.0	159.5	0.14	63.66
	0.0042	0.12	1.1	6.3 (6.9)		
700	0.0650	1.17	48.27	116.9	0.32	60.18
	0.0019	0.12	0.79	3.7 (4.2)		
750	0.0321	0.0946	37.36	112.3	1.56	74.60

	0.0010	0.0082	0.98	2.8 (3.4)		
800	0.0057	0.1591	28.21	107.04	3.56	94.03
	0.00018	0.0082	0.18	0.67 (1.95)		
850	0.0072	0.00924	28.44	106.18	5.71	92.50
	0.00016	0.00098	0.17	0.61 (1.91)		
900	0.005458	0.001	27.88	106.02	13.53	94.22
	0.000095	0.00087	0.16	0.56 (1.90)		
950	0.00209	0.0185	26.81	105.71	10.79	97.69
	0.00015	0.0016	0.15	0.56 (1.89)		
1000	0.00313	0.02065	27.22	106.11	11.68	96.60
	0.00012	0.00074	0.16	0.56 (1.90)		
1050	0.00424	0.02548	27.71	106.75	22.87	95.48
	0.000051	0.0004	0.20	0.59 (1.92)		
1100	0.003	0.02241	27.25	106.38	18.53	96.75
	0.00091	0.00043	0.16	0.55 (1.90)		
1150	0.00363	0.04049	27.47	106.50	9.03	96.09
	0.00014	0.00015	0.18	0.58 (1.91)		
1200	0.00682	0.614	28.56	107.1	1.57	92.94
	0.00076	0.011	0.34	1.6 (2.4)		
1250	0.0097	10.688	39.06	144.5	0.45	92.67
	0.0027	0.048	0.84	4.5 (5.1)		
1300	0.044	31.02	83.7	272.0	0.13	84.50
	0.011	0.11	3.3	16 (17)		
1400	0.718	26.18	217.0	18	0.04	2.01
	0.059	0.15	22.0	114 (114)		
Integrated Values	0.005223	0.13884	28.063	107.0	100.00	94.50
	0.000052	0.00096	0.069	0.23 (1.84)		

Table 4.13. Step heating argon isotopic compositions and apparent ages of sample SV-12 (Phlogopite from Sung Valley Carbonatite). Errors on age are without and with (bracketed) error on J. Errors quoted are at 1σ .

(J = 0.00229 ± 0.00004)

Temp. (°C)	$^{36}Ar/^{39}Ar$ ±1σ	$^{37}Ar/^{39}Ar$ ±1σ	$^{40}Ar/^{39}Ar$ ±1σ	AGE (Ma) ±1σ	^{39}Ar (%)	$^{40}Ar^*$ (%)
650	0.364	3.47	205.3	365	0.06	47.58
	0.017	0.38	4.6	18 (19)		
700	0.1215	7.005	107.0	272.4	0.18	66.43
	0.0079	0.060	5.2	6.4 (7.8)		
750	0.06182	1.0109	55.89	149.3	1.0	67.31
	0.00098	0.0097	0.40	1.8 (3.1)		
800	0.01761	0.0358	31.95	107.4	2.35	83.71
	0.00053	0.0094	0.27	1.2 (2.2)		
850	0.01265	0.00008	30.61	107.91	4.16	87.79
	0.00026	0.0000002	0.22	0.84 (2.02)		
900	0.01133	0	30.17	107.71	12.35	88.90
	0.00016	0	0.18	0.63 (1.94)		
950	0.00473	0.0093	28.31	108.08	10.66	95.06
	0.00024	0.00035	0.17	0.64 (1.95)		
1000	0.00617	0.0058	28.58	107.47	13.0	93.62
	0.00015	0.0019	0.17	0.60 (1.93)		
1050	0.00426	0.00701	28.02	107.48	28.43	95.51
	0.0001	0.00013	0.32	0.56 (1.92)		
1100	0.00220	0.01209	27.35	107.26	15.32	97.63
	0.00016	0.00013	0.16	0.59 (1.92)		
1150	0.00171	0.0273	27.13	106.95	10.88	98.14
	0.00026	0.0011	0.17	0.66 (1.94)		
1200	0.0068	0.8105	28.39	106.0	1.22	92.92
	0.0016	0.0038	0.61	2.9 (3.5)		
1250	0.0171	12.757	38.1	132	0.31	86.76
	0.0074	0.050	1.9	11 (11)		

1300	0.018	56.37	66.6	238	0.10	92.16
	0.023	0.11	6.6	35 (35)		
Integrated Values	0.06582	0.14037	28.99	108 58	100.00	93.29
	0.000077	0.00049	0.11	0.25 (1.87)		

Table 4.14. Summary of results of ^{40}Ar-^{39}Ar dating of Sung Valley samples.

Sample	Plateau			Isochron			Inverse Isochron			Integrated Age
	steps	% ^{39}Ar	Age (Ma)	Age (Ma)	Trap	MSWD	Age (Ma)	Trap	MSWD	(Ma)
SV-4	4	91.84	108.8 ±2.0	108.0 ±3.9	342.0 ±60.0	0.108	107.7 ±27.0	352.0 ±62.0	0.078	118.8 ±4.2
SV-7	9	97.27	106.4 ±1.3	106.6 ±3.9	284.0 ±71.0	0.128	105.9 ±34.5	319.0 ±73.0	0.088	107.0 ±3.7
SV-12	9	98.37	107.5 ±1.4	107.5 ±3.8	299.0 ±30.0	0.068	107.3 ±16.0	304.9 ±31.0	0.057	108.6 ±3.7

Note: Trap: Initial $^{40}Ar/^{36}Ar$ (trapped argon); MSWD: Mean Square Weighted Deviate.
Errors are 2σ.

4.5.2. Discussion

The contemporanity of alkali pyroxenite and carbonatites of Sung Valley complex probably indicates a genetic relationship between these two. The 106.9±0.9 Ma age of this complex suggests that this complex is much younger than most of the dates reported earlier and is younger than Rajmahal Traps by ~10 Ma. This age of Sung Valley also suggests that this alkaline activity is coeval with Kerguelen plume related magmatisms such as Damodar Valley and Darjeeling Lamprophyres (121-105 Ma; Sarkar et al., 1980), Prince Charles Mountains Lamprophyres (108-110 Ma; Walker and Mond, 1971) and Bundbury Basalt (88-105 Ma, McDougall and Wellman, 1976). Hence the age along with the location of Sung Valley carbonatite-alkaline complex (present within the Kerguelen plume affected region) can be put forward as a circumstantial evidence for Kerguelen plume origin for this complex.

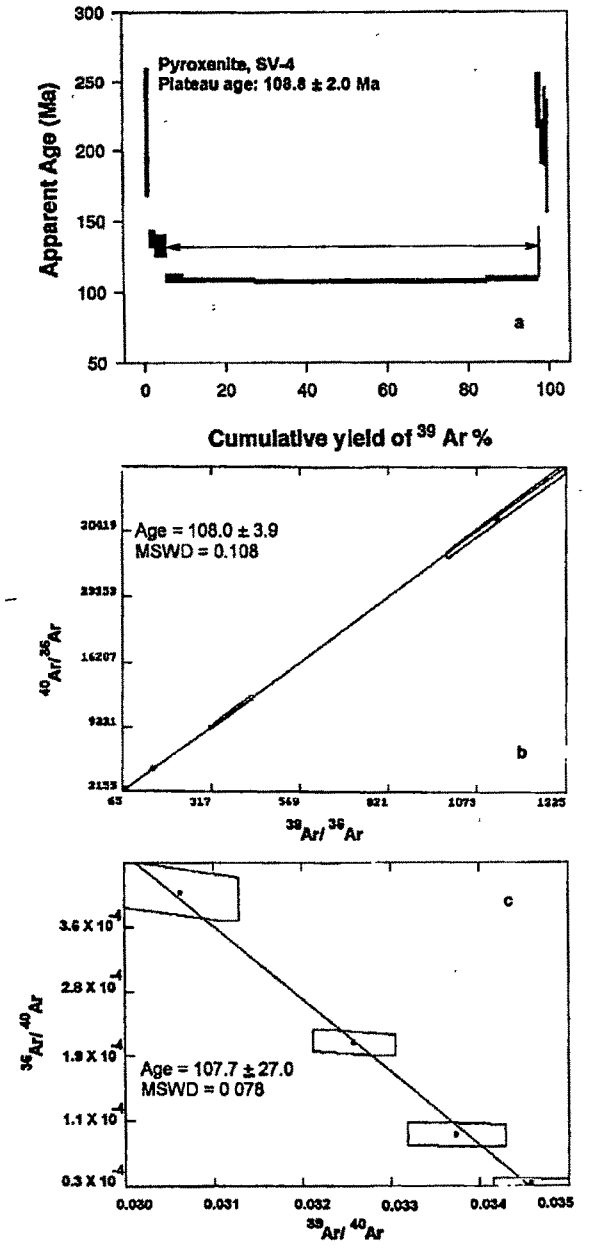

Fig. 4.32. *(a) Step heating $^{40}Ar/^{39}Ar$ apparent age spectrum for SV-4 (Sung Valley Pyroxenite) with plateau age. The spectrum shows a saddle shaped pattern with a four temperature steps plateau (see text for discussion). (b) $^{40}Ar/^{36}Ar$ vs. $^{39}Ar/^{36}Ar$ correlation diagram of SV-4 showing 2σ error envelopes and regression line. Isochron age and MSWD value are also shown. (c) $^{36}Ar/^{40}Ar$ vs. $^{39}Ar/^{40}Ar$ correlation diagram of SV-4 showing 2σ error envelopes and regression line. Inverse isochron age and MSWD value are also shown. Please also see the caption of Fig. 4.1.*

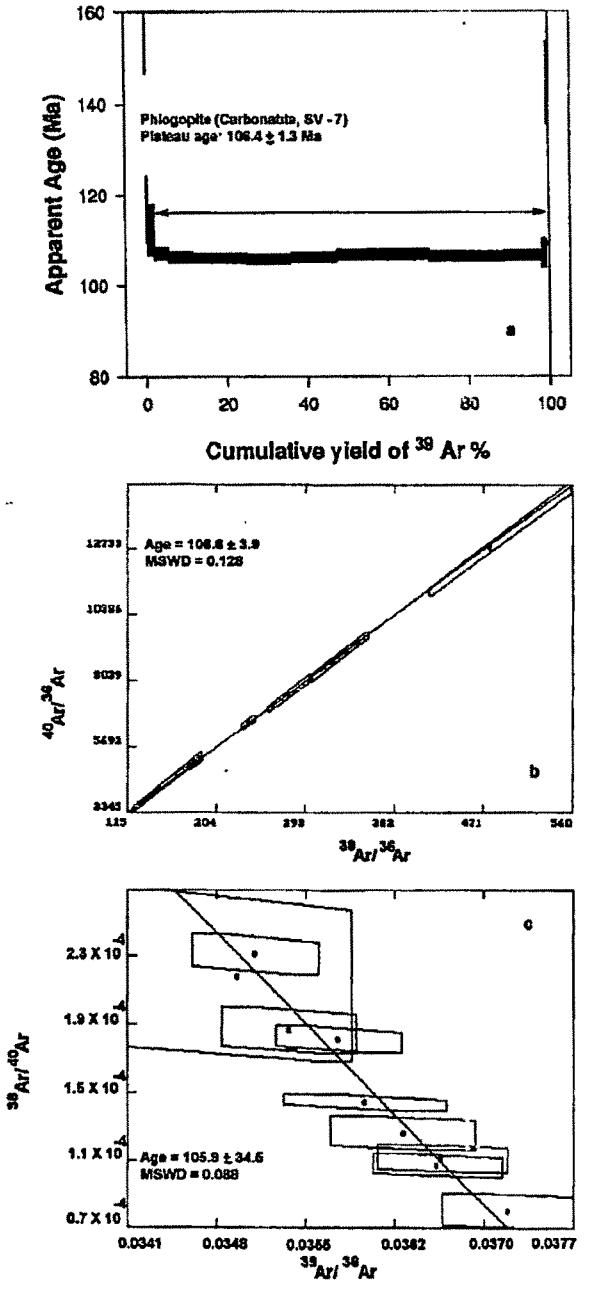

Fig.4.33. *(a) Step heating of $^{40}Ar/^{39}Ar$ apparent age spectrum for SV-4(phlogopite separate from a carbonatite of Sung Valley) with the plateau age. (b) $^{40}Ar/^{36}Ar$ vs. $^{39}Ar/^{36}Ar$ correlation diagram of SV-7 with isochron age and MSWD value. (c) $^{36}Ar/^{40}Ar$ vs. $^{39}Ar/^{40}Ar$ correlation diagram of SV-7 with inverse isochron age and MSWD value. Please also see the caption of Fig.4.1 and Fig. 4.32.*

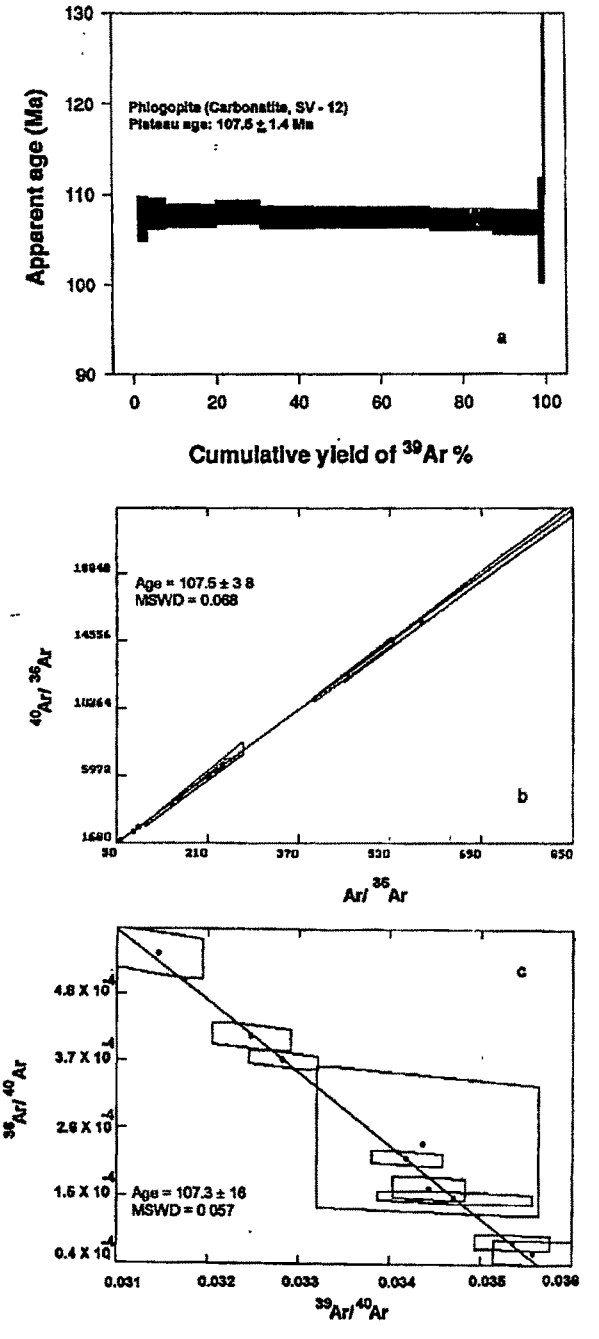

Fig. 4.34. *(a) Step heating of $^{40}Ar/^{39}Ar$ apparent age spectrum for SV-12 (phlogopite separate from a carbonatite of Sung Valley) with plateau age. (b) $^{40}Ar/^{36}Ar$ vs. $^{39}Ar/^{36}Ar$ correlation diagram of SV-12 with isochron age and MSWD value. (c) $^{36}Ar/^{40}Ar$ vs. $^{39}Ar/^{40}Ar$ correlation diagram of SV-12 with inverse isochron age and MSWD value. Please also see the captions of Fig. 4.1 and Fig. 4.32.*

4.5.3. Summary

The Sung Valley carbonatite-alkaline complex is 107 Ma old. The pyroxenites and carbonatites of this complex are coeval and hence, are probably genetically related. The temporal and spatial relation of this complex with Rajmahal Traps, Bengal basin magmatisms and other Kerguelen related activities suggest that this complex was generated by the Kerguelen plume.

4.6 Sr ISOTOPIC STUDIES IN SUNG VALLEY

4.6.1. Results

Sr isotope ratio and concentration were measured in samples of carbonatites, a phlogopite separate and a pyroxenite. The results are summarized in Table 4.15. The table also gives the initial $^{87}Sr/^{86}Sr$ ratios calculated using the age of 107 Ma for Sung Valley (^{40}Ar-^{39}Ar age). An attempt was made to date Sung Valley complex by Rb-Sr isochron method of dating and for this, two calcite carbonatite whole rocks (SV-11 and SV-12), and phlogopite separate (SV-12/P) from the calcite carbonatite and a pyroxenite whole rock (SV-4) were used. The Rb-Sr isochron age (using the method proposed by Provost, 1990) for this complex was found to be 106±11 (2σ) Ma (Fig. 4.35) and the y-intercept gave an initial ratio [$(^{87}Sr/^{86}Sr)_i$] for the complex of 0.70508±0.00004 (2σ). This isochron age matches well with the ^{40}Ar-^{39}Ar age for the complex within the error. The initial Sr ratios of carbonatites and the pyroxenite are essentially same as the initial ratio found from isochron diagram (Fig. 4.35) considering the errors associated with them. The average Sr concentration in carbonatites is ~4000 ppm.

Table 4.15. Results of Sr isotopic measurements in samples from Sung Valley complex.

Sample	Rb (ppm)	Sr (ppm)	$(^{87}Sr/^{86}Sr)_m$ (atomic)	$(^{87}Rb/^{86}Sr)_m$ (atomic)	$(^{87}Sr/^{86}Sr)_i$
Carbonatites					
SV-1	0.1	4076	0.7055±3	0.00007	0.7055

SV-5	0.12	4030	0.7049±2	0.00009	0.7049
SV-6	0.15	3859	0.7053±2	0.00011	0.7053
SV-10	0.1	4148	0.7046±5	0.00007	0.7046
SV-11	0.18	3831	0.7051±1	0.00014	0.7051
SV-12	0.22	3418	0.7053±3	0.00019	0.7053
SV-13	0.18	3956	0.7050±1	0.00013	0.7050
Phlogopite (carbonatite)					
SV-12/P	153	207	0.7083±3	2.1369	0.7050
Pyroxenite					
SV-4*	10	700	0.70514±4	0.04132	0.70508

Note: * = sample analyzed at NGRI; subscript 'm' stands for measured ratios and 'i' for initial ratio (at 107 Ma). The errors quoted on the measured Sr ratios are at 2σ.

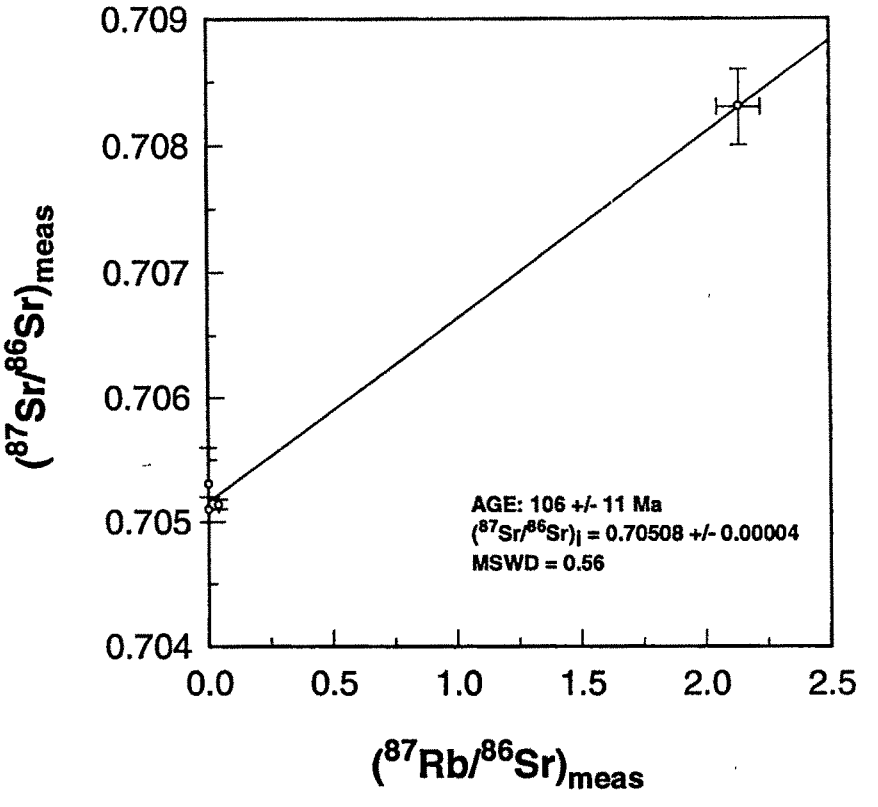

Fig. 4.35. *Rb-Sr conventional isochron diagram for Sung Valley complex. Two whole rock carbonatites and one whole rock pyroxenite plot close to $^{87}Rb/^{86}Sr$ = 0, whereas a phlogopite separate from carbonatite with very high $^{87}Rb/^{86}Sr$ (~2.14) and very high $^{87}Sr/^{86}Sr$ plots on the extreme right of the figure. Error bars are at 2σ.*

4.6.2. Discussion

The consistency of Rb-Sr isochron age with the ^{40}Ar-^{39}Ar age and the homogeneous initial $^{87}Sr/^{86}Sr$ ratio in the rocks of Sung Valley suggests that the Sr reservoir of this complex has remained a closed system since the emplacement of the complex. The similarity of initial $^{87}Sr/^{86}Sr$ ratio of carbonatites and pyroxenites indicates that these rocks types were derived from similar sources and are genetically related.

The initial $^{87}Sr/^{86}Sr$ ratio of Sung Valley complex, i.e., 0.70508 (found from isochron diagram, Fig.4.35) falls within the initial ratio fields of Rajmahal tholeiites and the 105-115 Ma old basalts from Kerguelen plateau (Storey et al, 1992). This observation

along with the chronology clearly supports the generation of this complex by the Kerguelen plume activity.

4.6.3. Summary

The Rb-Sr isochron age a Sung Valley is 106±11 (2σ) Ma, which is same as the ^{40}Ar-^{39}Ar age of this complex. The homogenous initial Sr ratio in rocks of this complex suggests that the complex has remained a closed system since its formation. Similarity of the initial $^{87}Sr/^{86}Sr$ of Sung Valley with that of other Kerguelen plume generated rocks suggest a similar origin (i.e., generation from Kerguelen plume) for this complex.

4.7 STABLE CARBON AND OXYGEN ISOTOPES

4.7.1. Results

The carbon and oxygen isotopic compositions of carbonatites from all the three complexes (Sung Valley, Samchampi and Swangkre) were measured. Isotopic compositions of coexisting calcites and dolomites in samples of dolomite bearing calcite carbonatites from Sung Valley were measured following the selective CO_2 extraction produces discussed in section 3.2.2b of Chapter-III. Table 4.16 summarizes the results of these measurements. The $\delta^{13}C$ and $\delta^{18}O$ values of calcite from calcite carbonatites from all the three complexes are plotted in Fig. 4.36. The isotopic compositions of coexisting calcite and dolomite of Sung Valley samples are plotted in Fig. 4.37. These figures also show the primary carbonatite box, which is modified after Taylor (1967) and Keller and Hoefs (1995).

As seen in Fig.4.36, the carbonatites from Sung Valley, except two samples, from a cluster around $\delta^{13}C$ value of -3.0‰ and $\delta^{18}O$ value of 7.4‰. Similarly carbonatites from Samchampi form a cluster around $\delta^{13}C$ = -3.5‰ and $\delta^{18}O$ = 7.2‰ and the only sample from Swangkre plots at $\delta^{13}C$ = -3.7‰ and $\delta^{18}O$ = 9.6‰. All these complexes plot above the primary carbonatite box.

Table 4.16. Carbon and Oxygen isotopic compositions of samples from carbonatite-alkaline complexes of Assam-Meghalaya Plateau.

Sample	$\delta^{13}C_{calcite}$ (‰)	$\delta^{18}O_{calcite}$ (‰)	$\delta^{13}C_{dolomite}$ (‰)	$\delta^{18}O_{dolomite}$ (‰)
Sung Valley				
SV-1	-2.6	7.5	-2.2	6.8
SV-2	-1.8	15.3	-2.2	7.1
SV-5	-3.0	7.2	---	---
SV-6	-2.9	7.5		
SV-10	-2.9	7.1		
SV-11	-3.0	7.2		
SV-12	-3.0	7.2		
SV-15	-3.0	7.1		
SV-18	-2.8	7.2	-2.4	6.7
SV-19	-2.8	8.4	-3.1	8.8
SV-20	-2.8	7.3	-2.4	6.7
PKS-145	-3.0	7.6		
PKS-164	-3.1	7.8		
PKS-270	-2.9	7.5		
PKS-241	-3.1	15.3		
PKS-279	-3.1	7.1		
Samchampi				
71	-3.8	7.2		
C1/93	-3.7	7.5		
165	-3.0	7.3		
177	-3.7	7.0		
179	-3.5	7.1		
Swangkre				
WKS-1	-3.7	9.6		

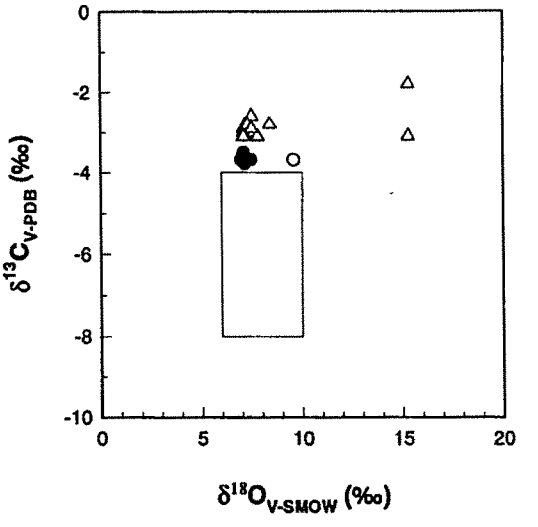

Fig. 4.36. *Carbon and oxygen isotopic compositions of calcites from calcite carbonatites and dolomite bearing calcite carbonatites of all the three complexes of Assam-Meghalaya plateau. Open triangles = Sung Valley, filled circles = Samchampi, and open circles = Swangkre. The box is for primary carbonatites (modified after Taylor et al., 1967 and Keller and Hoefs, 1995).*

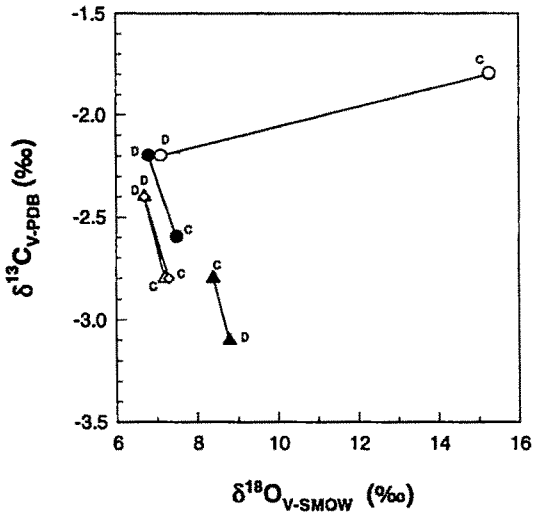

Fig. 4.37. *$\delta^{13}C$ vs. $\delta^{18}O$ of coexisting calcites (marked as c) and dolomite (marked as d) joined by tie lines from dolomite bearing calcite carbonatites of Sung Valley complex.*

4.7.2. Discussion

It has been postulated that the $\delta^{13}C$ and $\delta^{18}O$ variations of carbonatites depends on their emplacement levels (Deines and Gold,1973) and the isotopic compositions of deep-seated complexes are less variable than those of the shallow seated complexes. The carbonatites of Assam-Meghalaya plateau being the deepest complex (Section 2.8 of Chapter-II) of all the Mesozoic complexes studied in this work, shows less variable (in fact, homogeneous) isotopic composition, consistent with the observations made by Deines and Gold (1973). This is probably because these rocks have not been affected by any near surface alteration processes. Only the two samples (which are collected close to a river-cut section) from Sung Valley, which show higher $\delta^{18}O$ values than the rest but similar $\delta^{13}C$ values, possibly have been affected by meteoric water alteration.

4.7.2.a. Mantle Source Regions

All the samples from Sung Valley, Samchampi and Swangkre, except the two altered ones, show $\delta^{18}O$ value in the range of 7.0 to 9.6‰, consistent with the predictions made by Deines (1989) for the $\delta^{18}O$ of the primary carbonatites. However, the $\delta^{13}C$ values are higher than the generally observed $\delta^{13}C$ values for primary carbonatites (Deines, 1989; Keller and Hoefs, 1995). Homogeneous initial of Sr isotopic ratios (as discussed in the previous section) of Sung Valley rules out crustal contamination and the homogeneous nature of $\delta^{13}C$ and $\delta^{18}O$ values rules out the isotopic fractionation due to fractional crystallization in these complexes. In such a case the $\delta^{13}C$ and $\delta^{18}O$ values of the carbonatites directly reflect the isotopic composition of the parent magma. If so, then the parent magmas of these three complexes had higher $\delta^{13}C$ compositions (> 3.5%) than what is observed for most of the carbonatite complexes of the world. Deines (1989) suggested that during the formation of carbonate magma a fairly complete extraction of elemental carbon from the source takes place and hence the magma would simply inherit the carbon isotopic composition of the mantle source without fractionating it. Hence, the $\delta^{13}C$ of the primary magmas for the complexes under discussion are essentially the $\delta^{13}C$ values of their source regions which would mean that the mantle source regions of these complexes were enriched in carbon isotopes compared to an average mantle ($\delta^{13}C$ = -5.0‰, Nelson et al., 1988). If we assume that all the three complexes of Assam-Meghalaya plateau were derived from a

single source than the source had $\delta^{13}C$ values of -3.2‰ (average of all $\delta^{13}C$ values), which is 1.8‰ higher than an average mantle. This kind of carbon isotope enrichment of the mantle source is probably because of contamination of recycled crustal carbon with the juvenile carbon. Phanerozoic pelagic carbonates and secondary carbonates in altered oceanic crust generally have $\delta^{13}C$ values between 0-2‰ (Nelson et al., 1988); if such an oceanic crust got recycled into the mantle in the past, with a mixing of 26-36%, it could have generated higher $\delta^{13}C$ value in the carbonatite source region as observed. However, such an effect may not be detected in $\delta^{18}O$ of carbonatites as the reservoir for oxygen is much larger compared to that of carbon. As all these complexes were derived from Kerguelen plume, with the present findings, one would except that either the plume itself was enriched in carbon isotopes or it entrained subcontinental upper mantle material which was already enriched by mantle metasomatic processes. The latter explanation seems to be more reasonable as experiments (Yaxley and Green, 1994) have shown that calcite and dolomite can survive in the subducting oceanic crust as refractory phases up to 130-150 km depth, which can in turn provide the required carbon isotope enrichment upon dissociation of carbonates and subsequent metasomatism by the fluids (CO_2) removed from the oceanic crusts. It is not known yet whether the carbonates of subducting oceanic crust can survive up to core-mantle boundary in order to enrich the plume source regions. Hence, a plausible explanation for the generation of enriched carbonate magmas from the plume (like Sung Valley, Samchampi and Swangkre) would be melting of entrained carbon enriched subcontinental upper mantle material.

4.7.2b. Dolomite bearing calcite carbonatites from Sung Valley

Fig. 4.37 shows $\delta^{13}C$ and $\delta^{18}O$ values of coexisting calcite and dolomite from dolomite bearing calcite carbonatites. Calcites have lower $\delta^{13}C$ compared to dolomite and similar $\delta^{18}O$, except for two samples where calcites have higher $\delta^{13}C$ and $\delta^{18}O$ values compared to the dolomite. Except for these two samples, in all other samples (three of them) there is a clear indication of equilibrium between calcite and dolomite. The temperature of equilibration for these samples, calculated using the carbon isotopic fractionation equation of Sheppard and Schwartz (1970), is found to be ~600°C. This suggests that the carbonatites of Sung Valley complex were crystallized above 600°C.

3.7.3. Summary

Unlike carbonatites of Deccan Province, the carbonatites from Assam-Meghalaya plateau show homogeneous $\delta^{13}C$ (also $\delta^{18}O$) compositions. Except for two samples from Sung Valley (which are altered by meteoric water), others seem not to have experienced fractional crystallization or secondary alteration. The oxygen isotopic composition of these carbonatites suggest their magmatic nature. The carbon isotopic composition of these rocks suggest that the mantle source regions of these carbonatites were enriched compared to a isotopically normal mantle and this enrichment has been attributed to the incorporation of recycled crustal carbon.